ENERGY LABORATORY

MASSACHUSETTS INSTITUTE
OF TECHNOLOGY

SIMULATION OF SODIUM BOILING EXPERIMENTS WITH THERMIT SODIUM VERSION

by

Kang Yul Huh

MIT-EL 82-023

May 1982

SIMULATION OF SODIUM BOILING EXPERIMENTS

WITH THERMIT SODIUM VERSION

by

KANG YUL HUH

B.S., Seoul National University
(1980)

SUBMITTED IN PARTIAL FULFILLMENT
OF THE REQUIREMENTS FOR THE
DEGREE OF

MASTER OF SCIENCE

at the

MASSACHUSETTS INSTITUTE OF TECHNOLOGY

May 1982

SIMULATION OF SODIUM BOILING EXPERIMENTS WITH THERMIT SODIUM VERSION

by

KANG YUL HUH

Submitted to the Department of Nuclear Engineering on May 7, 1982, in partial fulfillment of the requirements for the Degree of Master of Science

ABSTRACT

Natural and forced convection experiments(SBTF and French) are simulated with the sodium version of the thermal-hydraulic computer code THERMIT. Simulation is done for the test secti--on with the pressure-velocity boundary condition and subsequ--ently extended to the whole loop. For the test section simu--lation, a steady-state and transient calculations are perform--ed and compared with experimental data. For the loop simula--tion, two methods are used, a simulated 1-D loop and an actual 1-D loop. In the simulated 1-D loop analysis, the vapor densi--ty is increased by one hundred and two hundred times to avoid the code failure and the results still showed some of the impor--tant characteristics of the two-phase flow oscillation in a loop. A mathematical model is suggested for the two-phase flow oscillation. In the actual 1-D loop, only the single phase calculation was performed and turned out to be nearly the same as the simulated 1-D loop single phase results.

In the process of simulation, it is discovered that the energy conservation equations of THERMIT fails to conserve energy by a small amount due to interfacial mass transfer and frictional dissipation of mechanical into thermal energy. The problems and applicability of the THERMIT physical models are also discussed.

Thesis Supervisor: Neil F. Todreas
Professor of Nuclear Engineering Department

ACKNOWLEDGEMENTS

I wish to express my sincere gratitude to my thesis supervisor Professor Neil E. Todreas for his guidance and advice, and to Professor Mujid S. Kazimi as my thesis reader. Finally I will never forget Andrei L. Schor for his friend--ship and advice throughout all the difficulties I encoun--tered for the last sixteen months.

TABLE OF CONTENTS

LIST OF FIGURES

LIST OF TABLES

NOMENCLATURE

Letter	Definition
A	flow area in axial direction
A_t	true interfacial area between liquid and vapor
cfℓ	wall contact fraction of liquid
cfv	wall contact fraction of vapor
c_p	specific heat at constant pressure
D	diameter of the tube
De	equivalent hydraulic diameter
e	internal energy per unit mass
f	wall friction factor
F	friction force
g	gravity
h	enthalpy per unit mass
H	wire wrap lead of the helical spacer
h_{fg}	enthalpy change between liquid and vapor at saturation
hℓfc	wall heat transfer coefficient through liquid convection
hℓnb	wall heat transfer coefficient through nucl--eate boiling
hvfc	wall heat transfer coefficient through vapor convection
k	thermal conductivity

L	axial length
$\dot{m}$	mass flow rate
M	mass
M	geometry factor for wall friction calculation
P	pressure
P	pitch between adjacent rods
P_i	pressure at the top face of the lower plenum
P'_i	pressure at the bottom face of the lower plenum
P_0	pressure at the top face of the upper plenum
P'_0	pressure at the bottom face of the upper plenum
Pe	Peclet number
Pr	Prandtl number
q	heat transfer rate per unit area
Q	heat transfer rate per unit volume
Re	Reynold's number
R_g	gas constant of sodium
S	slip ratio
t	time
T	temperature
tℓ	liquid temperature
tsat	saturation temperature
tv	vapor temperature
u	velocity

v	velocity
V	volume
v_{fg}	specific volume change between liquid and vapor at saturation
x	flow quality
z	axial coordinate

Greek

α	void fraction
Γ	interfacial mass transfer rate per unit volume
λ	interfacial mass transfer coefficient
μ	viscosity
ρ	density
σ	surface tension

Superscript

n	time step at n

Subscipt

c	condensation
dry	dryout
e	evaporation
i(in, inlet)	inlet
k	spatial point at k
ℓ	liquid

lam	laminar
m	mixture of liquid and vapor
0(out)	outlet
r	return loop
s	(used with T) saturation
s	(used with ρ, e, u, V) single-phase liquid
T	total of the liquid and vapor contributions
trans	transition between laminar and turbulent
turb	turbulent
v	vapor
w	wall
z	axial coordinate

Chapter 1. Introduction

This thesis is primarily concerned with applying the computer code THERMIT (sodium version) to actual experiments to examine the applicability of the numerical and physical models in the code by comparing calculational results with experimental data.

THERMIT is a component code for thermal-hydraulic calculations of a nuclear reactor core. It was originally written for water coolant, and revised for use in LMFBR's by Andrei L. Schor at MIT. Schor has also prepared the 4-Eq model as part of the sodium version of THERMIT so that there are now three two-phase flow models, i.e. a 6-Eq, a 4-Eq and a HEM model. The THERMIT version that is used throughout this thesis is the Schor version (as of January, 1981) which has all the three two-phase flow models as options.

The basic THERMIT code uses the two-fluid model with mass, momentum and energy conservation equations for each phase, hence six conservation equations. Presently the constitutive relations of the two fluid model are not in a well-established state so that in some cases it may be better to use the 4-Eq model than the 6-Eq model.

The 4-Eq model has mixture mass and energy conservation

equations in addition to a separate momentum conservation equation for each phase. Physically this equation set requires that the liquid and vapor phases should always be in thermal equilibrium. Consequently if a high degree of thermal disequilibrium between phases does not exist, the 4-Eq model can give good results. However in case of a severe transient in which the vapor phase may exist in subcooled liquid, the 4-Eq model may be a poor model to use. Since the code tends to fail in such a severe transient due to numerical problems, the 4-Eq model gave almost identical results to the 6-Eq model in the scope of my experience.

The HEM model assumes large interfacial momentum transfer so that the slip ratio is equal to one. Practically this is not a good assumption since the slip ratio is much greater than one due to the high density ratio (>2000) at atmospheric pressure. Thus the HEM model shows wide discrepancy with low pressure experimental data.

THERMIT is a component code, which needs appropriate boundary conditions at the top and bottom ends. Two types of boundary conditions can be used in THERMIT. One is the pressure-pressure set and the other is the pressure-velocity set. In case of loop simulation, however, the starting point corresponds to the end point so that only one boundary

condition is needed.

There are two experiments simulated in this thesis, an ORNL natural convection experiment and a French forced convection experiment. The experiment reported in ORNL/TM--7018 is a single-channel natural convection sodium boiling experiment that was performed in the Sodium Boiling Test Facility of the Oak Ridge National Laboratory. It is chosen for simulation because of its simple geometry and well--documented output data. The French experiment is a single channel forced convection sodium boiling experiment performed at the CEA, Grenoble, France. The geometry of the French experiment is simplified to have a uniform flow area and calculation is done for the simplified geometry.

In Chapter 2 the details of the simulation methods are given for these two experiments. For the ORNL/TM-7018 experiment, first only the test section is simulated with appropriate boundary conditions and subsequently the analysis is extended to the whole loop. In simulating the loop as a whole, there are two methods possible, i.e. a simulated 1-D loop analysis and an actual 1-D loop analysis. For the loop analysis, condensation in the upper plenum should be taken into consideration. However the code presently fails when conden--sation occurs. The difficulty is circumvented by decreasing the density ratio of the liquid and vapor phases artificially.

For this purpose, the vapor density is increased by 100 and 200 times with all the other properties intact. These changes in the density ratio correspond to actual pressures of 10.0 Mpa (1470 psia) and 15.7 Mpa (2300 psia). The simulation of the French experiment is essentially the same as the test section simulation of ORNL/TM-7018.

In Chapter 3, numerical and physical models are listed and explained. Physical models are the constitutive relations that close the conservation equations.

As part of the numerical model, the energy loss problem is considered. With the present form of the energy conservation equations, some portion of the total energy is lost due to disregard for the frictional dissipation and some extra terms that come from the mass transfer between phases.

As for the physical model, geometry plays an important role. The geometry of THERMIT is a rod-bundle geometry with wire wraps, whereas the ORNL/TM-7018 experiment was done in a single circular tube. Hence either translation should be done between the different geometries or constitutive rela--tions from the same geometry should be used. In this thesis the former approach is taken for all the calculations. The present contitutive relations and their problems are also summarized in Chapter 3.

In Chapters 4 and 5, all the computer results and

experimental data are presented and analyzed. For the test section simulation, the difference of the pressure drops between calculation and experiment is presented and the results from the HEM, 4-Eq and 6-Eq models are compared and discussed. For the loop simulation an analysis explaining why there should be an oscillatory behavior under two-phase flow conditions is presented. The oscillation period is calculated analytically.

In Chapter 6, it is concluded that THERMIT is a good numerical tool, although it still has some problems to be solved. Stabilization of the numerical scheme and verification of the physical models are major problems.

In Chapter 7, recommendations for future works are given for further improvement of THERMIT and better understanding of two-phase flow phenomena.

Chapter 2. Simulation of the cases

2.1 Natural convection

2.1.1 Explanation of the experiment ORNL/TM-7018

This is a single-channel sodium boiling experiment that was performed in the SBTF (Sodium Boiling Test Facility) at Oak Ridge National Laboratory. The object of the test was to determine the maximum power that could be transferred to the sodium coolant in an LMFBR fuel assembly subchannel when the flow is driven by natural convection.

Fig 2.1 shows the whole test loop and Fig 2.2 shows the test section. The test section is composed of a heated zone and an adiabatic zone. Lower and upper plena are attached to the ends of the test section. The temperatures of the lower and upper plena are fixed at 420°C and 590°C by sodium--to-air heat exchangers located inside the plena. The upper plenum pressure is always maintained at atmospheric pressure, 100 kPa (14.5 psia).

As shown in Fig 2.1, the system is a loop with no bypass flow. The heat is input by a radiant furnace and measured indirectly by measuring the furnace coolant temperature rise, furnace coolant mass flow rate and the electric power input to the furnace. Since the heat input is the only controlled variable, its accurate determination is important in analyzing

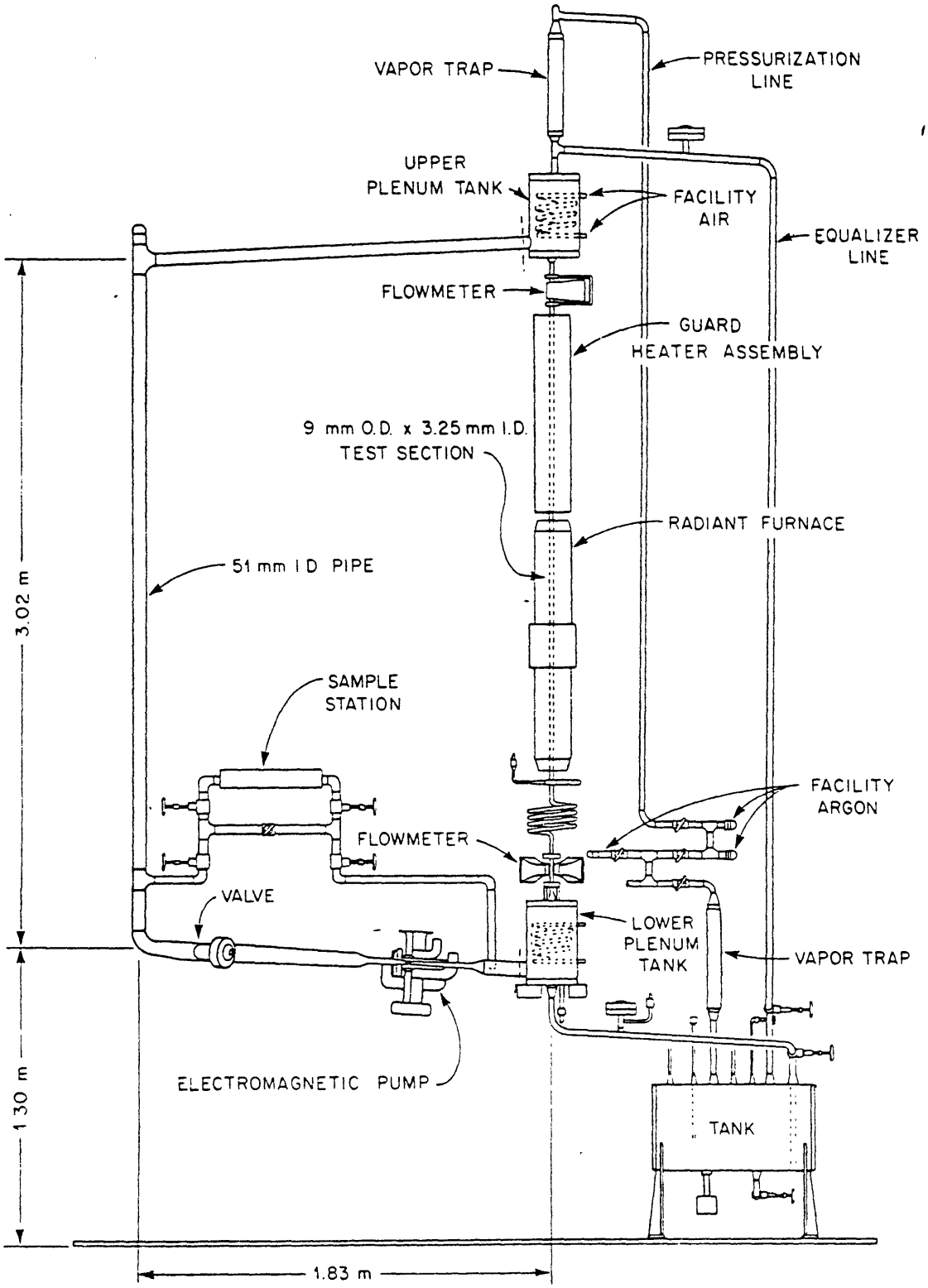

Fig 2.1 Sodium Boiling Test Facility - loop (taken from ORNL/TM-7018)

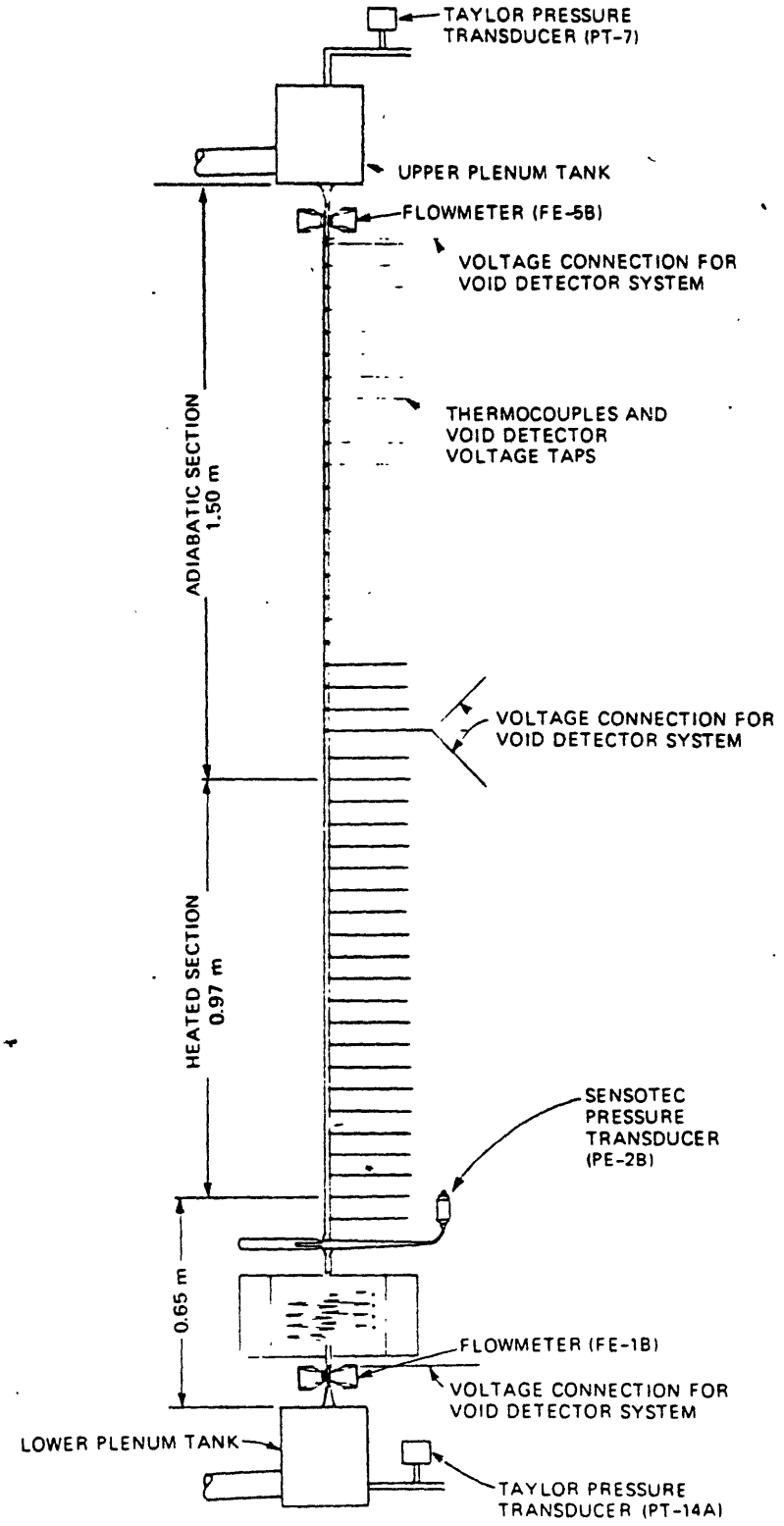

Fig 2.2 Sodium Boiling Test Facility - test section

(taken from ORNL/TM-7018)

the experiment. It was found in the process of simulation that there was a systematic error in measuring the heat input to the test section.

2.1.2 Calibration of heat input

Table 2.1 shows the summary of the data given in the report ORNL/TM-7018 for all the test runs performed in the SBTF. From Table 2.1 it can be observed that boiling began when the test section power was about 900 W. In simulation, however, boiling began at a lower power. Therefore the inlet flow rate and heat input data in Table 2.1 are not consistent because the energy convected out by sodium is not equal to the heat input under steady-state condition.

There are two sources of error which may be responsible for the deviation. One is the error in the inlet flow deter--mination which might have underestimated the inlet flow rate. The other is the error in the test section heat input which might be lower than the values given in Table 2.1.

Permanent magnet flow meters are used to determine the inlet flow rate. The report ORNL/TM-7018 states that the flow meters were calibrated after installation and the calcu--lated flow as determined by heat balance was within 15% of the measured values in the forced flow tests.

Regarding the test section heat input, there is a high

Table 2.1 SBTF natural convection results

(taken from ORNL/TM-7018)

Test No.	Test section power[a] (W)	Heat flux[b] (W/cm^2)	Power density[c] (W/cm^3)	Inlet flow, mean (mℓ/s)	Outlet flow, mean[d] (mℓ/s)	Frequency[e] (Hz)	Phase angle[e,f] (deg)
			Single phase				
107R2	300	3	40	0.7	0.4	N/A	N/A
109R1[g]	340	3	42	2.0	1.9	N/A	N/A
108R2	500	5	60	0.9	0.6	N/A	N/A
100R3	700	7	90	1.0	0.6	N/A	N/A
100R2	700	7	90	0.9	0.7	N/A	N/A
100R4	800	8	100	1.1	0.8	N/A	N/A
			Chugging				
131R1	1000	10	130				
132R1	1100	11	140				
130R1	1300	13	160	2.4	2.2	0.9[h]	130
			Steady boiling				
129R1	1300	13	160	1.0	0.7	0.7	130
121R1	1400	14	180	0.8	0.5	0.8	120
125R1	1400	14	180	0.9	0.6	1.0	110
125R2	1400	14	180	0.7	0.4	1.0	110
127R1	1500	15	190	0.8	0.6	1.0	110
120R1	1500	15	190	2.4	2.1	0.8	130
119R1	1600	16	200	1.1	0.9	0.5	140
126R2	1600	16	200	0.9	0.7	1.2	100
			Dryout				
122R1	1600	16	200				
128R1[i,j]	1700	17	210	0.9	0.7	1.3	100
				0.3	0.0	1.0	110
123R1[i,j]	1700	17	210	1.0	0.7	1.1	100
				0.4	0.1	0.9	110
124R1	1700	17	210				
126R1	1700	17	210				

[a] Furnace power + furnace clamshell power − furnace coolant enthalpy rise − furnace losses to ambient.

[b] Based on tube ID (98.6 cm^2).

[c] Based on heated coolant volume (8.0 cm^3).

[d] Outlet flowmeter was calibrated at inlet temperature (420°C) — not corrected for actual temperature.

[e] Corresponds to dominant frequency based on power spectral density analysis of the inlet flowmeter (FE-1B) signal.

[f] Angle by which inlet flow (FE-1B) leads pressure at inlet of heated section (PE-2B).

[g] Forced flow run used for flowmeter calibration check (see Appendix C).

[h] Unstable flow pattern; frequency is average of two distinct frequencies, 0.7 and 1.5 Hz.

[i] Conditions preceding dryout.

[j] Conditions during dryout.

probability of overestimation due to bending of the tube, which might move the test section out of the focal plane of the radiant heating source.

It is difficult to find out which error is responsible for the inconsistency, but in this thesis it is assumed that the heat input was overestimated. The heat input as determi--ned by heat balance with inlet flow data is about 30% less than the values listed in Table 2.1. For all the code inputs, 70% of the listed values is therefore used as the test section heat input. The detailed procedure of the test section heat input calibration is given in Appendix A.

2.1.3 Test section simulation

2.1.3.1 Steady-state

2.1.3.1.1 Boundary conditions

Initially only the test section is simulated with steady--state boundary conditions. At the outlet, the pressure boundary condition is applied because the pressure at the upper plenum is always kept at atmospheric pressure. At the inlet, either the pressure or velocity boundary condition may be applied using the values measured in the experiment. After the steady-state has been reached, there is no differ--ence in the computational procedure between the pressure and velocity boundary conditions at the inlet. However in

reaching the steady-state, the computation with the inlet pressure boundary condition undergoes more severe transients than that with the inlet velocity boundary condition.

For example a large reverse flow occurs at the inception of boiling with the inlet pressure boundary condition, whereas there is no reverse flow with the inlet velocity boundary condition.

It is usually tougher to do the calculation with the p-p boundary condition set than with the p-v boundary condition set. Thus the velocity boundary condition is chosen at the inlet in spite of the fact that the inlet flow rate is not well characterized.

As shown in the data of the experiment, every measured parameter shows a highly oscillatory behavior and there does not exist a steady-state in its strict sense. However if only a time averaged value is of concern, it is possible to assume a quasi-steady-state with an average value of the inlet velocity as the inlet boundary condition.

2.1.3.1.2 Geometry

The test section is composed of a heated zone and an adiabatic zone. Each zone is divided into five uniform meshes. A mesh in the heated zone is 0.194 m long and a mesh in the adiabatic zone is 0.3 m long.

Since the geometry in the code is a rod-bundle geometry which is quite different from the simple tube in the experi--ment, appropriate translation should be done between diffe--rent geometries.

In this thesis the constitutive relations for the rod--bundle geometry are used directly for the circular tube under the assumption that the tube represents one fuel rod and the coolant channel around the rod as in Fig 2.4. The dotted line in Fig 2.4 represents the symmetry line between the fuel rods, and it is assumed that there is no interaction with adjacent rods across the dotted line. This assumption is true if there is an infinite array of equally powered rods.

In the rod-bundle geometry, a pitch-to-diameter ratio and a wire-wrap-lead-to-diameter ratio are necessary to calculate the wall heat transfer and wall friction. An equivalent pitch--to-diameter ratio in the circular tube geometry is calculated in the following manner.

The coolant channel in Fig 2.5 can be made hydraulically identical to the circular channel in Fig 2.6 under the follow--ing conditions.

(1) The flow areas should be same.

(2) The equivalent hydraulic diameters should be same.

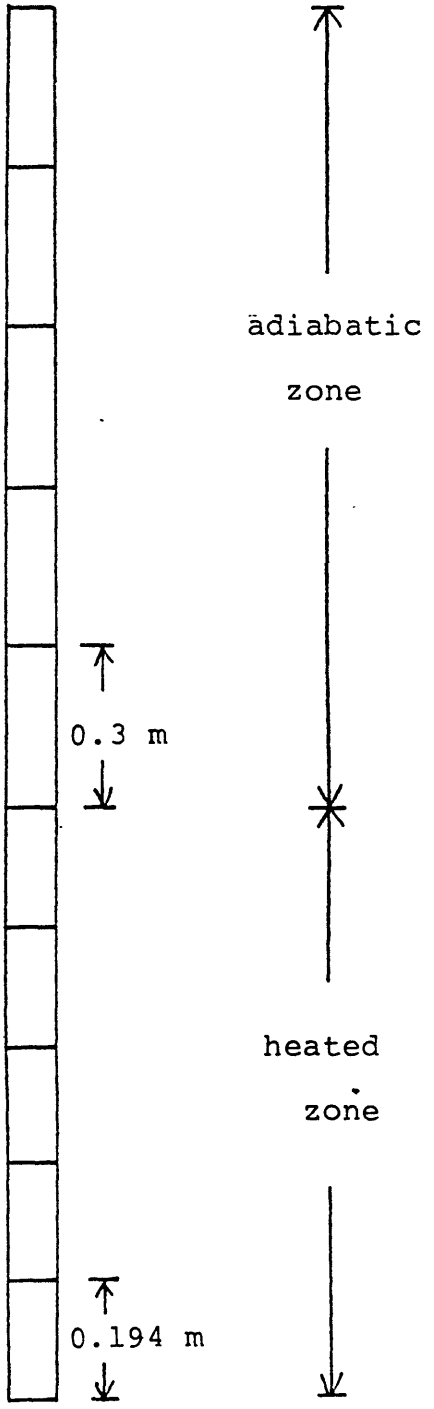

Fig 2.3 Geometry for the test section simulation

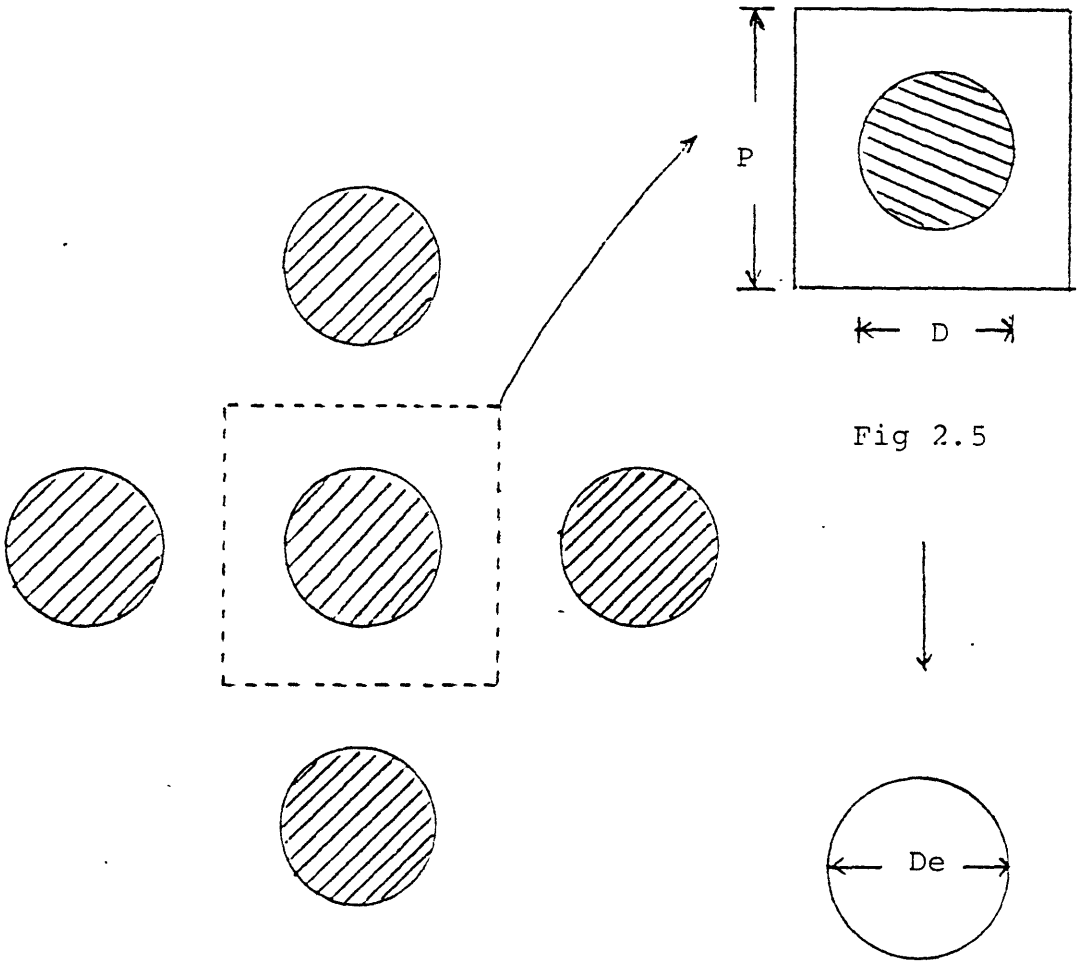

Fig 2.4

Fig 2.5

Fig 2.6

Schematic diagram for geometry transformation

$$p^2 - \frac{\pi D^2}{4} = \frac{\pi D_e^2}{4} \qquad (2.1)$$

$$\frac{4\ (p^2 - \frac{\pi D^2}{4})}{\pi D} = D_e \qquad (2.2)$$

Elimininating D_e from Eq 2.1 and Eq 2.2,

$$P/D = \sqrt{\pi/2} = 1.2533$$

Since there is no wire wrap, a very large value is input to the wire-wrap-lead-to-diameter ratio.

It may be better to use the correlations that are derived from the same geometry, i.e. a circular tube. However from the practical point of view there is no need to use correlations more directly applicable to circular tubes, because other uncertainties seem to be greater than the uncertainty arising from the difference in geometry.

2.1.3.2 Transient

The transient calculation in this section has the same geometry and type of boundary condition as the steady-state calculation in the previous section.

After the steady-state boiling has been reached, the inlet velocity is oscillated with the period of one second.

One second is the typical period of the experimental data.

Fig 2.7 shows the variation of the inlet velocity in the transient calculation and the experiment.

It should be mentioned that this is the transient for the steady-state boiling, and not the transient between the boiling inception and the steady-state boiling.

2.1.4 Whole loop simulation

The loop can generally be simulated in two ways, as a simulated 1-D loop and as an actual 1-D loop. The simulated 1-D loop is obtained by cutting some point of the loop and extending it into a straight line. The direction of gravity should be determined according to the position in the loop. The actual 1-D loop is obtained by putting a solid block in the center of a two-dimensional rectangular pool.

2.1.4.1 Geometry and boundary conditions of the simulated 1-D loop

Fig's 2.8 and 2.9 show the geometry of the simulated 1-D loop analysis. The upper face of the upper plenum in Fig 2.8 is cut and the loop is straightened into a one dimensional tube in Fig 2.9.

The boundary conditions at the top and bottom ends of Fig 2.9 should be identical because they are the same point

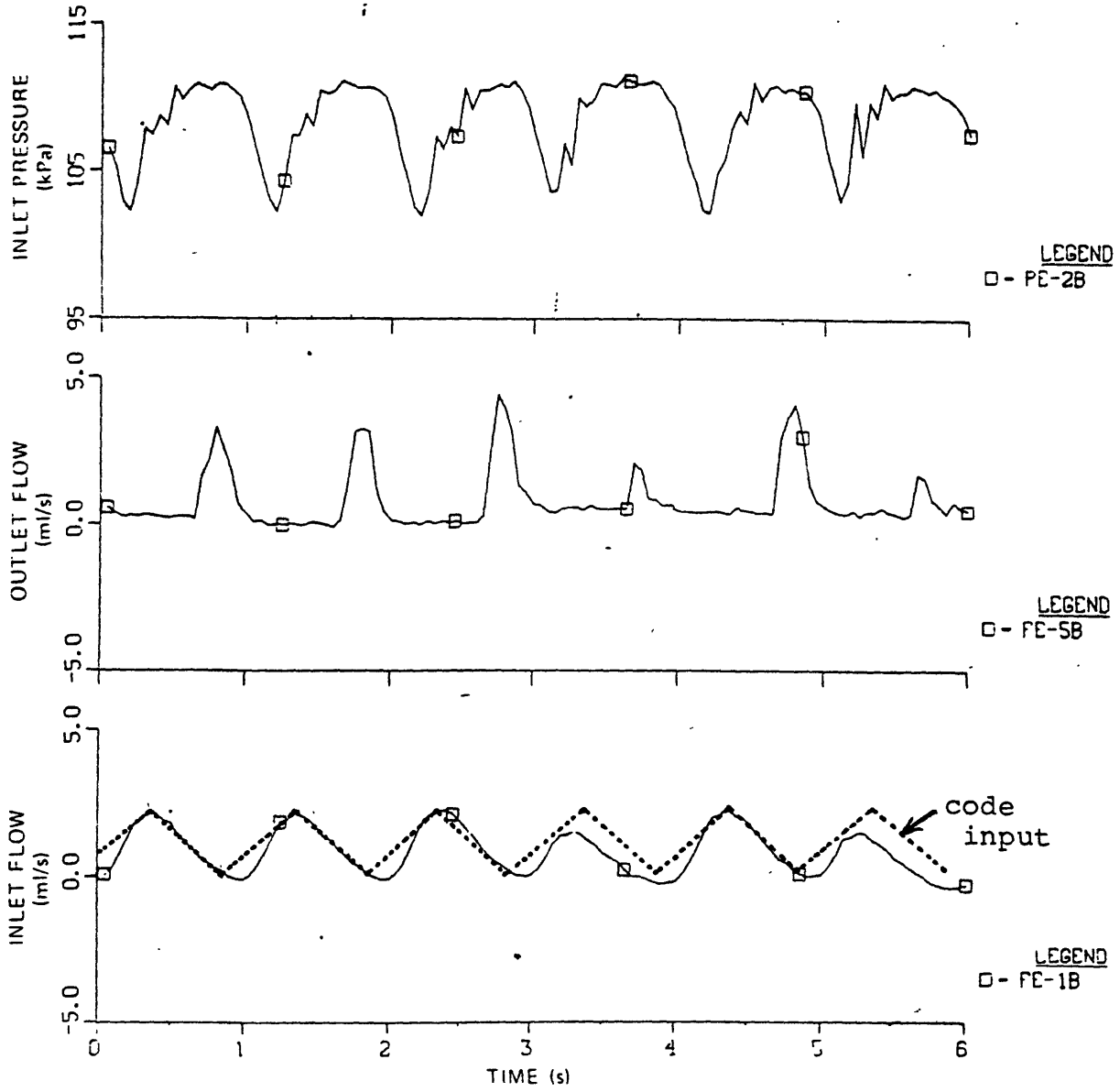

Fig 2.7 Typical experimental data for steady-state boiling experiment (taken from ORNL/TM-7018)

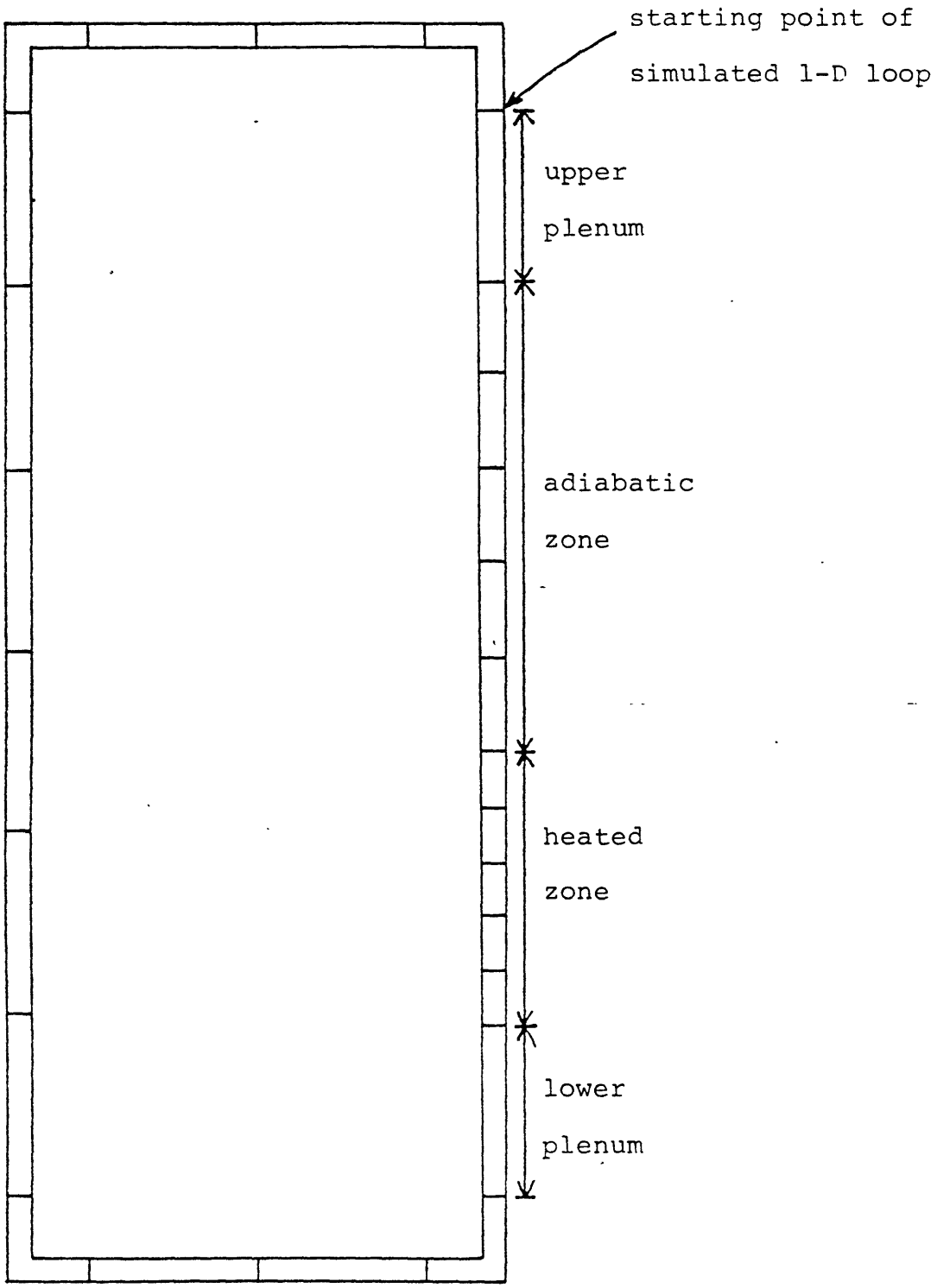

Fig 2.8 Geometry for the simulated 1-D loop

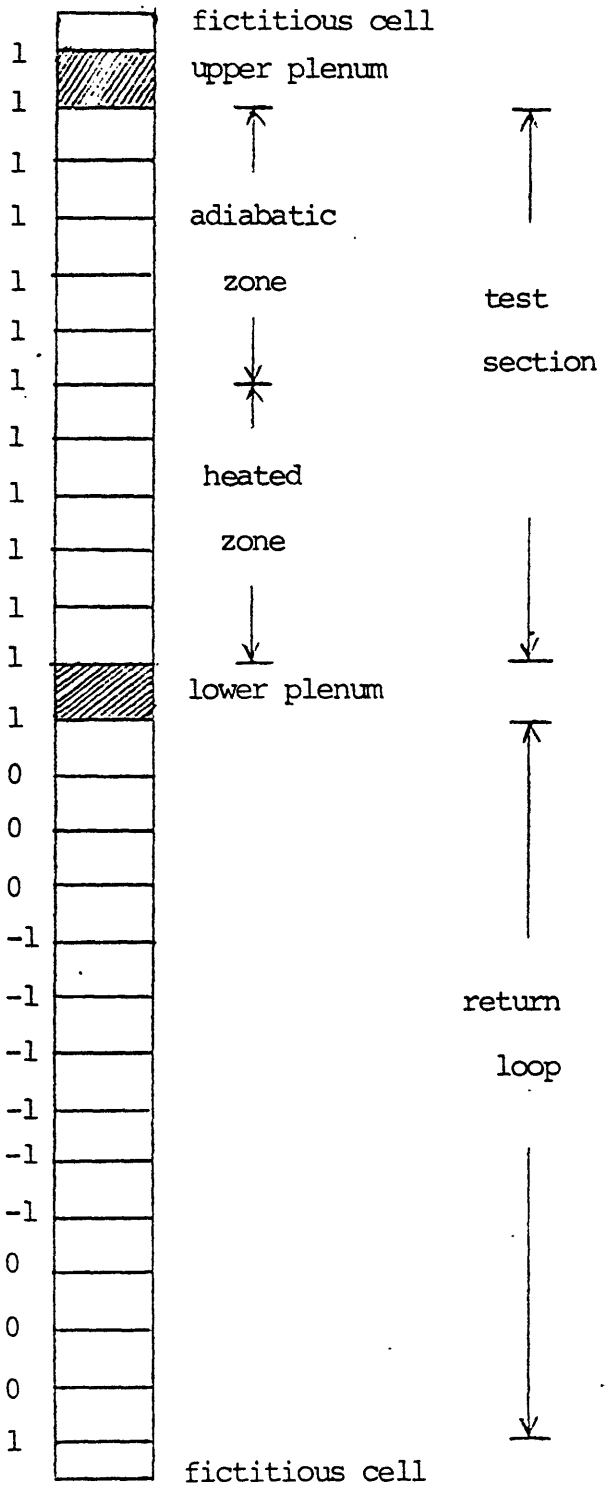

Fig 2.9 Geometry for the code inputs of the simulated 1-D loop

in the loop. Thus the pressure-pressure boundary condition is used for Fig 2.9 so that the pressures at the top and bottom boundaries are both atmospheric pressure.

Fig 2.9 shows that fictitious cells are defined at boun--daries according to the code format. Since the boundary pressures are defined at the center points of the fictitious cells, not at the interface of meshes, an error enters the calculation. In order to reduce the error, very thin ficti--tious cells are used. The length of the fictitious cells is 1.0×10^{-10} m, whereas the length of the upper and lower plena is 0.6175 m.

As can be seen in Fig 2.8, the direction of gravity is different for different parts of the loop. The direction of gravity is defined at the interface of mesh cells and denoted by the numbers ' 0, 1,-1' at each interface in Fig 2.9.

One of the major problems in simulating the loop experi--ment ORNL/TM-7018 was to keep the plenum temperatures cons--tant throughout each transient. In THERMIT calculations the plenum temperature cannot be determined a priori, but is determined from the heat input and boundary conditions.

Since the temperatures in the upper and lower plena are kept at 590°C and 420°C in the experiment, a new scheme was needed to keep plenum temperatures constant in the calculation.

There are two ways of keeping the plenum conditions constant. One is to use the implicit scheme which solves the conservation equations with the plenum temperatures at the next time step already determined. The heat extraction from the plenum is determined as a result of the calculation for each time step. There will be no error of the plenum temperature in this method, but a fundamental change of the numerical scheme is required. The other way is the trial and error method which varies the heat extraction until satisfac--tory plenum temperatures are obtained. Since the plenum temperature decreases as the heat extraction increases, the plenum temperature is a monotonously decreasing function with respect to the heat extraction. The unknown function between the plenum temperature and the heat extraction is fitted by a parabola and a new heat extraction is obtained from the parabolic function. The same procedure is repeated until the required plenum temperature is obtained. The details of the method are given in Appendix C.

2.1.4.2 Artificial vapor density in the simulated 1-D loop analysis

One of the major difficulties of the loop simulation is that the code fails at the inception of boiling and when the

vapor reaches the upper plenum and begins condensation. The failure is a numerical problem induced by the high density ratio, since the density ratio of the liquid and vapor phases of sodium is over 2000 at atmospheric pressure.

In order to avoid the code failure, the density ratio is reduced by one hundred and two hundred times with all the other properties intact. Then the density ratios are approximately 24 and 12 and these correspond to the actual pressures of 10.0 MPa (1470 psia) and 15.7 MPa (2300 psia). With the increased vapor densities the code did not have any numerical problem and the results still showed the important characteristics of the two-phase flow in a loop. Note that the artificial vapor density was used only for the loop simulations and not for the test section simulations.

2.1.4.3 Geometry and boundary conditions of the actual 1-D loop

The geometry of the actual 1-D loop analysis is shown in Fig 2.10 and Fig 2.11. It is a two-dimensional rectangu--lar array of cells with a coolant channel around an internal solid block. As Fig 2.8 and 2.10 show, the geometries of the simulated and actual 1-D loops are exactly the same.

The coolant volume in any mesh cell should not be zero due to the numerical scheme in the code, but the coolant

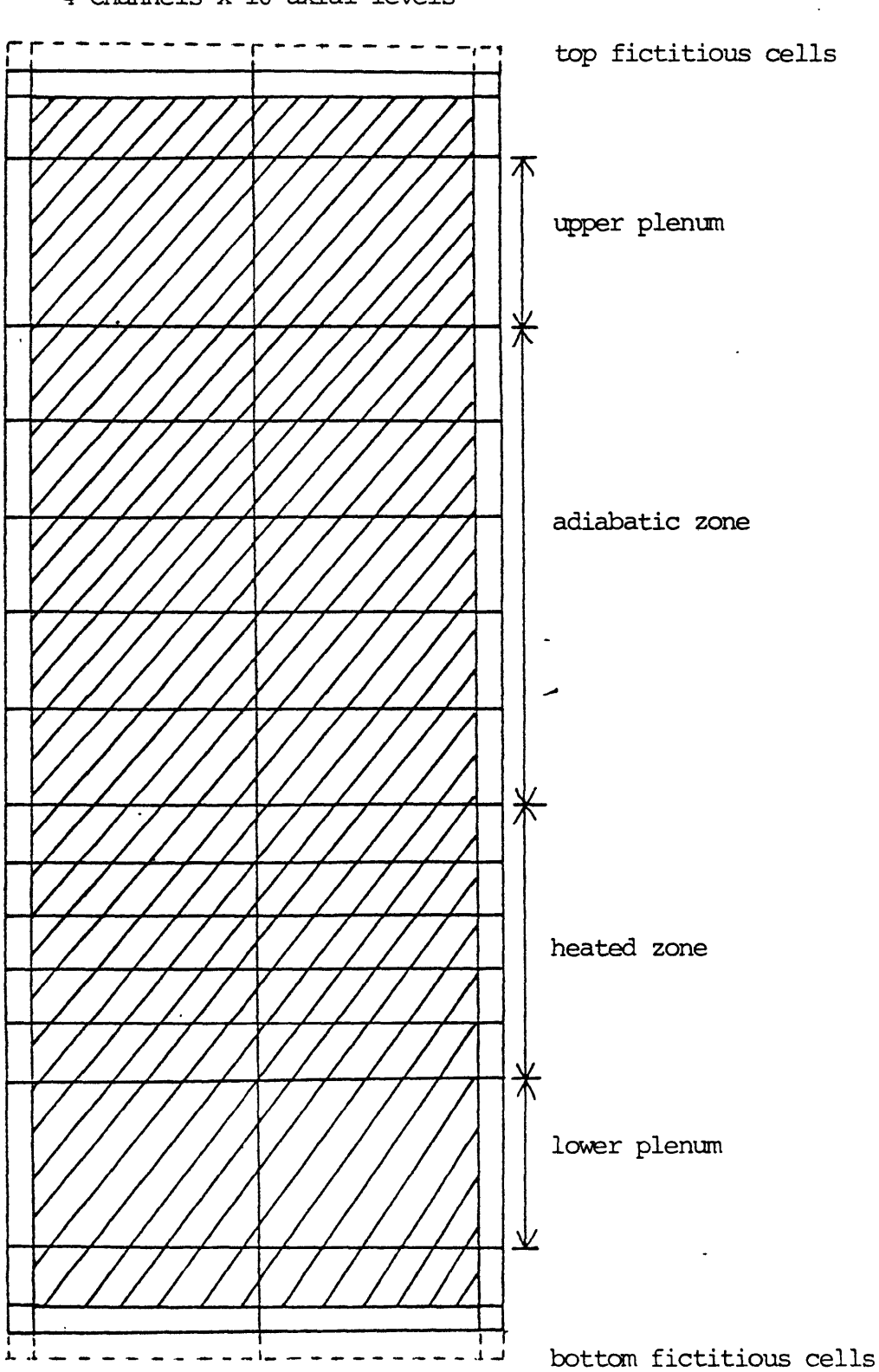

Fig 2.10 Geometry for actual 1-D loop

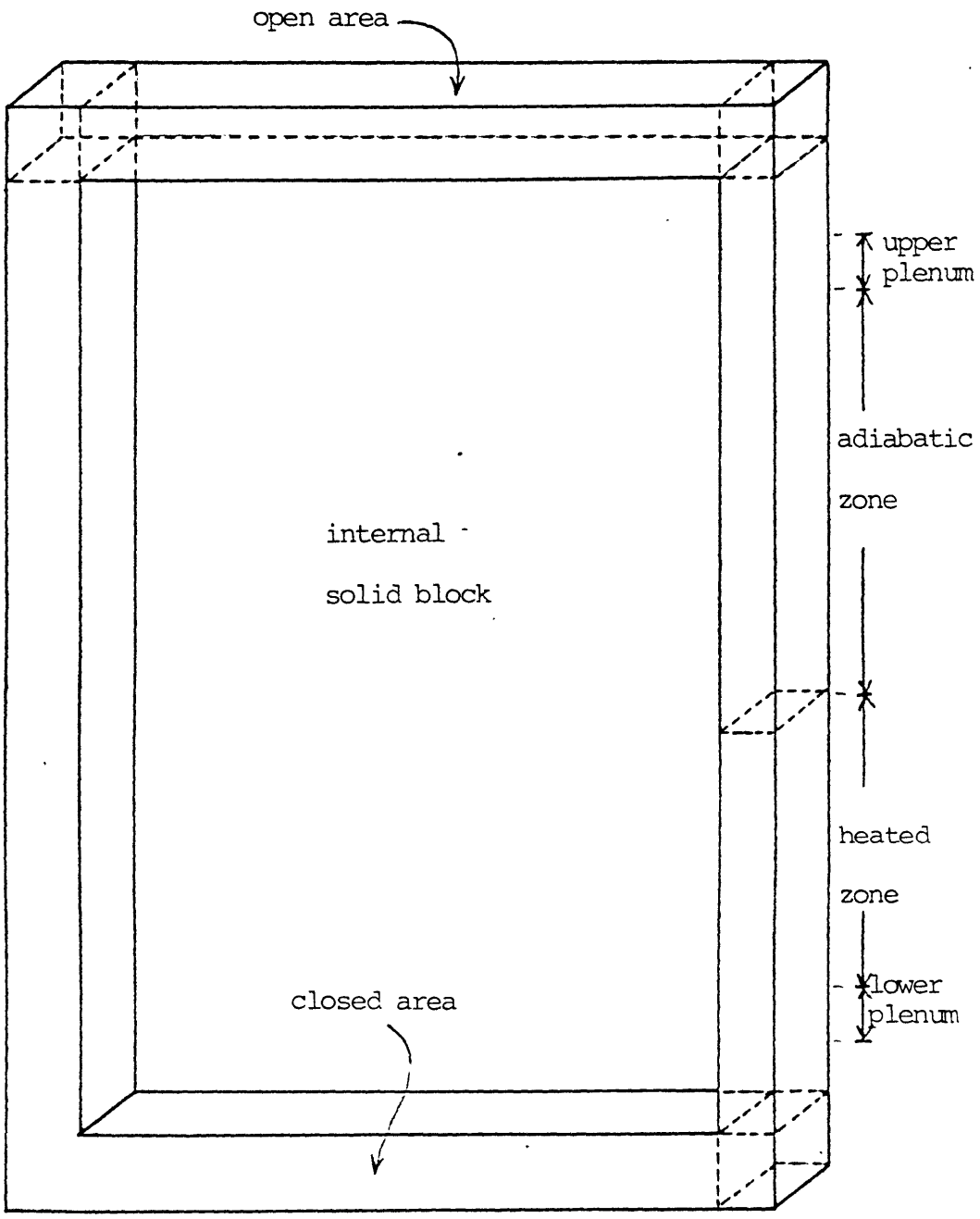

Fig 2.11 Geometry of actual 1-D loop analysis

volume inside the solid block is of no relevance to the results.

Since the interfacial area with the solid block is closed, there is no coolant flow across the solid interface. The inter--facial area with the bottom fictitious cells is also closed and the bottom boundary condition is the velocity boundary con--dition that the inlet velocity at the closed interface is zero. However it does not matter what bottom boundary condition is used, because there is no interaction between the bottom ficti--tious cells and the loop.

The interfacial area with the top fictitious cells is open so that there can be a little vertical velocity component due to thermal expansion of the sodium coolant. The pressure at the top fictitious cells is atmospheric pressure.

The upper and lower plenum temperatures are kept constant using the same scheme as used in the simulated 1-D loop analy--sis, which is given in Appendix C.

Only a single-phase case has been run because the two--dimensional geometry of the actual 1-D loop takes much longer computation time than the one-dimensional geometry of the simulated 1-D loop. However two-phase computations can be made without any modification to this approach.

2.2 Forced convection

2.2.1 Explanation of the experiment

This is a hypothetical experiment which is based on the data of a forced convection experiment performed in France. The French experiment could not be simulated with THERMIT because of its complicated geometry as shown in Fig 2.12. The momentum conservation equations in THERMIT assume that the flow area is uniform in axial direction. The variable flow area in axial direction cannot be taken into considera--tion, unless the differential and difference forms of the momentum conservation equations are altered.

Hence a hypothetical experiment with a uniform cross sectional area, but with the same input parameters as the French experiment was run with THERMIT to obtain calculational results. These calculational results cannot be checked with the experimental data.

From the computational point of view, there is no diff--erence between the natural and forced convections except that one has a low-speed and low-power and the other has a high--speed and high-power.

2.2.2 Geometry and boundary conditions

Fig 2.13 shows the geometry of the hypothetical forced convection experiment. The simulation is done for two

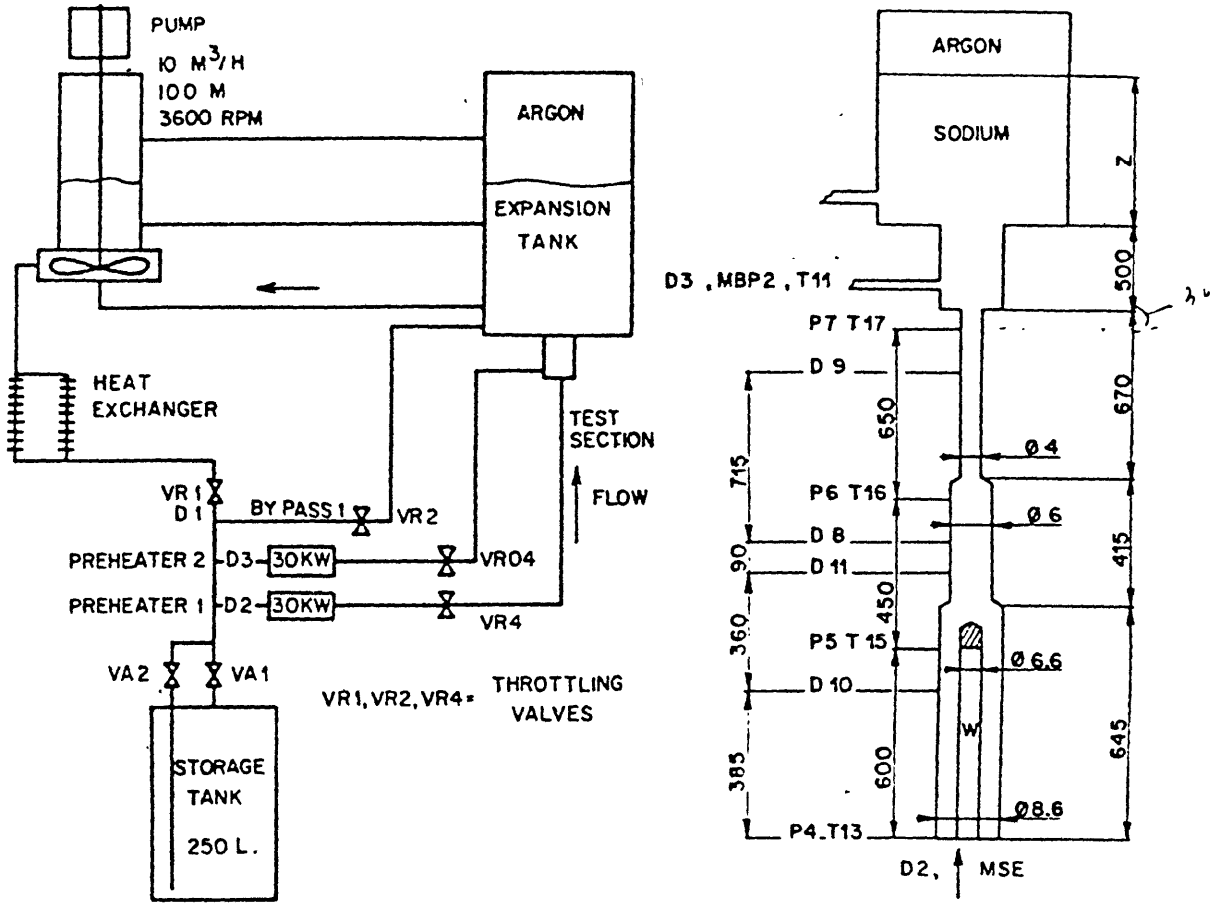

Fig 2.12 French experiment facility

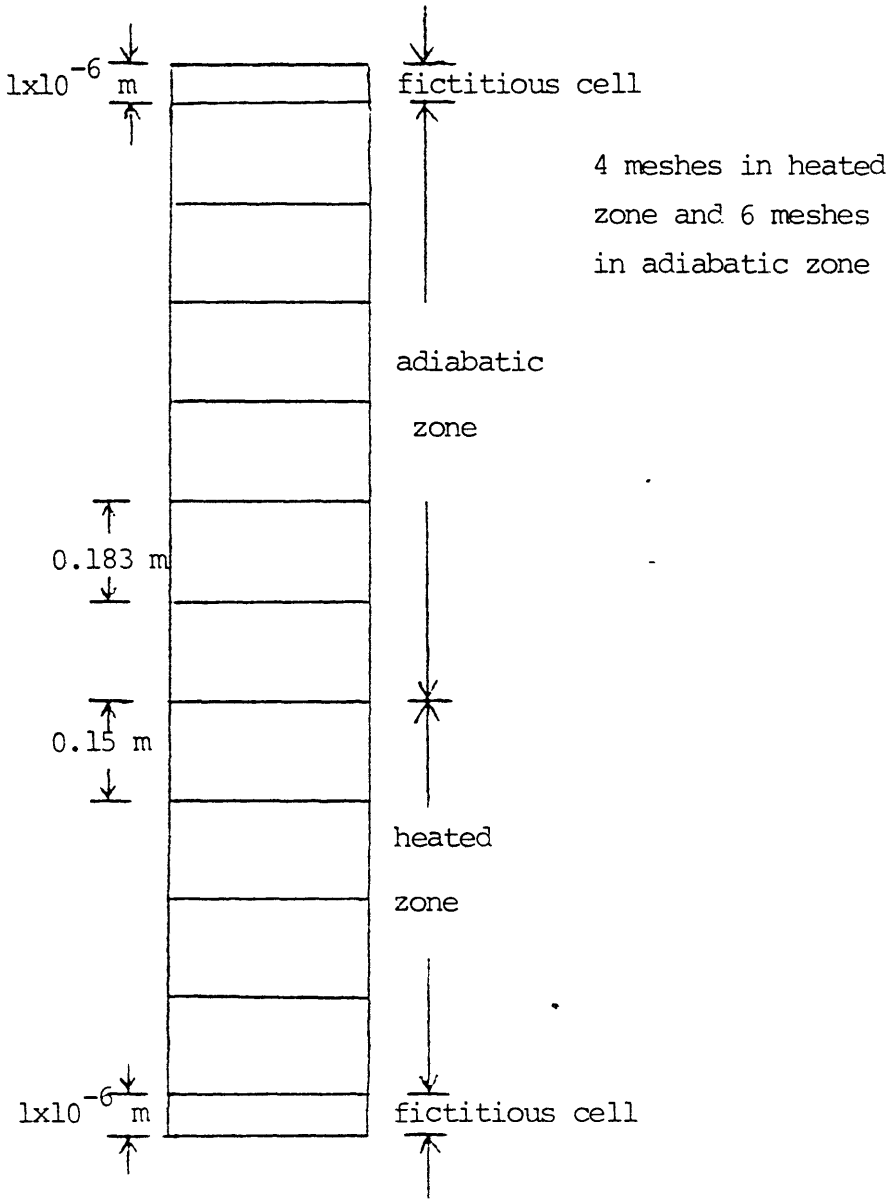

Fig 2.13 Geometry of the hypothetical forced-convection French experiment

different radii, r = 0.002 m and r = 0.003 m. These are the typical radii of the French experiment facility.

The test section is composed of two parts, a heated zone and an adiabatic zone, and the heat input to the test section is 10 kW.

The pressure-velocity boundary condition is used for the top and bottom ends of the test section.

Chapter 3. Numerical and physical models

3.1 Numerical models

3.1.1 THERMIT conservation equations

3.1.1.1 HEM, 4-Eq and 6-Eq models

THERMIT conservation equations for the two-fluid model are:

Mass

$$\frac{\partial}{\partial t}(\alpha\rho_v) + \nabla\cdot(\alpha\rho_v\vec{v}_v) = \Gamma \tag{3.1}$$

$$\frac{\partial}{\partial t}[(1-\alpha)\rho_\ell] + \nabla\cdot[(1-\alpha)\rho_\ell\vec{v}_\ell] = -\Gamma \tag{3.2}$$

Momentum

$$\frac{\partial}{\partial t}(\alpha\rho_v\vec{v}_v) + \nabla\cdot(\alpha\rho_v\vec{v}_v\vec{v}_v) + \alpha\nabla P = -\vec{F}_{wv} - \vec{F}_i - \alpha\rho_v\vec{g}_z \tag{3.3}$$

$$\frac{\partial}{\partial t}[(1-\alpha)\rho_\ell\vec{v}_\ell] + \nabla\cdot[(1-\alpha)\rho_\ell\vec{v}_\ell\vec{v}_\ell] + (1-\alpha)\nabla P =$$

$$-\vec{F}_{w\ell} + \vec{F}_i - (1-\alpha)\rho_\ell\vec{g}_z \tag{3.4}$$

Energy

$$\frac{\partial}{\partial t}(\alpha\rho_v e_v) + \nabla\cdot(\alpha\rho_v e_v\vec{v}_v) + P\nabla\cdot(\alpha\vec{v}_v) + P\frac{\partial\alpha}{\partial t} =$$

$$Q_{wv} + Q_i \tag{3.5}$$

$$\frac{\partial}{\partial t}[(1-\alpha)\rho_\ell e_\ell] + \nabla\cdot[(1-\alpha)\rho_\ell e_\ell\vec{v}_\ell] + P\nabla\cdot[(1-\alpha)\vec{v}_\ell]$$

$$-P\frac{\partial\alpha}{\partial t} = Q_{w\ell} - Q_i \tag{3.6}$$

The leftmost terms of the above equations represent the rate of change of mass, momentum and energy in the control volume when integrated over the control volume. The $P\frac{\partial \alpha}{\partial t}$ term in the energy conservation equation denotes the rate of work done between the liquid and vapor phases.

These time derivatives are omitted in the following analysis and only the steady-state with one spatial variable z is considered. However the analysis can be easily extended to the transient three-dimensional case.

Following equations represent the steady-state, one-dimensional conservation equations for the 6-Eq model.

Mass

$$\frac{\partial}{\partial z}(\alpha \rho_v v_{vz}) = \Gamma \tag{3.7}$$

$$\frac{\partial}{\partial z}[(1-\alpha)\rho_\ell v_{\ell z}] = -\Gamma \tag{3.8}$$

Momentum

$$\frac{\partial}{\partial z}(\alpha \rho_v v_{vz}^2) + \alpha\frac{\partial P}{\partial z} = -F_{wv} - F_i - \alpha\rho_v g_z \tag{3.9}$$

$$\frac{\partial}{\partial z}[(1-\alpha)\rho_\ell v_{\ell z}^2] + (1-\alpha)\frac{\partial P}{\partial z} = -F_{w\ell} + F_i - (1-\alpha)\rho_\ell g_z \tag{3.10}$$

Energy

$$\frac{\partial}{\partial z}(\alpha \rho_v e_v v_{vz}) + P\frac{\partial}{\partial z}(\alpha v_{vz}) = Q_{wv} + Q_i \tag{3.11}$$

$$\frac{\partial}{\partial z}[(1-\alpha)\rho_\ell e_\ell v_{\ell z}] + P\frac{\partial}{\partial z}[(1-\alpha)v_{\ell z}] = Q_{w\ell} - Q_i \tag{3.12}$$

The previous set of conservation equations can be reduced to four conservation equations with the assumption that the liquid and vapor phases are always at a thermal equilibrium state.

The constitutive relations that are related with the liquid and vapor temperatures are:

$$\Gamma_e = C_1(T_\ell - T_s) \tag{3.13}$$

$$\Gamma_c = C_2(T_v - T_s) \tag{3.14}$$

$$\Gamma = \Gamma_e - \Gamma_c \tag{3.15}$$

$$Q_i = C_3(T_\ell - T_v) \tag{3.16}$$

where

Γ_e : interfacial mass transfer due to evaporation

Γ_c : interfacial mass transfer due to condensation

Q_i : interfacial heat transfer

If it is assumed that the constants C_1, C_2 and C_3 are very large, the liquid and vapor temperatures are driven to the saturation temperature, i.e. $T_\ell = T_v = T_s$, because Γ and Q_i cannot get infinite physically. With the relation $T_\ell = T_v = T_s$, determination of the interfacial mass and heat transfer is not of interest, so that the phasic mass and energy

equations can each be added to yield mixture mass and energy conservation equations. This reduces to the set of conserva--tion equations to 4 from 6.

In the 6-Eq model, the parameters ρ_v, ρ_ℓ, e_v and e_ℓ are functions of T_v or T_ℓ and P, but with the assumption that $T_\ell = T_v = T_s$, they all become functions of the saturation temperature T_s only. This is shown in the following relations.

$$
\begin{aligned}
&\rho_v = f(T_v, P) \\
&\rho_\ell = f(T_\ell, P) \\
&e_v = f(T_v, P) \\
&e_\ell = f(T_\ell, P)
\end{aligned}
\qquad \rightarrow \qquad
\begin{aligned}
&\rho_v = f(T_s) \\
&\rho_\ell = f(T_s) \\
&e_v = f(T_s) \\
&e_v = f(T_s) \\
&e_\ell = f(T_s) \\
&T_v = T_\ell = T_s \\
&P = f(T_s)
\end{aligned}
\qquad (3.17)
$$

Hence three unknowns T_v, T_ℓ and P are reduced to only one unknown T_s and the number of conservation equations is also reduced by two, from six to four yielding,

4-Eq model

Mass
$$\frac{\partial}{\partial z}[\alpha\rho_v v_{vz} + (1-\alpha)\rho_\ell v_{\ell z}] = 0 \qquad (3.18)$$

Momentum
$$\frac{\partial}{\partial z}(\alpha\rho_v v_{vz}^2) + \frac{\partial P}{\partial z} = -F_{wv} - F_i - \alpha\rho_v g_z \qquad (3.19)$$

$$\frac{\partial}{\partial z}[(1-\alpha)\rho_\ell v_{\ell z}^2] + (1-\alpha)\frac{\partial P}{\partial z} = -F_{w\ell} + F_i$$

$$-(1-\alpha)\rho_\ell g_z \qquad (3.20)$$

Energy
$$\frac{\partial}{\partial z}[\alpha\rho_v e_v v_{vz} + (1-\alpha)\rho_\ell e_\ell v_{\ell z}]$$

$$+P\frac{\partial}{\partial z}[\alpha v_{vz} + (1-\alpha)v_{\ell z}] = Q_{wv} + Q_{w\ell} \qquad (3.21)$$

If the same procedure is repeated for the phasic momentum equations, the HEM conservation equations result. Here we deal with the issue of mechanical equilibrium embodied in the constitutive relation linking the phasic velocities.

$$F_i = C_4(v_{vz} - v_{\ell z}) \qquad (3.22)$$

where F_i: interfacial momentum transfer

Assuming C_4 goes to infinity, the velocities v_{vz} and $v_{\ell z}$ should have the same value to keep F_i bounded. This reduces

the unknown velocities to a single homogeneous parameter and suggests the combination of the phasic momentum equations. Consequently the following set of HEM conservation equations is obtained.

Mass $$\frac{\partial}{\partial z}[\alpha\rho_v + (1-\alpha)\rho_\ell]v_z = 0 \qquad (3.23)$$

Momentum $$\frac{\partial}{\partial z}[\alpha\rho_v + (1-\alpha)\rho_\ell]v_z^2 + \frac{\partial P}{\partial z} = -(F_{wv} + F_{w\ell}) - [\alpha\rho_v + (1-\alpha)\rho_\ell]g_z \qquad (3.24)$$

Energy $$\frac{\partial}{\partial z}[\alpha\rho_v e_v + (1-\alpha)\rho_\ell e_\ell]v_z + P\frac{\partial v_z}{\partial z} = Q_{wv} + Q_{w\ell} \qquad (3.25)$$

where $\alpha\rho_v + (1-\alpha)\rho_\ell = \rho_m$: mixture density

$\alpha\rho_v e_v + (1-\alpha)\rho_\ell e_\ell = e_m\rho_m$: mixture internal energy

3.1.1.2 Energy loss due to dissipation and interfacial mass transfer

The suggested form of energy conservation equations for THERMIT is:

$$\frac{\partial}{\partial z}(\alpha\rho_v e_v v_{vz}) + P\frac{\partial}{\partial z}(\alpha v_{vz}) = Q_{wv} + Q_i + \frac{\Gamma}{2} v_{vz}^2 - zg_z\Gamma$$

$$+(F_{wv} + F_i)v_{vz} \qquad (3.26)$$

$$\frac{\partial}{\partial z}[(1-\alpha)\rho_\ell e_\ell v_{\ell z}] + P\frac{\partial}{\partial z}[(1-\alpha)v_{\ell z}] = Q_{w\ell} - Q_i - \frac{\Gamma}{2} v_{\ell z}^2$$

$$+zg_z\Gamma + (F_{w\ell} - F_i)v_{\ell z} \qquad (3.27)$$

In order to satisfy the first law of thermodynamics, the above form of energy conservation equations should be used. The terms that contain Γ are produced by the transformation of pressure drop into kinetic and potential energy increase. If Γ were zero, Bernoulli's theorem would have resulted, but with Γ not equal to zero, the additional terms with Γ should appear.

The terms $\frac{\Gamma}{2} v_{vz}^2$ and $\frac{\Gamma}{2} v_{\ell z}^2$ may be interpreted as kinetic energy that mass should carry at the time of evaporation or condensation. However this is not the energy that is interchanged between phases, because the sum of the terms $\frac{\Gamma}{2}(v_{vz}^2 - v_{\ell z}^2)$ is not equal to zero. Rather it is the energy produced by the transformation of momentum flux into kinetic energy flux, due to the fact that there is a source term Γ in the mass conservation equations.

The potential energy terms with Γ are produced by the transformation of gravitational force into potential energy

flux.

In the THERMIT energy conservation equations, frictional dissipation terms were neglected because they were quantita--tively negligible. However in sodium two-phase flow at atmospheric pressure, they cannot be neglected safely as shown in the results of Chapter 4. Pressure drop occurs due to friction and that pressure drop is used in the energy conservation equations of THERMIT. Physically it means that the thermal energy that is transformed from mechanical energy due to frictional dissipation is lost to the environment. Actually that portion of thermal energy is not lost, but contributes to the increase of internal energy of the coolant. These contributions are neglected in the THERMIT energy equations. Detailed derivation of the suggested form of energy conservation equations is given in Appendix B. Note that the old form of the energy conservation equations has been used throughout this thesis.

3.1.2 Explanation of the code from the numerical point of view

Overall solution scheme of THERMIT

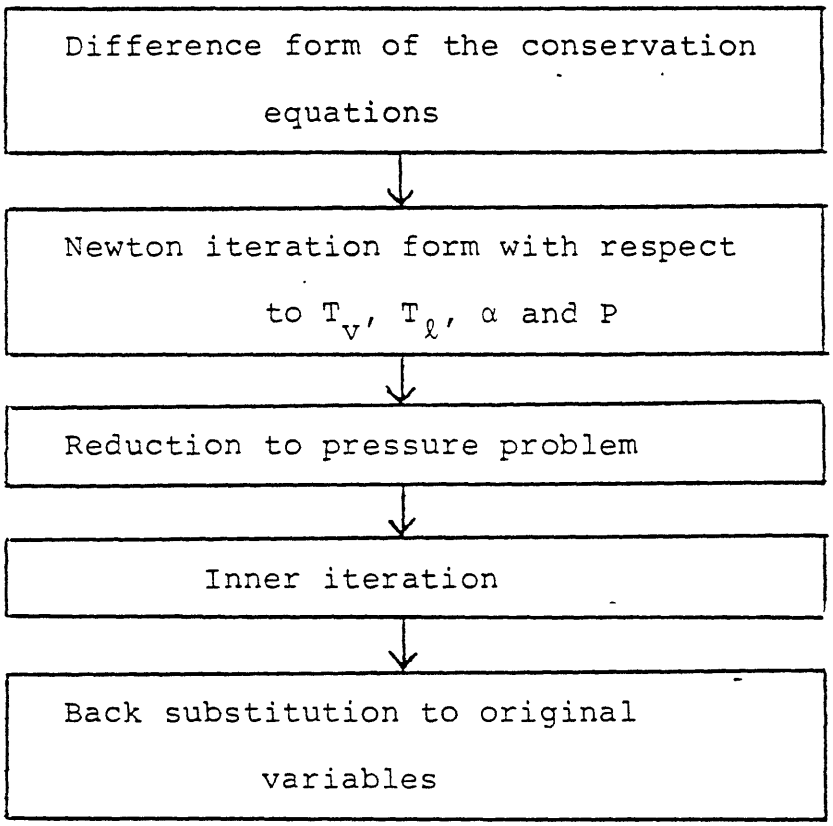

6-Eq model for 1-D transient

Mass
$$\frac{\partial}{\partial t}(\alpha\rho_v) + \frac{\partial}{\partial z}(\alpha\rho_v v_{vz}) = \Gamma \tag{3.28}$$

$$\frac{\partial}{\partial t}[(1-\alpha)\rho_\ell] + \frac{\partial}{\partial z}[(1-\alpha)\rho_\ell v_{\ell z}] = -\Gamma \tag{3.29}$$

Momentum
$$\frac{\partial}{\partial t}(\alpha\rho_v v_{vz}) + \frac{\partial}{\partial z}(\alpha\rho_v v_{vz}^2) + \frac{\partial P}{\partial z} = -F_{wv}$$

$$-F_i - \alpha\rho_v g_z \tag{3.30}$$

$$\frac{\partial}{\partial t}[(1-\alpha)\rho_\ell v_{\ell z}] + \frac{\partial}{\partial z}[(1-\alpha)\rho_\ell v_{\ell z}^2] + (1-\alpha)\frac{\partial P}{\partial z}$$

$$= -F_{w\ell} + F_i - (1-\alpha)\rho_\ell g_z \qquad (3.31)$$

Energy $$\frac{\partial}{\partial t}(\alpha\rho_v e_v) + \frac{\partial}{\partial z}(\alpha\rho_v e_v v_{vz}) + P\frac{\partial}{\partial z}(\alpha v_{vz}) + P\frac{\partial \alpha}{\partial t}$$

$$= Q_{wv} + Q_i \qquad (3.32)$$

$$\frac{\partial}{\partial t}[(1-\alpha)\rho_\ell e_\ell] + \frac{\partial}{\partial z}[(1-\alpha)\rho_\ell e_\ell v_{\ell z}] + P\frac{\partial}{\partial z}[(1-\alpha)v_{\ell z}]$$

$$- P\frac{\partial \alpha}{\partial t} = Q_{w\ell} - Q_i \qquad (3.33)$$

The above momentum conservation equations have a conservative form, whereas a nonconservative form is used in the code. In the nonconservative form, the α, ρ_v and ρ_ℓ are outside the time derivatives and can be treated explicitly utilizing the quantities at time step n, as shown in Eq 3.38. The momentum is not strictly conserved according to the difference form of Eq 3.38, but the degree of nonconservation must be tolerable in all the practical calculations. The nonconservative form of the momentum conservation equations are,

$$\alpha\rho_v\frac{\partial v_{vz}}{\partial t} + \alpha\rho_v v_{vz}\frac{\partial v_{vz}}{\partial z} + \frac{\partial P}{\partial z} = -F_{wv} - F_{iv} - \alpha\rho_v g_z \qquad (3.34)$$

$$(1-\alpha)\rho_\ell \frac{\partial v_{\ell z}}{\partial t} + (1-\alpha)\rho_\ell v_{\ell z}\frac{\partial v_{\ell z}}{\partial z} + (1-\alpha)\frac{\partial P}{\partial z} = -F_{w\ell} - F_i$$

$$-(1-\alpha)\rho_\ell g_z \qquad (3.35)$$

where $F_{iv} = F_i + \Gamma v_{vz}$

$$F_{i\ell} = -F_i - \Gamma v_{\ell z}$$

The difference forms of the one dimensional, six conservation equations are set up as follows.

Mass

vapor $$\frac{(\alpha\rho_v)^{n+1} - (\alpha\rho_v)^n}{\Delta t} + \frac{1}{V}\{[A(\alpha\rho_v)^n v_{vz}^{n+1}]_{k+1/2}$$

$$-[A(\alpha\rho_v)^n v_{vz}^{n+1}]_{k-1/2}\} = \Gamma^{n+1/2} \qquad (3.36)$$

liquid: α replaced by $(1-\alpha)$, subscript v by ℓ and Γ by $-\Gamma$

Energy

vapor $$\frac{(\alpha\rho_v e_v)^{n+1} - (\alpha\rho_v e_v)^n}{\Delta t} + \frac{1}{V}\{[P^n + (\rho_v e_v)^n_{k+1/2}][A\alpha^n$$

$$(v_{vz})^{n+1}]_{k+1/2} - [P^n + (\rho_v e_v)^n_{k-1/2}][A\alpha^n$$

$$(v_{vz})^{n+1}]_{k-1/2}\} + P^n\frac{\alpha^{n+1}-\alpha^n}{\Delta t} = Q_{wv}^{n+1/2} + Q_i^{n+1/2}$$

(3.37)

liquid: α replaced by $(1-\alpha)$, subscript v by ℓ and

Q_i by $-Q_i$

Note that the quantities without subscripts are at point k.

Momentum

vapor

$$(\alpha\rho_v)^n_{k+1/2}\frac{[v^{n+1}_{vz}-v^n_{vz}]_{k+1/2}}{\Delta t} + (\alpha\rho_v)^n_{k+1/2}\{(v_{vz})^n_{k+1/2}$$

$$[\frac{\Delta_z v_{vz}}{\Delta z}]^n_{k+1/2}\} + \alpha^n_{k+1/2}\frac{(P_{k+1}-P_k)^{n+1}}{\Delta z_{k+1/2}} = -(F_{wv})^{n+1/2}_{k+1/2}$$

$$-(F_{iv})^{n+1/2}_{k+1/2} - (\alpha\rho_v)^n_{k+1/2}g_z \qquad (3.38)$$

liquid: α replaced by $(1-\alpha)$ and subscript v by ℓ

The momentum conservation equations are differenced about the center of a face of a mesh cell whereas the mass and energy conservation equations are differenced about the center of a mesh cell volume.

In the above difference equations, some quantities are required at positions where they are not defined. These quantities are calculated using the concept of donor-cell differencing and spatial averages. The specific approach used is well explained in Ref.[1] section 2.2.2.

Now the difference equation forms are completely set up and they should be solved numerically.

First the momentum equations are transformed to reduce the velocities to spatial pressure differences. In the process the frictional terms $(F_{iv})^{n+1/2}_{k+1/2}$ and $(F_{wv})^{n+1/2}_{k+1/2}$ are treated semi-implicitly in the following way.

$$(F_{iv})^{n+1/2}_{k+1/2} = [(v_{vz})^{n+1}_{k+1/2} - (v_{\ell z})^{n+1}_{k+1/2}]\ \hat{F}_{iv} \tag{3.39}$$

$$(F_{wv})^{n+1/2}_{k+1/2} = [(v_{vz})^{n+1}_{k+1/2}]\ \hat{F}_{wv} \tag{3.40}$$

where $\hat{F}_{iv}$ and $\hat{F}_{wv}$ are explicit quantities at time step n that should be given from constitutive relations.

The momentum conservation equations may be written as follows.

$$\begin{aligned}&(v_{vz})^{n+1}_{k+1/2}\cdot arv + arv\cdot tcv\cdot delt + alpva\cdot rdsdt\cdot(P^{n+1}_{k+1}-P^{n+1}_{k})\\ &\quad -arv\cdot vv = -(v_{vz})^{n+1}_{k+1/2}\cdot delt\cdot fwv - [(v_{vz})^{n+1}_{k+1/2}\\ &\quad -(v_{\ell z})^{n+1}_{k+1/2}]\cdot delt\cdot fiv\ \cdot\end{aligned} \tag{3.41}$$

$$\begin{aligned}&(v_{\ell z})^{n+1}_{k+1/2}\cdot arl + arl\cdot tcl\cdot delt + alpla\cdot rdsdt\cdot(P^{n+1}_{k+1}-P^{n+1}_{k})\\ &\quad -arl\cdot vl = -(v_{\ell z})^{n+1}_{k+1/2}\cdot delt\cdot fwl - [(v_{\ell z})^{n+1}_{k+1/2}\\ &\quad -(v_{vz})^{n+1}_{k+1/2}]\cdot delt\cdot fil\end{aligned} \tag{3.42}$$

where the following notations have been used.

$$fiv = F_{iv} \qquad fwv = F_{wv}$$

$$arv = (\alpha\rho_v)^n_{k+1/2}$$

$$vv = (v_{vz})^n_{k+1/2}$$

$$tcv = [(v_{vz})^n_{k+1/2} [\frac{\Delta_z v_{vz}}{\Delta z}]^n_{k+1/2}]$$

$$alpva = \alpha^n_{k+1/2}$$

$$rdsdt = \frac{\Delta t}{\Delta z_{k+1/2}}$$

$$delt = \Delta t$$

The corresponding notations for liquid may be obtained by replacing the vapor notation v with the liquid notation ℓ and α with $(1-\alpha)$.

In the Eq's 3.41 and 3.42 there are two unknowns $(v_{vz})^{n+1}_{k+1/2}$ and $(v_{\ell z})^{n+1}_{k+1/2}$ that can be expressed in terms of the pressure difference $(P^{n+1}_{k+1} - P^{n+1}_k)$ at time step (n+1) and other explicit terms at time step n.

Therefore the momentum conservation equations can be linearized in the following form.

$$(v_{vz})^{n+1}_{k+1/2} = cpv\ (P^{n+1}_{k+1} - P^{n+1}_k) + fv \qquad (3.43)$$

$$(v_{\ell z})^{n+1}_{k+1/2} = cp\ell\ (P^{n+1}_{k+1} - P^{n+1}_k) + f\ell \qquad (3.44)$$

These velocities are substituted in the mass and energy

conservation equations to get a set of equations with P, α, ρ_v, ρ_ℓ, e_v, e_ℓ, Γ, Q_{wv}, $Q_{w\ell}$ and Q_i at time step (n+1). Using the equations of state and constitutive relations, the quantities ρ_v^{n+1}, ρ_ℓ^{n+1}, e_v^{n+1}, e_ℓ^{n+1}, Γ^{n+1}, Q_{wv}^{n+1}, $Q_{w\ell}^{n+1}$ and Q_i^{n+1} are approxi-mated in terms of those quantities at time step n and the first order derivatives with respect to the parameters α, T_v, T_ℓ and P. For example,

$$\rho_v = f(T_v, P) \tag{3.45}$$

$$\rho_v^{n+1} = \rho_v^n + \frac{\partial \rho_v}{\partial T_v}(T_v^{n+1} - T_v^n) + \frac{\partial \rho_v}{\partial P}(P^{n+1} - P^n) \tag{3.46}$$

Now for the mass and energy conservation equations for each phase, there are four unknowns α^{n+1}, T_v^{n+1}, T_ℓ^{n+1} and P^{n+1}. In matrix form, they may be written as follows.

$$\begin{bmatrix} C_{11} & C_{12} & C_{13} & C_{14} \\ C_{21} & C_{22} & C_{23} & C_{24} \\ C_{31} & C_{32} & C_{34} & C_{34} \\ C_{41} & C_{42} & C_{43} & C_{44} \end{bmatrix} \begin{bmatrix} \Delta P \\ \Delta\alpha \\ \Delta T_v \\ \Delta T_\ell \end{bmatrix} = \begin{bmatrix} f_1 \\ f_2 \\ f_3 \\ f_4 \end{bmatrix} \tag{3.47}$$

Eq 3.4 is a local matrix equation for one Newton iteration step. For each Newton iteration step, the coeffi-cient matrix on the lefthand side and the column vector on

the righthand side should be recalculated. The above local matrix is inverted to eliminate $\Delta\alpha$, ΔT_v and ΔT_ℓ in favor of ΔP. Then the global matrix equation over the entire spatial mesh is set up and solved by the inner iteration scheme.

The Newton and inner iteration convergence criteria are both such that ΔP between two successive iterates at any spatial mesh point should be less than some preset values.

In case of a one dimensional problem, the inner iteration is not necessary because the global matrix can be inverted directly with little computation time.

Now the spatial pressure distribution at time step (n+1) is completely calculated by the Newton and inner iterations. From the pressure distribution, the void fraction, vapor temperature and liquid temperature can also be calculated immediately and the calculation goes on to the next time step (n+2).

3.2 Physical models

3.2.1 Physical models in THERMIT*

3.2.1.1 Wall friction

For single phase, the THERMIT wall friction correlation is a mixture of Markley's laminar correlation[Ref. 4] with Novendstern's turbulent correlation[Ref. 4] with some

---

* sodium version THERMIT revised by Andrei L. Schor as of January, 1981.

appropriate transition formula. The single-phase correlation is extended to the two-phase case using the format of Autruffe's correlation. None of the Markley's, Novendstern's and Autruffe's correlations is satisfactory by itself due to their limited range of applicability. Therefore these three corre--lations are combined to produce a new wall friction correla--tion which has a proper applicable range. The present wall friction correlation in THERMIT is given in the following.

$$M = \left[\frac{1.034}{(P/D)^{0.124}} + \frac{29.7(P/D)^{6.94}Re^{0.086}}{(H/D)^{2.239}}\right]^{0.885} \qquad (3.48)$$

P/D : pitch-to-diameter ratio

H/D : wire-wrap-lead-to-diameter ratio

Re : Reynold's number

M is a geometry factor and appropriate Reynold's number should be used for the calculation of M for each phase. The Reynold's number for each phase is defined as follows.

$$Re_{\ell} = \frac{(1-\alpha)\rho_{\ell} v_{\ell} De}{\mu_{\ell}} \qquad (3.49)$$

$$Re_{v} = \frac{\alpha \rho_{v} v_{v} De}{\mu_{v}} \qquad (3.50)$$

Since the wall friction is composed of two parts, i.e. the liquid and vapor that contact the wall, the contact

fraction is defined for each phase. Before the dryout point, only the liquid contacts the wall and the contact fraction for vapor is zero.

$$cf\ell = \begin{cases} 1.0 & \alpha < \alpha_{dry} \\ \dfrac{1.0 - \alpha}{1.0-\alpha_{dry}} & \alpha_{dry} \leq \alpha \leq 1.0 \end{cases} \tag{3.51}$$

$$cfv = 1.0 - cf\ell \tag{3.52}$$

where $\alpha_{dry} = 0.957$

With the above definitions the wall friction factor is expressed in the following way.

For liquid

$$f_{turb,\ell} = \frac{0.316M}{Re^{0.25}} cf\ell \qquad 2600 \leq Re_\ell \leq 200,000 \tag{3.53}$$

$$f_{lam,\ell} = \frac{32}{\sqrt{H}}\left(\frac{P}{D}\right)^{1.5}\frac{cf\ell}{Re_\ell} \qquad Re_\ell \leq 400 \tag{3.54}$$

$$f_{trans,\ell} = f_{turb,\ell}^{\sqrt{\Psi}} + f_{lam,\ell}^{\sqrt{1-\Psi}} \qquad 400 < Re_\ell < 2600 \tag{3.55}$$

where $\Psi = \dfrac{Re_\ell - 400}{2200}$

For vapor

$$f_{turb,v} = \frac{0.316M}{Re^{0.25}} cfv \qquad 2600 \leq Re_v \leq 200,000 \tag{3.56}$$

$$f_{lam,v} = \frac{32}{\sqrt{H}}\left(\frac{P}{D}\right)^{1.5}\frac{cfv}{Re_v} \qquad Re_v \leq 400 \qquad (3.57)$$

$$f_{trans,v} = f_{turb,v}^{\sqrt{\Psi}} + f_{lam,v}^{\sqrt{1-\Psi}} \qquad 400 < Re_v < 2600 \qquad (3.58)$$

where $\Psi = \dfrac{Re_v - 400}{2200}$

Note that H is the wire-wrap-lead in [meter].

3.2.1.2 Interfacial mementum transfer

THERMIT has a Wallis-type correlation for the interfacial momentum transfer which is given in the following.

$$K = \frac{4.31}{2De}\rho_v|v_v - v_\ell|\{(1-\alpha)[1+75(1-\alpha)]\}^{0.95} \qquad (3.59)$$

$$F_i = K(v_v - v_\ell) \qquad (3.60)$$

where De is the equivalent hydraulic diameter.

3.2.1.3 Wall heat transfer

The wall heat transfer is assumed to be composed of three parts, i.e. liquid convection, nucleate boiling and vapor convection.

$$q = hvfc(twf-tv) + hlnb(twf-tsat) + hlfc(twf-t\ell) \qquad (3.61)$$

where tv, tℓ, tsat :vapor, liquid and saturation temperatures

hvfc :heat transfer coefficient through vapor convection

hlnb :heat transfer coefficient through nucleate boiling

hlfc :heat transfer coefficient through liquid convection

Three flow regimes are defined and the condition of existence for each flow regime is as follows.

a) single-phase liquid

$0.01 > \alpha$ or $twf \leq tsat$

b) two-phase annular flow

$0.01 \leq \alpha \leq 0.99$

c) single-phase vapor

$0.99 < \alpha$

The correlations used for each of these flow regimes are,

1) Schad's correlation for single-phase liquid

$$q = hlfc\ (twf - t\ell) \tag{3.62}$$

$$Pe_\ell > 150 \qquad hlfc = \frac{k_\ell}{De}\ rr\ (Pe_\ell)^{0.3} \tag{3.63}$$

$$Pe_\ell < 150 \qquad hlfc = \frac{k_\ell}{De}\ 4.5\ rr \tag{3.64}$$

where rr is defined in Eq 3.66.

2) Modified Chen's correlation for two-phase annular flow

$$q = hlnb\ (twf - tsat) + hlfc\ (twf - t\ell) \tag{3.65}$$

Define the following parameters.

$$rr = -16.15 + (P/D)[24.96 - (P/D)8.55] \tag{3.66}$$

$$xtti = \left(\frac{x}{1-x}\right)^{0.9}\left(\frac{\rho_\ell}{\rho_v}\right)^{0.5}\left(\frac{\mu_v}{\mu_\ell}\right)^{0.1} \tag{3.67}$$

$t\ell \geq tsat$

$$xtti > 0.1 \quad f = 2.35(xtti + 0.213)^{0.736} \tag{3.68}$$

$$xtti \leq 0.1 \quad f = 1.0 \tag{3.69}$$

$$gx = (1-\alpha)\rho_\ell |v_\ell| \tag{3.70}$$

$t\ell < tsat$

$$f = 1.0 \tag{3.71}$$

$$gx = \alpha\rho_v |v_v| + (1-\alpha)\rho_\ell |v_\ell| \tag{3.72}$$

Definitions for the parameters sig, relx and retp.

$$sig = 9.8066\ \sigma_\ell \tag{3.73}$$

$$relx = \frac{gx\ De}{\mu_\ell} \tag{3.74}$$

$$retp = 1.0x10^{-4}\ relx\ (f)^{1.25} \tag{3.75}$$

$$retp < 32.5 \qquad s = 1/(1+0.12\ retp^{1.14}) \tag{3.76}$$

$$32.5 \leq retp < 70.0 \qquad s = 1/(1+0.42\ retp^{0.78}) \tag{3.77}$$

$$retp \geq 70.0 \qquad s = 0.1 \tag{3.78}$$

$$h_s = 0.0012\ s\ \left(\frac{k_\ell c_{p\ell}}{sig}\right)^{0.5}(Pr_\ell)^{-0.29}(\rho_\ell)^{0.25}\left(\frac{c_{p\ell}\rho_\ell}{\rho_v h_{fg}}\right)^{0.24} \tag{3.79}$$

Now with these definitions the heat transfer coefficients are calculated in the following way.

$$hlfc = \frac{k_\ell}{De}\, rr\, (f)^{0.375} (Pe_\ell)^{0.3} \tag{3.80}$$

$$hlnb = h_s\, (twf - tsat)^{0.99} \left(\frac{h_{fg}}{tsat\ v_{fg}}\right)^{0.75} \tag{3.81}$$

3) Dittus-Boelter correlation for single-phase vapor

$$q = hvfc\ (twf - tv) \tag{3.82}$$

$$hvfc = \frac{k_v}{De}\, 0.023 (Pe_v)^{0.4} (Re_v)^{0.4} \tag{3.83}$$

3.2.1.4 Interfacial heat transfer

The interfacial heat transfer occurs by conduction and convection at the interface of the liquid and vapor phases. Presently a very large constant is input for the heat transfer coefficient 'hinter'.

$$q_i = hinter\ (tv - t\ell) \tag{3.84}$$

3.2.1.5 Interfacial mass transfer

The interfacial mass transfer model in THERMIT is a modified form of the Nigmatulin model.

True interfacial area;

$$\alpha < 0.6 \qquad A_t = \frac{4}{D}\sqrt{3\pi\alpha M} \tag{3.85}$$

$$0.6 \leq \alpha < 0.957 \qquad A_t = \frac{4\sqrt{\pi}}{D}[2\sqrt{3}(P/D\cdot M)^2 - \alpha M]^{0.5} \tag{3.86}$$

$$\alpha \geq 0.957 \qquad A_t = \frac{4\sqrt{\pi}}{D}[2\sqrt{3}(P/D\cdot M)^2 - \alpha M]^{0.5}\left(\frac{1-\alpha}{1-0.957}\right)^{0.5} \tag{3.87}$$

where $M = \dfrac{1}{2\sqrt{3}(P/D)^2 - \pi}$

D : rod diameter

Note that

$A = A_t/3$

$\lambda_e = 0.1$

$\lambda_c = 0.005$

$$\Gamma_e = \begin{cases} \dfrac{3}{\sqrt{2}} A\alpha(1-\alpha)\sqrt{R_g}\lambda_e \dfrac{\rho_v^2 h_{fg}}{P} \dfrac{T_\ell - T_s}{\sqrt{T_s}} & T_\ell > T_s \\ 0 & T_\ell \leq T_s \end{cases} \tag{3.88}$$

$$\Gamma_c = \begin{cases} \dfrac{3}{\sqrt{2}} A\alpha(1-\alpha)\sqrt{R_g}\lambda_c \dfrac{\rho_v^2 h_{fg}}{P} \dfrac{T_s - T_v}{\sqrt{T_s}} & T_v < T_s \\ 0 & T_v \geq T_s \end{cases} \tag{3.89}$$

Finally $\Gamma = \Gamma_e - \Gamma_c$ (3.90)

3.2.2 Problems of THERMIT physical models

3.2.2.1 Forced and natural convection

THERMIT physical models are derived from high-speed forced convection experiments whereas ORNL/TM-7018 is a low speed natural convection experiment. It is not yet known what amount of error will result, when the forced convection correlations are used for natural convection cases. For single-phase flow, one of the major differences between the two cases is the velocity and temperature profiles across the flow area. The peak velocity in forced convection is at the center region of the flow area, whereas the peak velocity in some natural convection cases is somewhere between the center and the wall. This is because the coolant is heated from the wall and the flow is driven by the buoyancy effect of the heated coolant. When there are different velocity and temperature profiles, different wall friction and wall heat transfer correlations should theoretically be used.

For the two-phase flow, the situation is much more complicated and it is difficult to say what the difference between the forced and natural convection would be.

3.2.2.2 Flow regime

There are two flow regimes in the THERMIT correlations for a sodium two-phase flow, i.e. bubbly and annular flow.

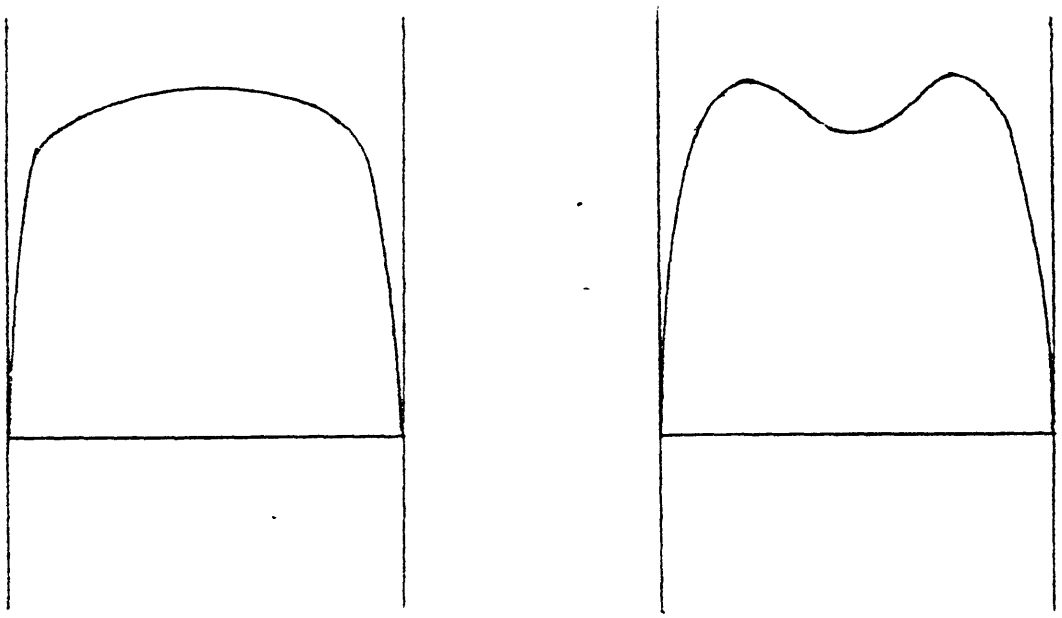

forced convection natural convection

Fig 3.1 Typical velocity profiles for forced and natural convection

Three points should be defined to determine the flow regimes, inception of boiling, transition from bubbly to annular flow and dryout.

In THERMIT physical models there are some inconsistencies regarding the flow regimes as listed below.

1) There is an inconsistency in determining the dryout point. For the wall friction, the dryout is assumed to occur at $\alpha = 0.957$ and the contact fraction of liquid is defined as $\frac{1-\alpha}{1-\alpha_{dry}}$ after the dryout point. However for the wall heat transfer the dryout occurs at $\alpha = 0.99$ and the wall is in contact only with vapor after the dryout point.

2) There is an inconsistency in determining the transition point between bubbly and annular flow. The bubbly flow regime is not defined for the wall friction and wall heat transfer, but only for the interfacial area calculation. The value $\alpha = 0.6$ is chosen for the transition from bubbly to annular flow just to make the interfacial area a continuous function with respect to the void fraction. There is no physical basis for the value $\alpha = 0.6$.

3) The droplets in the vapor core for an annular flow should be considered. The fraction of the liquid droplets should be determined because the droplets significantly affect the interfacial momentum transfer. Since the droplets may be assumed to flow at the same velocity as

the vapor, the interfacial momentum transfer is increased in comparison with the flow without droplets.

4) A physical model for the interfacial heat transfer is required. Presently a very large value is input for the interfacial heat transfer coefficient, but it must be a function of the interfacial area and flow regimes.

5) There seems to be a problem in determining the interfa--cial momentum transfer. In the present correlation, the interfacial momentum transfer is proportional to the square of the difference between the liquid and vapor average velocities. Actually the interfacial momentum transfer is a local phenomenon at the interface and has nothing to do with the bulk average quantities. The difference of bulk average velocities is sometimes a good measure of the velocity gradient at the interface. However if the liquid film Reynold's number is above 3000[Ref. 6], the wavy motion of liquid film is independent of the liquid film flow rate and determined from the vapor velocity. Hence the interfacial momentum transfer may depend not only on the difference of the liquid and vapor velocities but also on their absolute magnitudes.

3.2.2.3 Condensation modeling

In THERMIT, the liquid and vapor temperatures are

artificially made almost equal by using a large interfacial heat transfer coefficient. According to the Nigmatulin model, the interfacial mass transfer is proportional to the difference between the liquid or vapor temperature and the saturation temperature. Consequently the interfacial mass transfer is not reliable, because the liquid and vapor temperatures are not reliable.

The advantage of the 4-Eq model is that physical models for the interfacial mass and energy transfer are not necessary, but the 4-Eq model cannot describe a state of thermal disequili--brium between phases. Since a thermal disequilibrium state is expected to occur in case of the condensation of superheated vapor in subcooled liquid, the interfacial mass and energy transfer is of primary concern for condensation modeling of the 6-Eq model.

3.2.3 Translation of physical models to different geometry

3.2.3.1 Equivalent hydraulic diameter

The wall friction and wall heat transfer are the transport phenomena of momentum and energy from the wall. The transport phenomena from the wall are determined by the flow condition, properties of coolant, wall surface condition and the geometry of the wall. It has been shown by experiments that in some cases the transport from the wall is relatively independent of the geometry of the wall, e.g. circular or rectangular,

provided the equivalent hydraulic diameters are the same.

If the transport phenomenon from one portion of the perimeter affects the transport from another portion of the perimeter, the equivalent hydraulic diameter cannot be used. In other words, the equivalent hydraulic diameter cannot be used when the flow area is too far from being circular or the flow is laminar so that the wall effect is not uniform over the flow area, but is a function of the distance from the wall.

Consequently in translating the rod-bundle correlations to the circular geometry, two conditions should be satisfied. One is that the rod-bundle in LMFBR should not be too closely-packed so that the subchannel geometry is not too far from being circular and the other is that the flow should be turbulent.

Two equivalent hydraulic diameters are used in THERMIT, the wetted equivalent diameter for the wall friction and the heated equivalent diameter for the wall heat transfer. They are defined as follows.

$$De(\text{wetted}) = 4A/(\text{wetted perimeter}) \tag{3.91}$$

$$De(\text{heated}) = 4A/(\text{heated perimeter}) \tag{3.92}$$

The equivalent hydraulic diameter may be a good approximation if the previously mentioned two conditions are

satisfied, but the best way is to use the correlations that are developed in the same geometry.

3.2.3.2 Interfacial area

The interfacial area in a rod-bundle geometry is given in Section 3.2.1.5 'Interfacial mass transfer', and the basic idea of the derivation is given in Ref. 4 . If the same idea is used for the circular tube geometry, the following expressions for the interfacial area between liquid and vapor phases are derived.

$$A_t = 2\sqrt{6}\,\frac{\sqrt{\alpha}}{D} \qquad \text{in bubbly flow} \tag{3.93}$$

$$A_t = \frac{4\sqrt{\alpha}}{D} \qquad \text{in annular flow} \tag{3.94}$$

$$A_t = \frac{4\sqrt{\alpha}}{D}\left(\frac{1-\alpha}{1-\alpha_{dry}}\right)^{0.5} \qquad \text{after dryout} \tag{3.95}$$

where D is the diameter of the tube

In order to get a continuous interfacial area with respect to the void fraction α, an approximation to the above equations is made as follows.

$$A_t = \frac{4\sqrt{\alpha}}{D}\left(\sqrt{1.5} - \frac{\sqrt{1.5}-1}{(\alpha_{dry})^{1.5}}\,\alpha^{1.5}\right) \qquad \text{in bubbly and annular flow} \tag{3.96}$$

$$A_t = \frac{4\sqrt{\alpha}}{D}\left(\sqrt{1.5} - \frac{\sqrt{1.5}-1}{(\alpha_{dry})^{1.5}}\,\alpha^{1.5}\right)\left(\frac{1-\alpha}{1-\alpha_{dry}}\right)^{0.5} \qquad \text{after dryout} \tag{3.97}$$

Fig 3.2 shows the difference between the interfacial areas calculated by Eq 3.85, 3.86 and 3.87 with the equivalent hydraulic diameter of the rod-bundle and by Eq 3.96 and 3.97 with the diameter of the tube. Fig 3.2 shows that the inter--facial area between phases is dependent not only on the equivalent hydraulic diameter but also on the actual shape of coolant channel.

Although the equivalent hydraulic diameter may be a good approximation for calculating the wall friction and wall heat transfer, it is not so good for calculating the interfacial area which determines all the transfer terms between liquid and vapor phases.

3.2.4 Summary of physical models for circular tube geometry

Wall friction

Autruffe's wall friction correlation[Ref. 5]

$$F_\ell = \frac{0.18}{2De}(Re_\ell)^{-0.2}\ \rho_\ell v_\ell |v_\ell| \tag{3.98}$$

$$F_v = \frac{0.2}{2De}\ \alpha(Re_v)^{-0.2}\ \rho_v v_v |v_v| \tag{3.99}$$

where $Re_\ell = \dfrac{(1-\alpha)\rho_\ell v_\ell De}{\mu_\ell}$ $\quad Re_v = \dfrac{\alpha\rho_v v_v De}{\mu_v}$

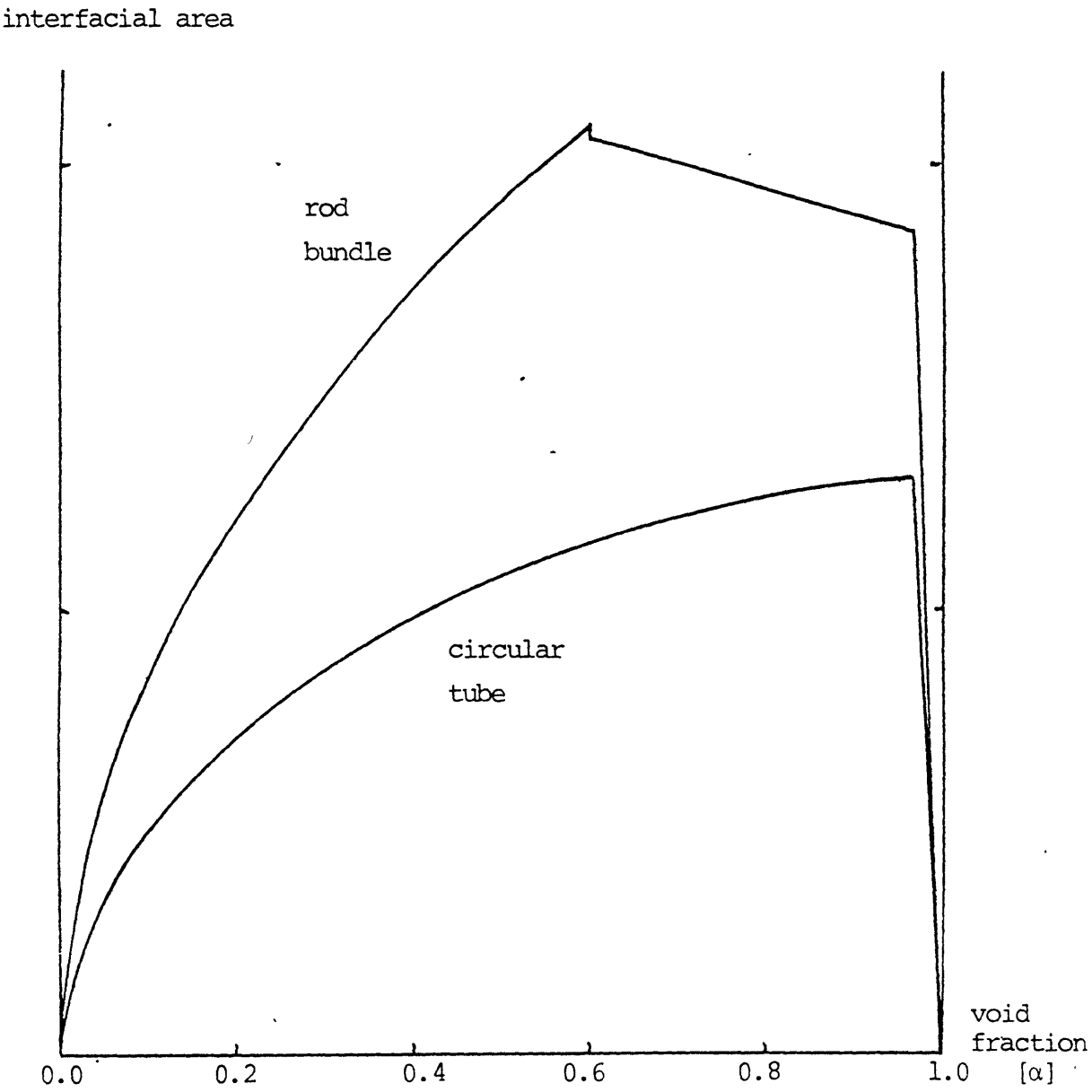

Fig 3.2 Interfacial area for rod-bundle and circular tube geometry with the same equivalent hydraulic diameter

$$F_T = \theta F_\ell + (1-\theta) F_v$$

$$\text{where} \begin{cases} \theta = 1 & \alpha \leq \alpha_{dry} \\ \theta = \dfrac{1-\alpha}{1-\alpha_{dry}} & \alpha > \alpha_{dry} \end{cases}$$

Interfacial area between liquid and vapor

$$A_t = \frac{4\sqrt{\alpha}}{D}\left(\sqrt{1.5} - \frac{\sqrt{1.5}-1}{(\alpha_{dry})^{1.5}}\,\alpha^{1.5}\right) \qquad \text{in bubbly and annular flow}$$

$$A_t = \frac{4\sqrt{\alpha}}{D}\left(\sqrt{1.5} - \frac{\sqrt{1.5}-1}{(\alpha_{dry})^{1.5}}\,\alpha^{1.5}\right)\left(\frac{1-\alpha}{1-\alpha_{dry}}\right) \qquad \text{after dryout}$$

Table 3.1 Summary of the constitutive relations used for the natural and forced convection simulations

constitutive relations	Natural convection (ORNL/TM-7018) circular tube		Forced convec--tion (French) circular tube
	4-Eq	6-Eq	4-Eq
Interfacial mass transf--er	none	Modified Nig--matulin model Eq 3.85 - 3.90	none
Interfacial momentum transfer	Wallis correlation Eq 3.59 - 3.60		
Interfacial energy transfer	none	large heat transfer coeff. Eq 3.84	none
Axial wall friction	Markley's, Novendstern's and Autruffe's correlation Eq 3.48 - 3.58		
Wall heat transfer	Schad's, Modified Chen's and Dittus-Boelter's correlation Eq 3.61 - 3.83		

Chapter 4. Results

4.1 Natural convection

The calculational results for the simulation of ORNL/TM--7018 are presented here. There are two parts in the simulation, the test section and the loop simulation. For the test section simulation, first the quasi-steady-state is assumed and calculation is done for all test runs using the average values of the oscillatory inlet velocity. After the quasi-steady-state (steady-state boiling) has been reached, the inlet velocity is oscillated with the period of one second and a transient calculation for the test run 129R1 is performed. For the loop simulation, the simulated and actual 1-D loop analysis results are presented. In the simulated 1-D loop analysis, a hypothetical vapor density is used to avoid the code failure.

4.1.1 Test section simulation

4.1.1.1 Steady-state

The steady-state here means the time average of the oscillatory behavior as discussed in Chapter 2.

The pressure-velocity boundary condition is used for all runs of the test section simulation. The inlet velocity is given from the inlet flow meter measurement.

In Table 4.1 the pressure drops in experiment and calculation are given for all test runs. The 4-Eq and 6-Eq models gave almost identical results and those results are plotted in Fig 4.1.

Note that the experiment and calculation pressure drops cannot be compared directly. The calculated pressure drop is between the center points of the fictitious cells, whereas the experiment pressure drop is between the upper and lower plena. The condensation effect in the upper plenum and the gravitational head between the center points of the fictitious cells and the actual manometer locations are not taken into consideration. These effects are bounded and discussed in Chapter 5.

In Table 4.2 the maximum number of Newton iterations, the convergence criteria for Newton iterations and the convergence criteria for steady-state are given. The negative number of maximum Newton iterations means that the time step size is automatically reduced after the maximum number of Newton iterations, if the Newton iteration convergence criterion is not satisfied. If a positive number of maximum Newton iterations is used, the calculation will continue to the next time step, although the Newton iteration convergence criterion is not satisfied. It may be safer to use a negative number of maximum Newton iterations.

Table 4.1 Steady-state test section pressure drop for 4-Eq/6-Eq models

	Test No.	Power[a] [W]	inlet velocity [cm/s]	ΔP_{calc} (4-Eq) [BAR]	ΔP_{calc} (6-Eq) [BAR]	$\Delta P_{exp't}$ [BAR]
Single phase	107R2	210	8.438	0.2013		0.20
	108R2	350	10.849	0.1974		0.18
	100R3	490	12.054	0.1930		0.08
	100R4	560	12.260	0.1901		0.16
Two phase	129R1	910	12.054	0.75149	0.75140	0.08
	121R1	980	9.644	0.86342	0.86334	0.08
	125R1	980	10.849	0.87640	0.87622	0.06
	125R2	980	8.438	0.82815	0.82829	0.08
	127R1	1050	9.644	0.92575	0.92577	0.07
	120R1[b]	1050	28.930	0.21965		0.06
	119R1	1120	13.260	1.02340	1.02280	0.08
	126R2	1120	10.849	1.02326	1.02315	0.08
	128R1	1190	10.849	1.08605		0.07

Note a 70% of the power given in the report ORNL/TM-7018

b In experiment it was a two-phase run, but in calculation it was a single-phase run with the given inlet velocity.

Table 4.2 Steady-state test section calculation convergence criteria for 4-Eq model

	Test No.	Power	nitmax[a]	epsn[b]	delpr[c]
Single phase	107R2	210	-5	1.0×10^{-5}	1.0×10^{-5}
	108R2	350	-5	1.0×10^{-5}	1.0×10^{-5}
	100R3	490	-5	1.0×10^{-5}	1.0×10^{-5}
	100R4	560	-5	1.0×10^{-5}	1.0×10^{-5}
Two phase	129R1	910	5	1.0×10^{-3}	1.0×10^{-7}
	121R1	980	3	1.0×10^{-4}	1.0×10^{-5}
	125R1	980	3	1.0×10^{-3}	1.0×10^{-5}
	125R2	980	3	1.0×10^{-3}	1.0×10^{-5}
	127R1	1050	3	1.0×10^{-4}	1.0×10^{-5}
	120R1	1050	3	1.0×10^{-3}	1.0×10^{-5}
	119R1	1120	3	1.0×10^{-4}	1.0×10^{-5}
	126R2	1120	3	1.0×10^{-3}	1.0×10^{-5}
	128R1	1190	3	1.0×10^{-4}	1.0×10^{-5}

Note a maximum number of Newton iterations

b convergence criterion for Newton iteration

c convergence criterion for steady-state

(delpr = delro = delem)

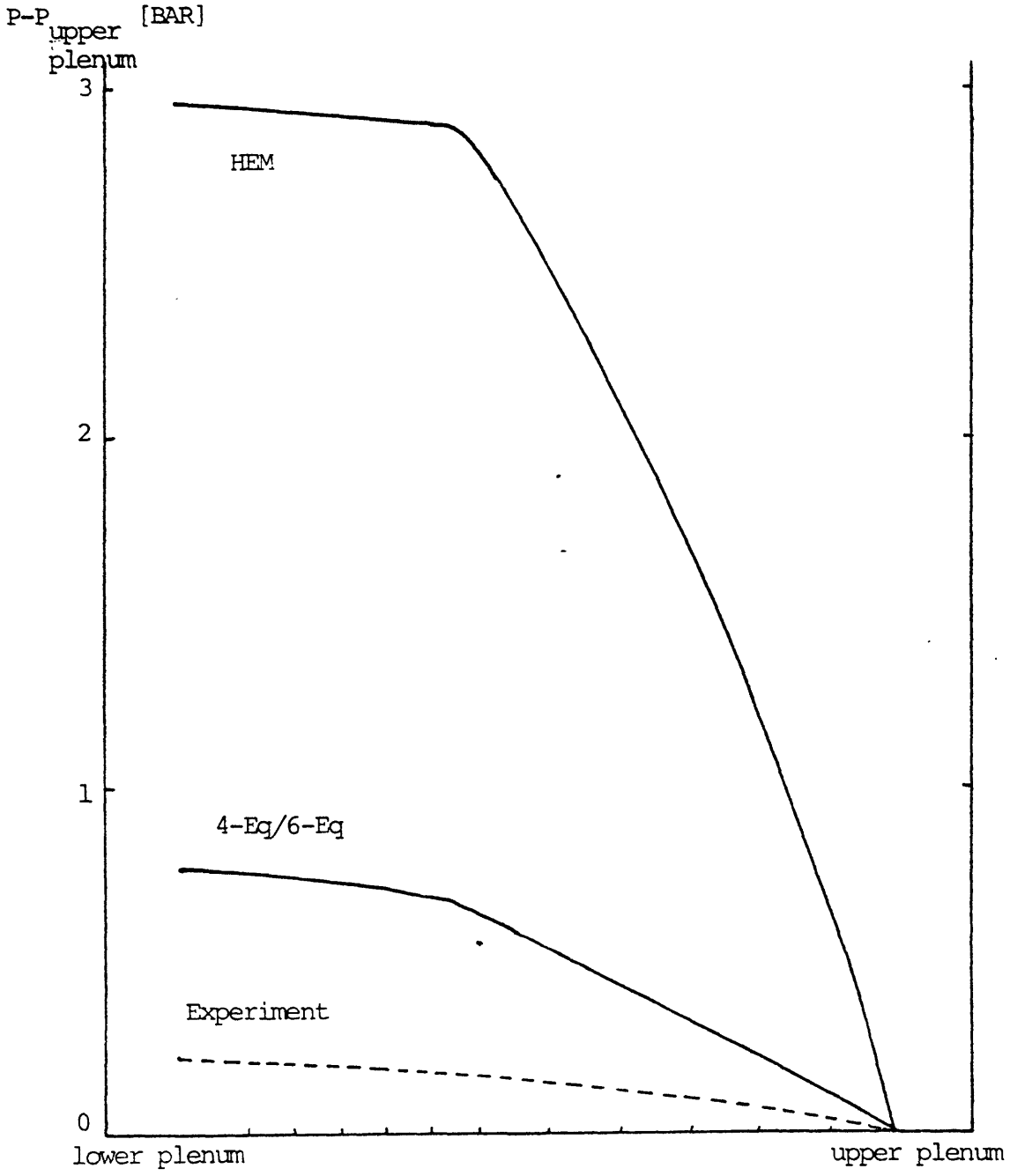

Fig 4.1 Pressure distribution for the test run 129P1

However it was impossible to satisfy any meaningful Newton iteration convergence criterion at the inception of boiling and condensation, whatever number of maximum Newton itera--tions might be used.

Although the Newton iteration convergence criterion is not satisfied at the inception boiling, the calculation goes on to the next time step and finally reaches the steady--state. Hence the intermediate results are not reliable, but the final steady-state does not depend on the interme--diate results, but only on the boundary conditions.

If the maximum fractional change in pressure, mixture density and mixture internal energy between successive time steps are less than delpr, delro and delem, it is concluded that the steady-state has been reached.

In Table 4.3 it is shown how the heat input is trans--formed and partitioned among the enthalpy, kinetic energy and potential energy rises of the coolant. About 1~2% of the total heat input is lost according to THERMIT calcula--tions for two-phase cases. The reason has been given in Chapter 3.

In Table 4.4 and 4.5, the liquid and vapor velocities of the HEM and 4-Eq/6-Eq models are given.

Table 4.3 Steady-state test section energy conservation for 4-Eq model

	Test No.	Power [W]	enthalpy rise[W]	K.E. rise [W]	P.E. rise [W]	% energy loss
Single phase	107R2	210	210	0.0	0.0	0.0
	108R2	350	350	0.0	0.0	0.0
	100R3	490	490	0.0	0.0	0.0
	100R4	560	560	0.0	0.0	0.0
Two phase	129R1	910	900	4.29×10^{-2}	2.06×10^{-2}	1.10
	121R1	980	963	11.66×10^{-2}	1.65×10^{-2}	1.74
	125R1	980	965	8.79×10^{-2}	1.85×10^{-2}	1.53
	125R2	980	962	15.11×10^{-2}	1.44×10^{-2}	1.84
	127R1	1050	1030	15.85×10^{-2}	1.65×10^{-2}	1.91
	120R1	1050	1050	0.0	0.0	0.0
	119R1	1120	1104	9.98×10^{-2}	2.26×10^{-2}	1.43
	126R2	1120	1098	16.56×10^{-2}	1.85×10^{-2}	1.96
	128R1	1190	1165	21.67×10^{-2}	1.85×10^{-2}	2.10

Table 4.4 Steady-state HEM model for test run 129R1

Inter-face No.	velocity[m/s]		slip ratio
	liquid	vapor	
1	0.121	0.121	1.0
2	0.126	0.126	1.0
3	0.133	0.133	1.0
4	0.140	0.140	1.0
5	0.975	0.975	1.0
6	5.932	5.932	1.0
7	6.006	6.006	1.0
8	6.977	6.977	1.0
9	8.402	8.402	1.0
10	10.738	10.738	1.0
11	15.394	15.394	1.0

Table 4.5 Steady-state 4-Eq/ 6-Eq model for test run 129R1

Inter-face No.	velocity[m/s]		slip ratio
	liquid	vapor	
1	0.121	0.121	1.0
2	0.126	0.126	1.0
3	0.133	0.133	1.0
4	0.140	0.140	1.0
5	1.318	9.748	7.40
6	2.208	20.232	9.16
7	2.268	21.535	9.50
8	2.327	23.372	10.04
9	2.400	25.621	10.68
10	2.464	28.483	11.56
11	2.605	32.163	12.35

Table 4.6 Dependence of the pressure drop on interfacial friction for test run 129R1

F_i/F_i(THERMIT)	ΔP [BAR]
no slip(HEM)	2.95734
1.0	0.75149
0.1	0.33761
0.05	0.26956
0.01	0.17535
0.005	0.15408

4.1.1.2 Transient

After the steady-state has been reached, the inlet velocity was oscillated with the period of one second. Then all the other parameters such as the pressure drop over the test section and the void fraction, mixture enthalpy and mixture density at the end of the heated zone oscillate according to the inlet velocity oscillation with some phase shifts.

Fig 4.2 and 4.3 show the oscillations of those parame--ters. It should be noted that the Newton iteration conver--gence criterion of 10^{-4} is satisfied at every time step in this calculation. Hence all the intermediate results are reliable within the limit of the convergence criterion.

In Fig 4.4 the variation of the outlet liquid and vapor velocities is shown during the transient.

4.1.2 Whole loop simulation

4.1.2.1 Simulated 1-D loop analysis

In order to avoid the failure of the code at the incep--tion of boiling and condensation, the vapor density has been artificially increased by one hundred and two hundred times as explained in Chapter 2. The transient with a real vapor density can be inferred from these two results.

Fig 4.5 and 4.6 are the simulated 1-D loop results of the

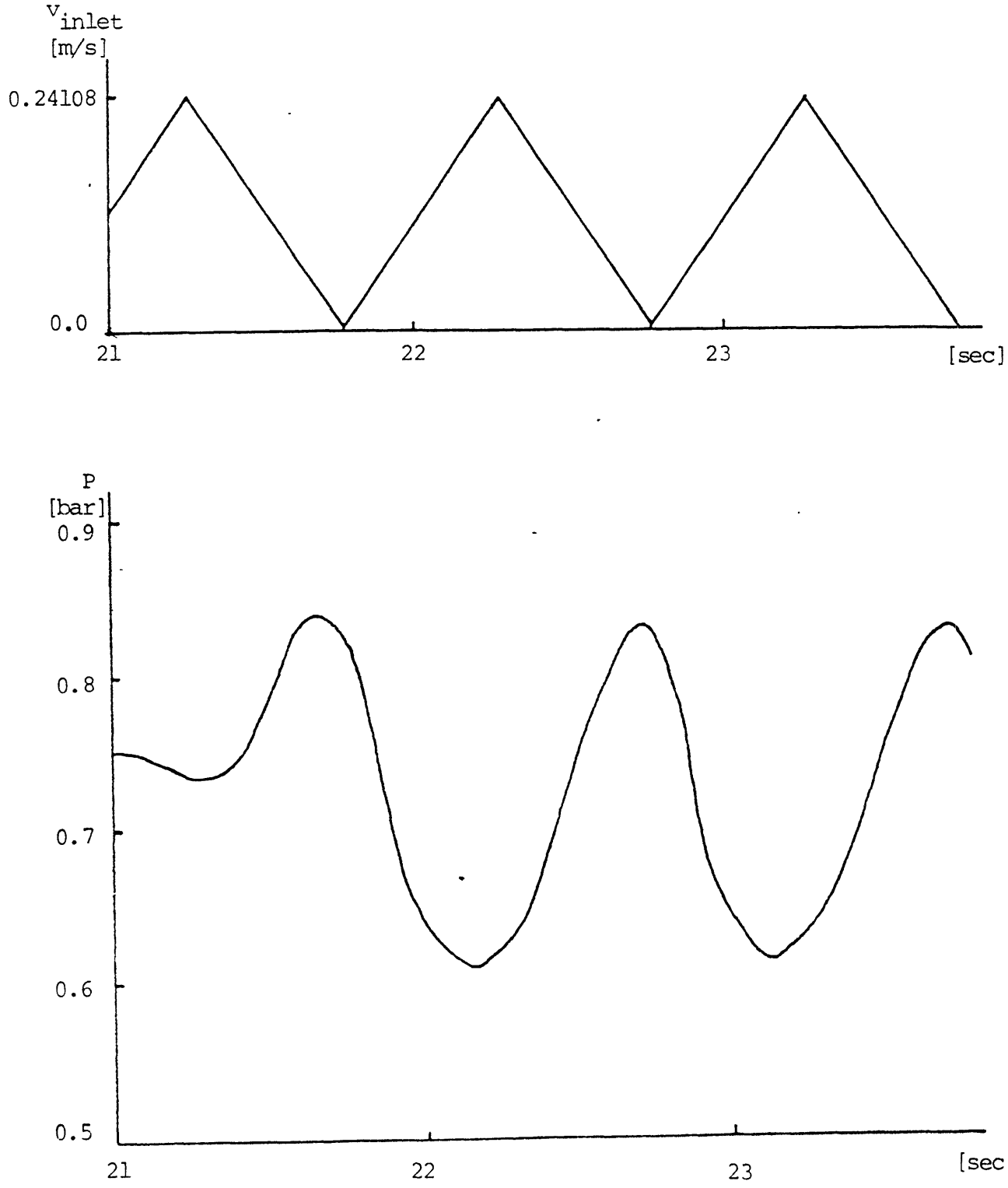

Fig 4.2 Oscillation of the pressure drop according to the inlet velocity for test run 129R1

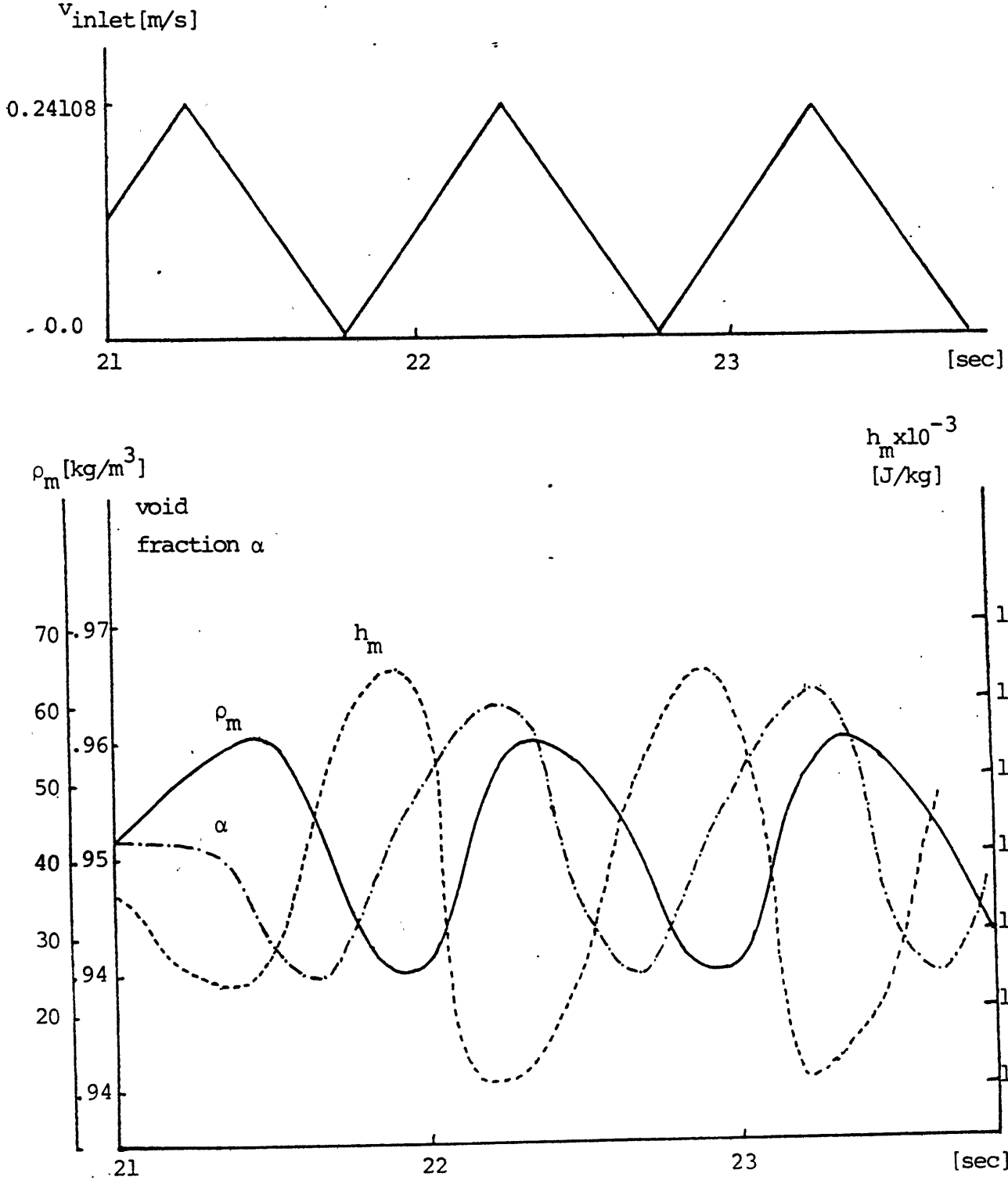

Fig 4.3 Oscillation of the void fraction, mixture enthalpy and mixture density at the end of the heated zone for 129R1

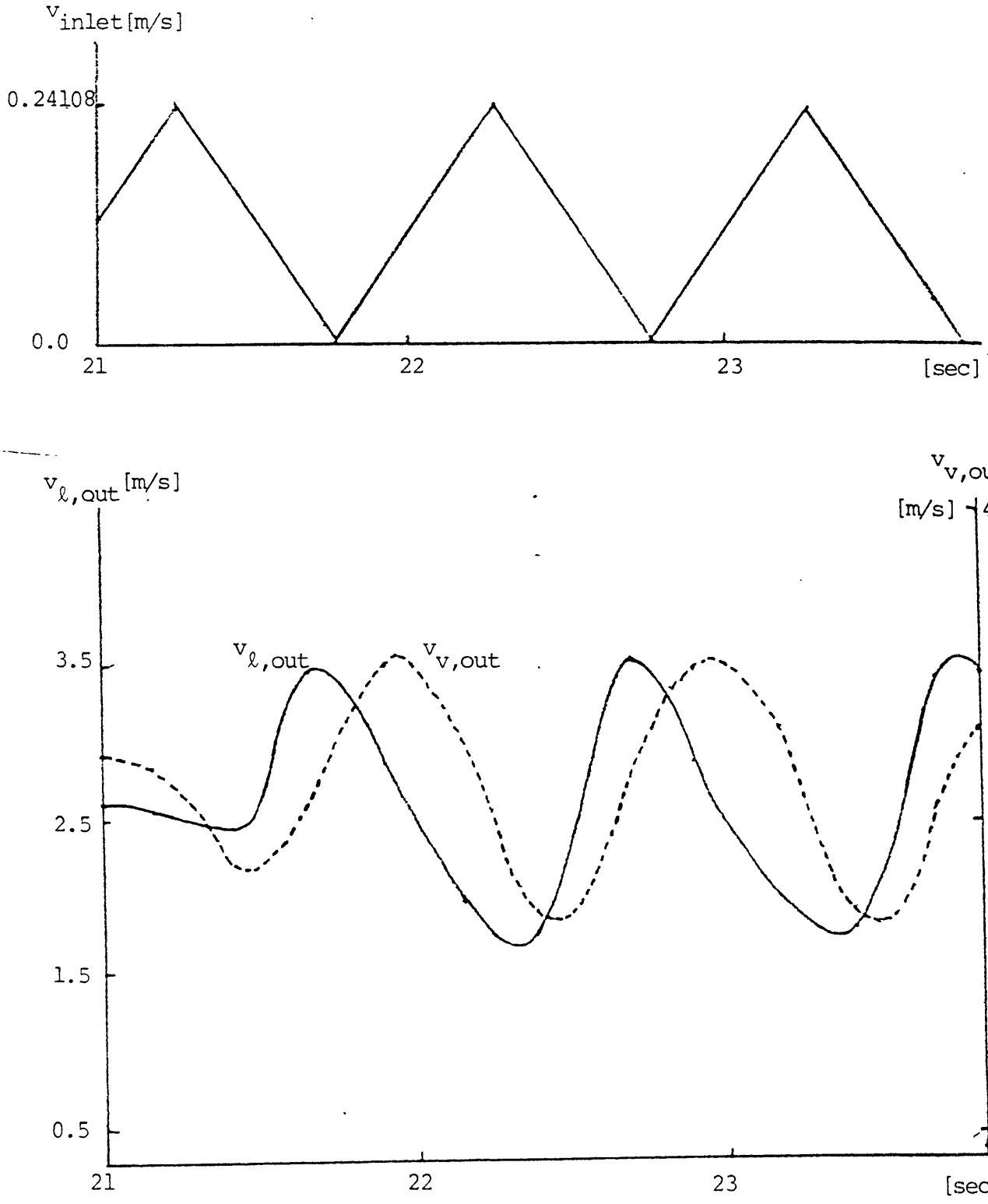

Fig 4.4 Oscillation of liquid and vapor velocities at the outlet for the transient of the test run 129R1

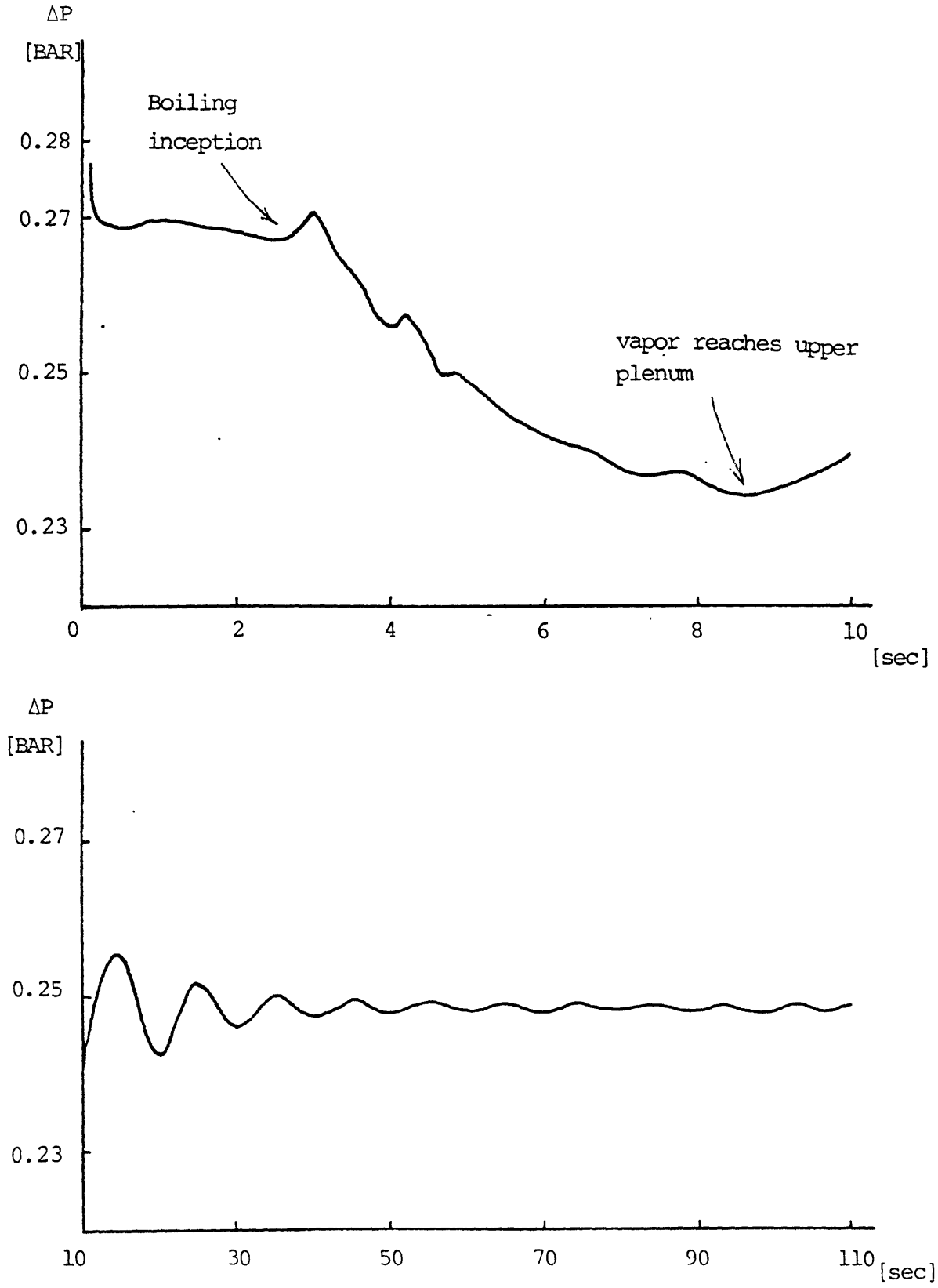

Fig 4.5 Pressure drop over the test section for simulated 1-D loop analysis with vapor density x200

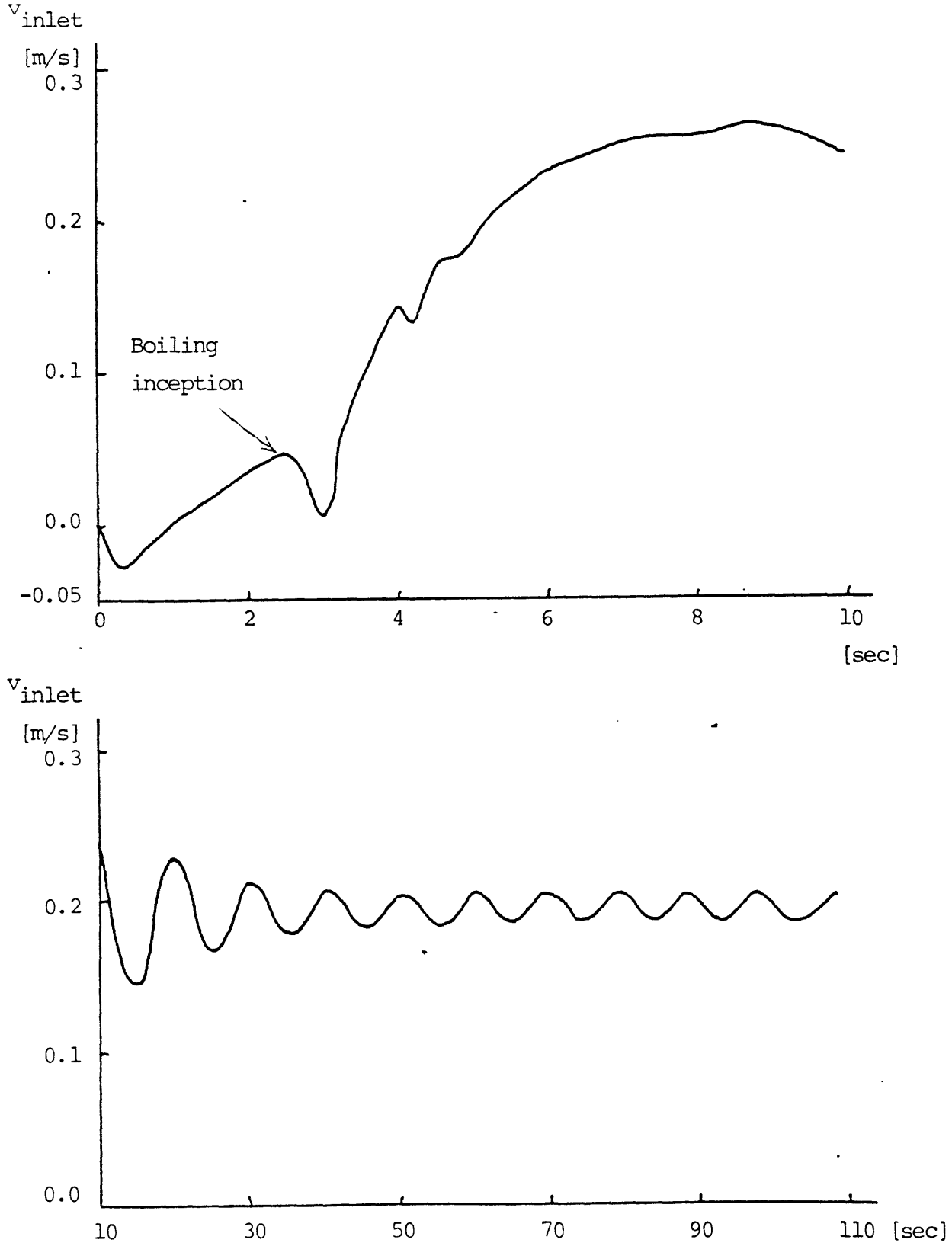

Fig 4.6 Inlet velocity of the test section for simulated 1-D loop analysis with vapor density x200

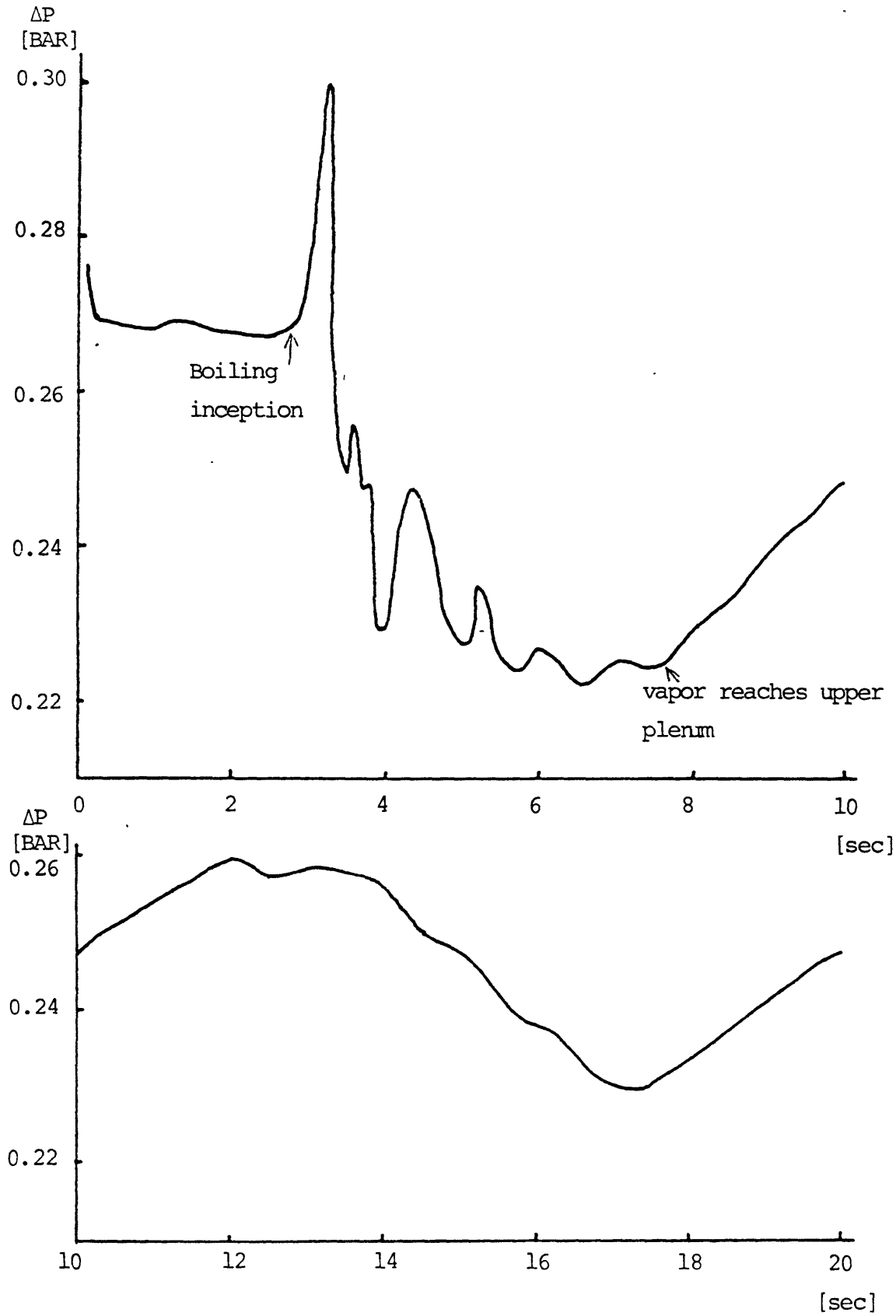

Fig 4.7 Pressure drop over the test section for simulated 1-D loop analysis with vapor density x100

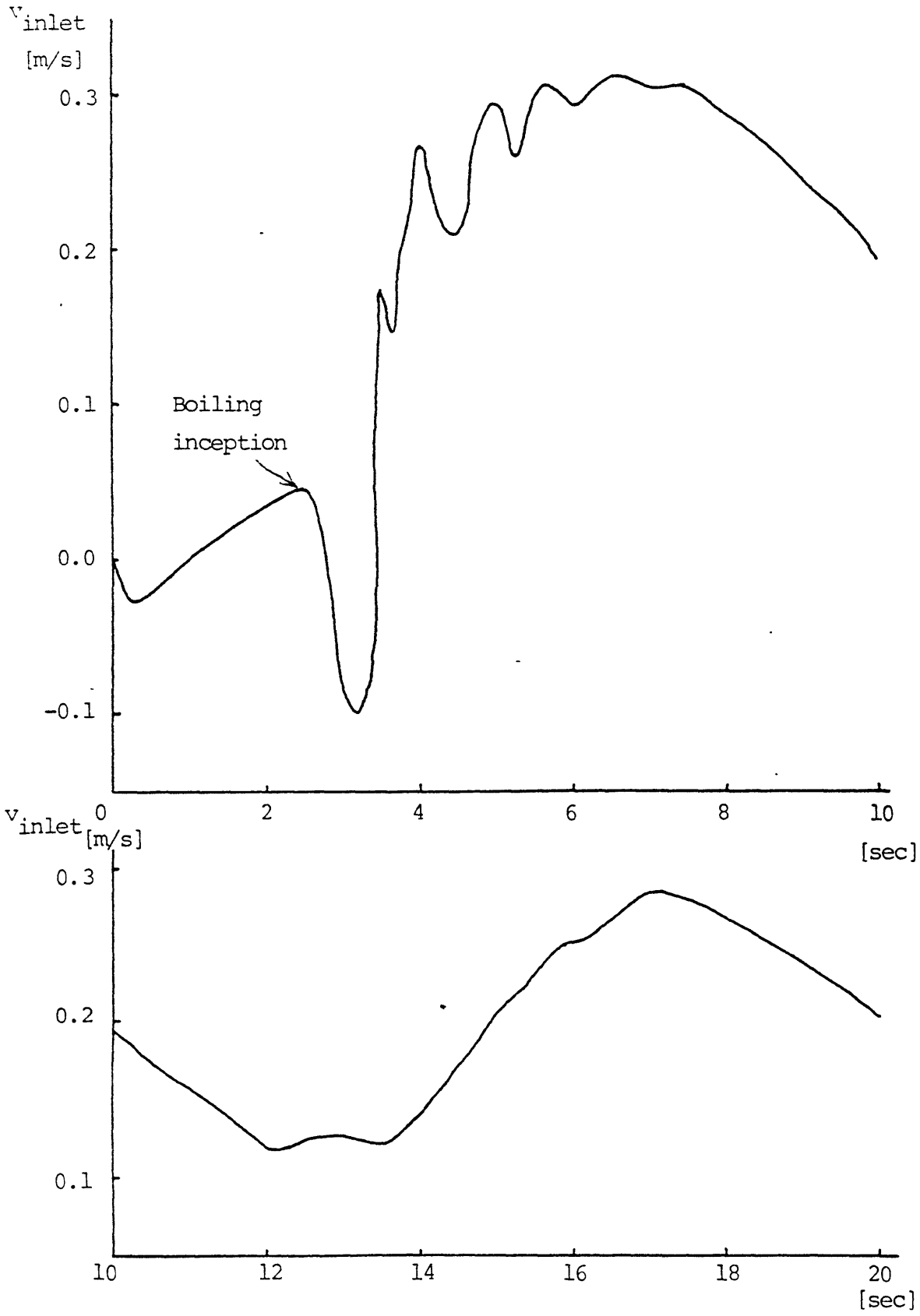

Fig 4.8 Inlet velocity of the test section for simulated 1-D loop analysis with vapor density x100

inlet pressure and velocity with the vapor density 200 times increased. Fig 4.7 and 4.8 are the results of the case which has exactly the same geometry, boundary conditions and inputs as Fig 4.5 and 4.6 except that the vapor density is increased by 100 times.

In Fig 4.5 there is a peak of the pressure drop at the inception boiling and the pressure drop decreases as boiling goes on, because the hydrostatic pressure drop decreases due to the lower density of vapor. A minimum value of the pressure drop is indicated when the vapor packet reaches the upper plenum and condensation begins. From that point on, the pressure drop oscillates with the period of about 10 seconds. Initially there is a damping of the oscillation amplitude. However after about 70 seconds, no damping is indicated up to the point of 130 seconds.

The inlet velocity varies in the opposite way from the pressure drop. When the inlet velocity is minimum, the pressure drop is maximum. Consequently there is a phase shift of 180° between the pressure drop and inlet velocity. Note also that the inlet velocity is minimum at the incep--tion of boiling.

Fig 4.7 and 4.8 show the same general tendency as Fig 4.5 and 4.6, but much more severe transient at the inception of boiling. A reverse flow is indicated in

Fig 4.8 and the code failed at the time of 20 seconds.

In Fig 4.9 the steady-state boiling oscillation with the vapor density 200 times increased is shown on a magni--fied scale. The period is about 9 seconds.

Fig 4.10 through 4.19 show the spatial distributions of the void fraction at discrete time intervals. Fig 4.10 through 4.15 show the inception of boiling at the end of the heated zone and propagation of the vapor packet and conden--sation in the upper plenum. Meanwhile another vapor packet is formed at the end of the heated zone and these two vapor packets are connected and undergoes a similar vapor packet propagation in the test section. Fig 4.16 through Fig 4.19 show the void distribution in the steady-state boiling region. It can be observed that the shape of the void distr--ibution oscillates with the same period of 9 seconds as in Fig 4.9.

4.1.2.2 Actual 1-D loop analysis

Fig 4.20 shows the steady-state pressure distributions in the test section for the simulated 1-D loop and actual 1-D loop analysis. It is the result of the single-phase run 107R2 the heat input of which is 210 W.

The steady-state inlet velocity is 0.070 m/s in the simulated 1-D loop and 0.063 m/s in the actual 1-D loop because the slope of the pressure distribution in the

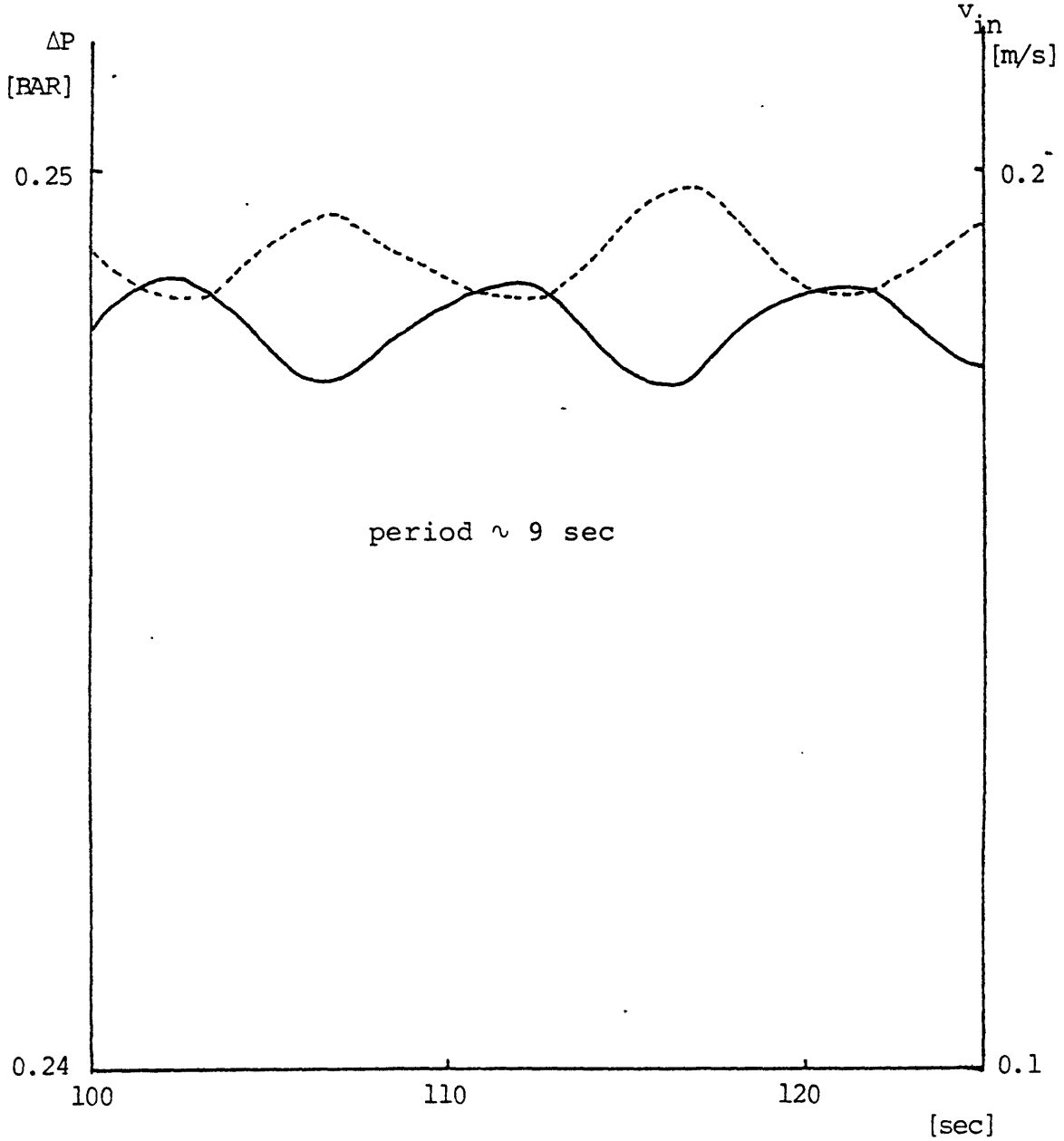

Fig 4.9 Stable boiling oscillation in the simulated 1-D loop with vapor density x200

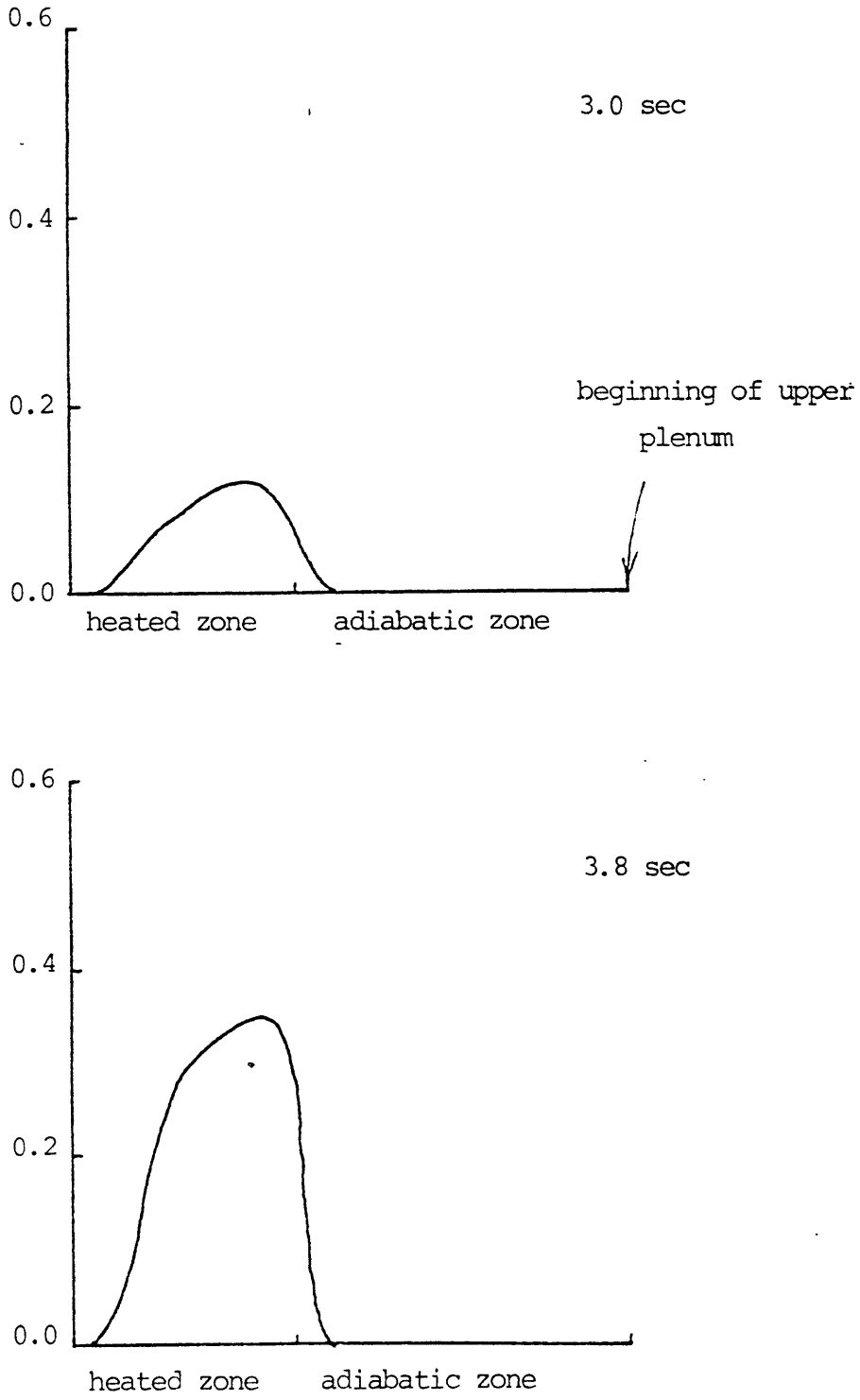

Fig 4.10 Spatial void distribution for simulated 1-D loop with vapor density x200

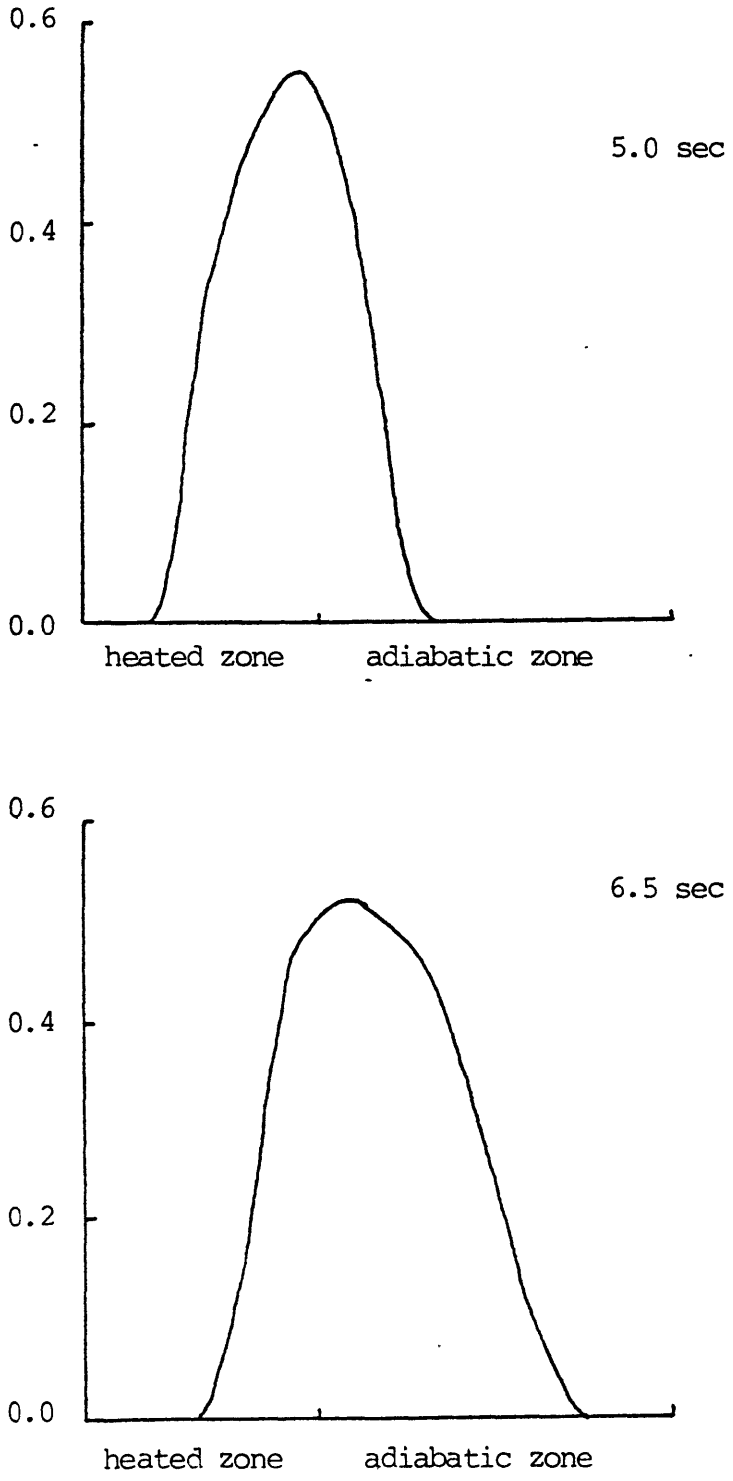

Fig 4.11 Spatial void distribution for simulated 1-D loop with vapor density x200

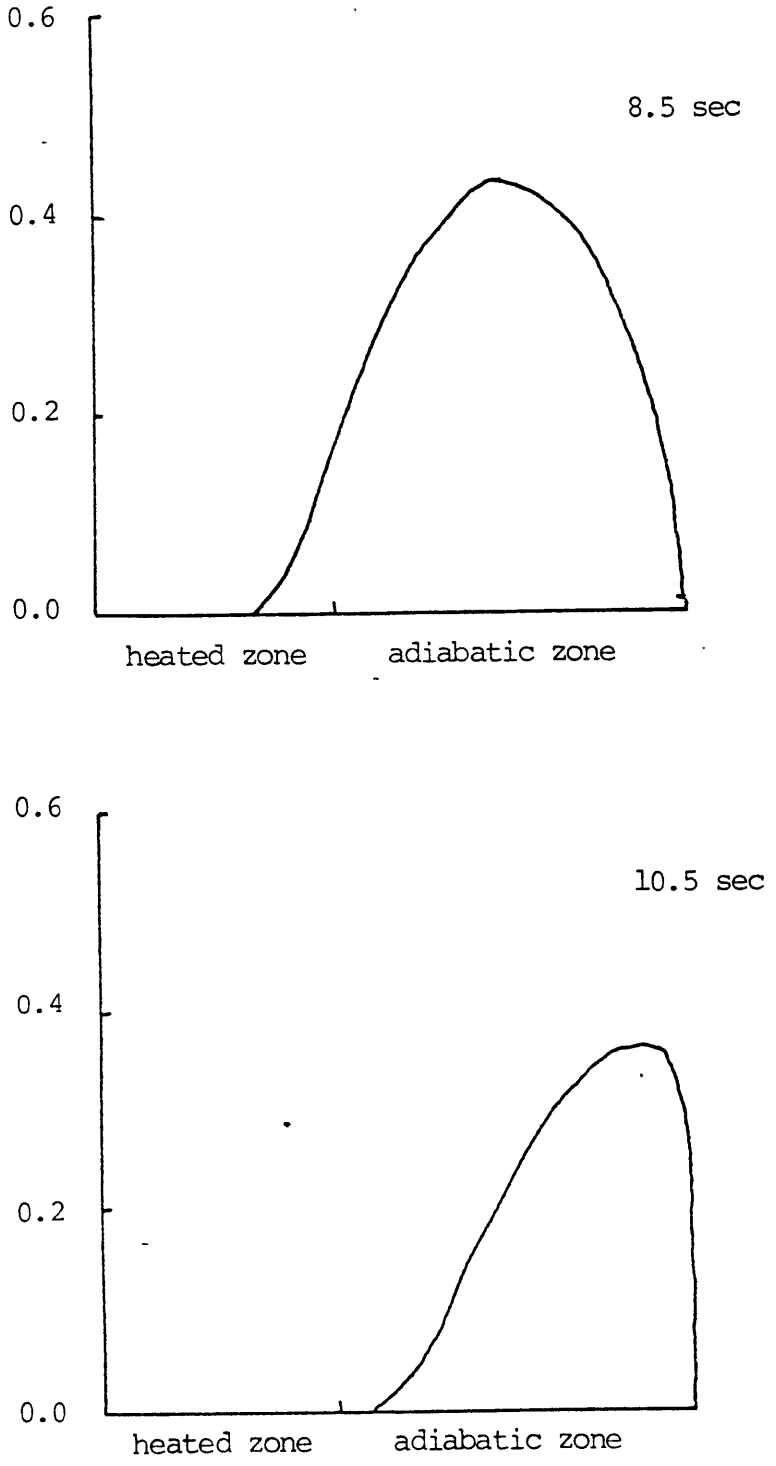

Fig 4.12 Spatial void distribution for simulated 1-D loop with vapor density x200

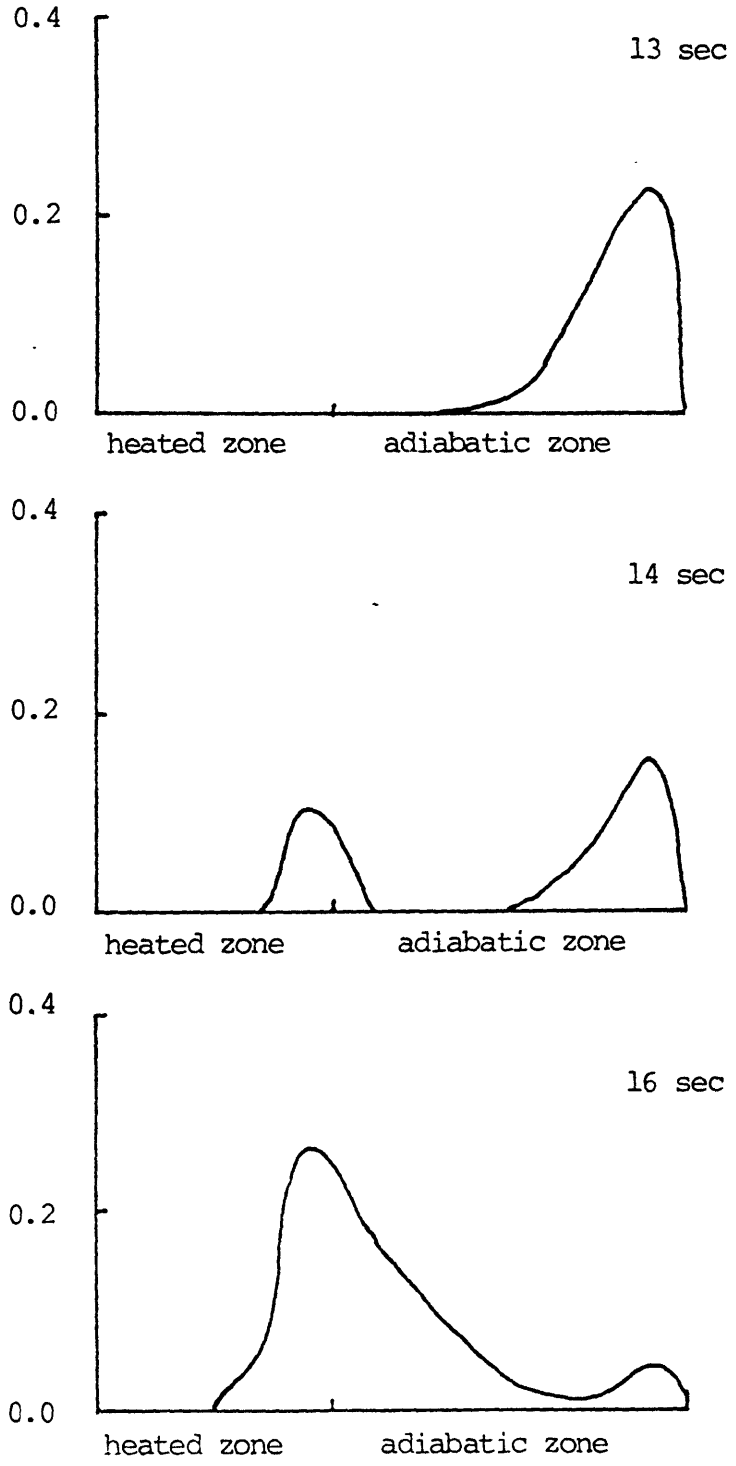

Fig 4.13 Spatial void distribution for simulated 1-D loop with vapor density x200

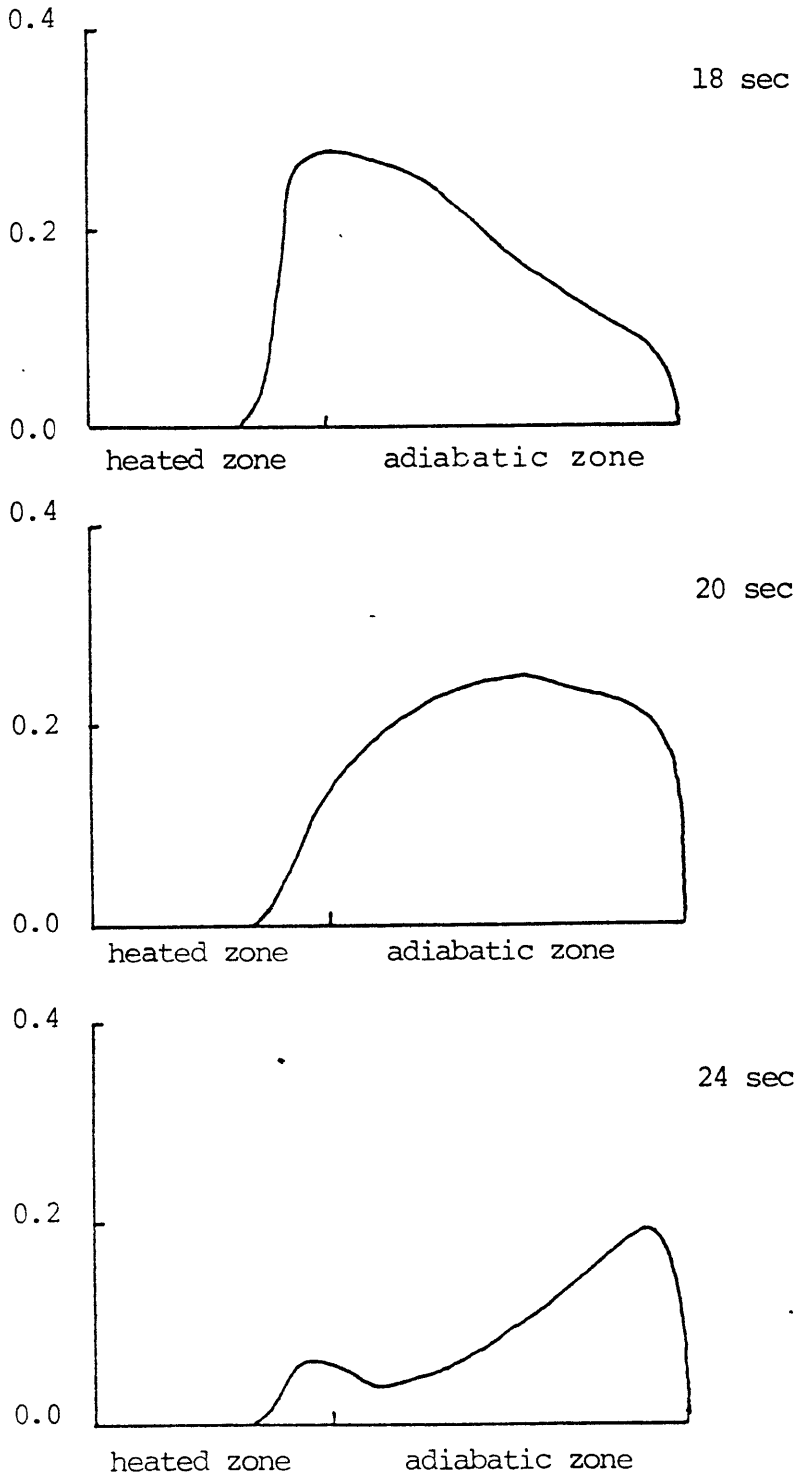

Fig 4.14 Spatial void distribution for simulated 1-D loop with vapor density x200

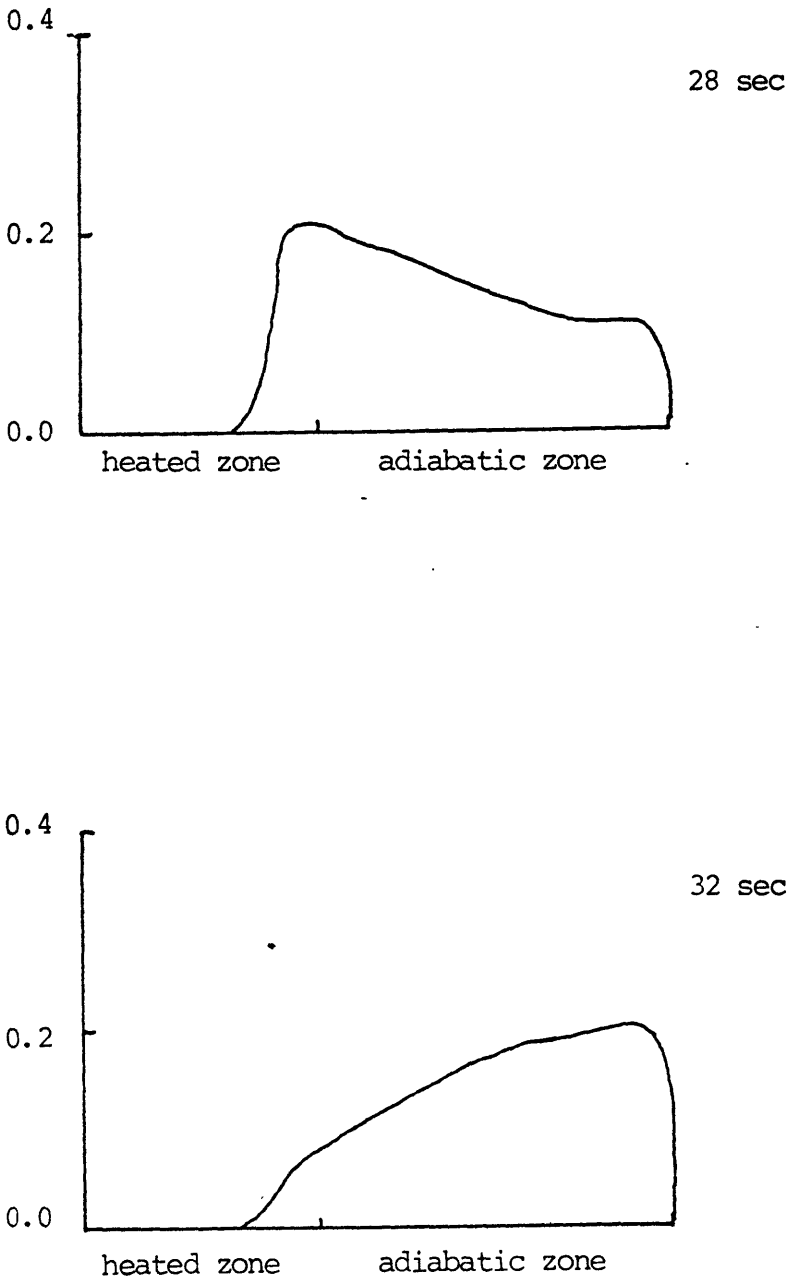

Fig 4.15 Spatial void distribution for simulated 1-D loop with vapor density x200

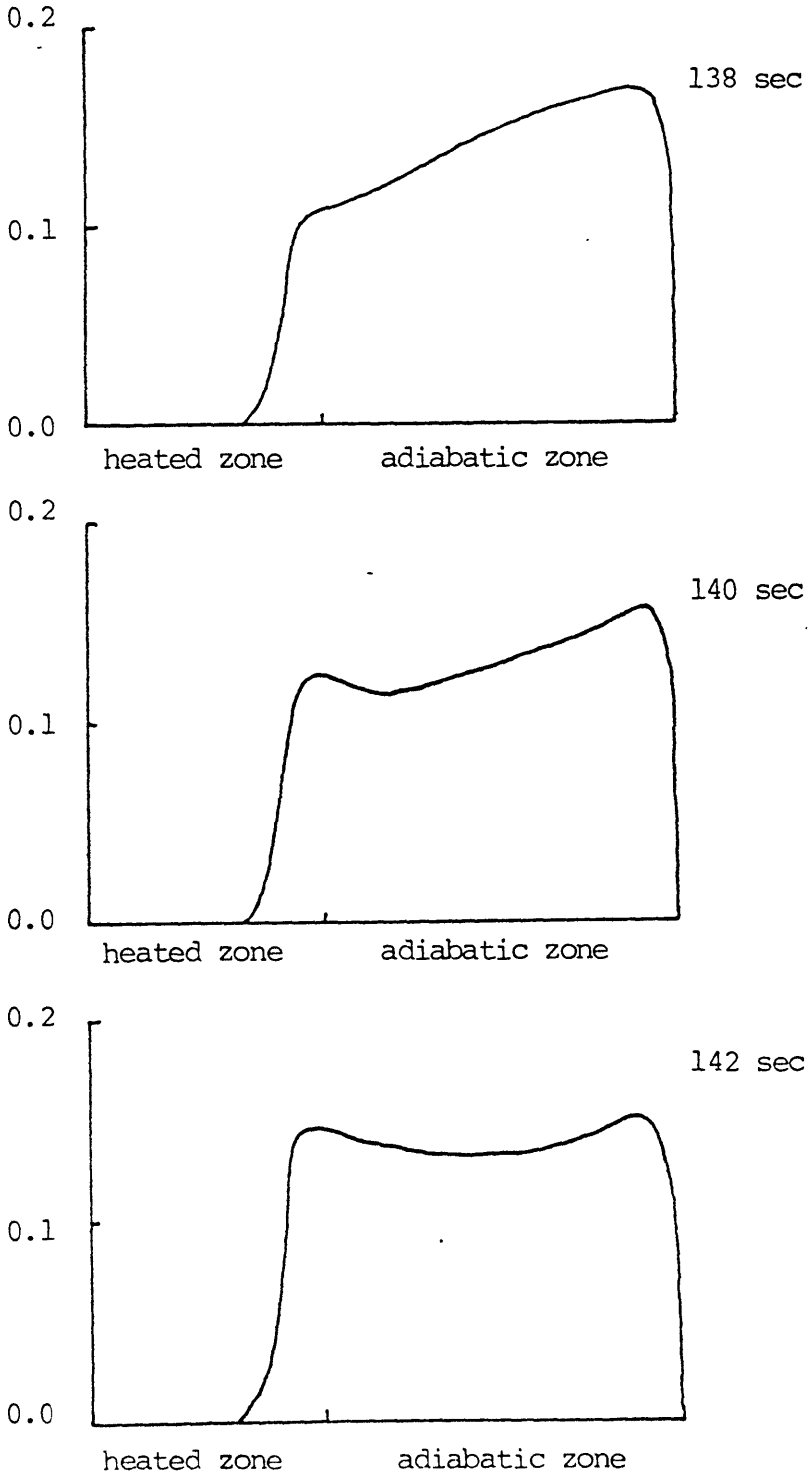

Fig 4.16 Spatial void distribution for simulated 1-D loop with vapor density x200

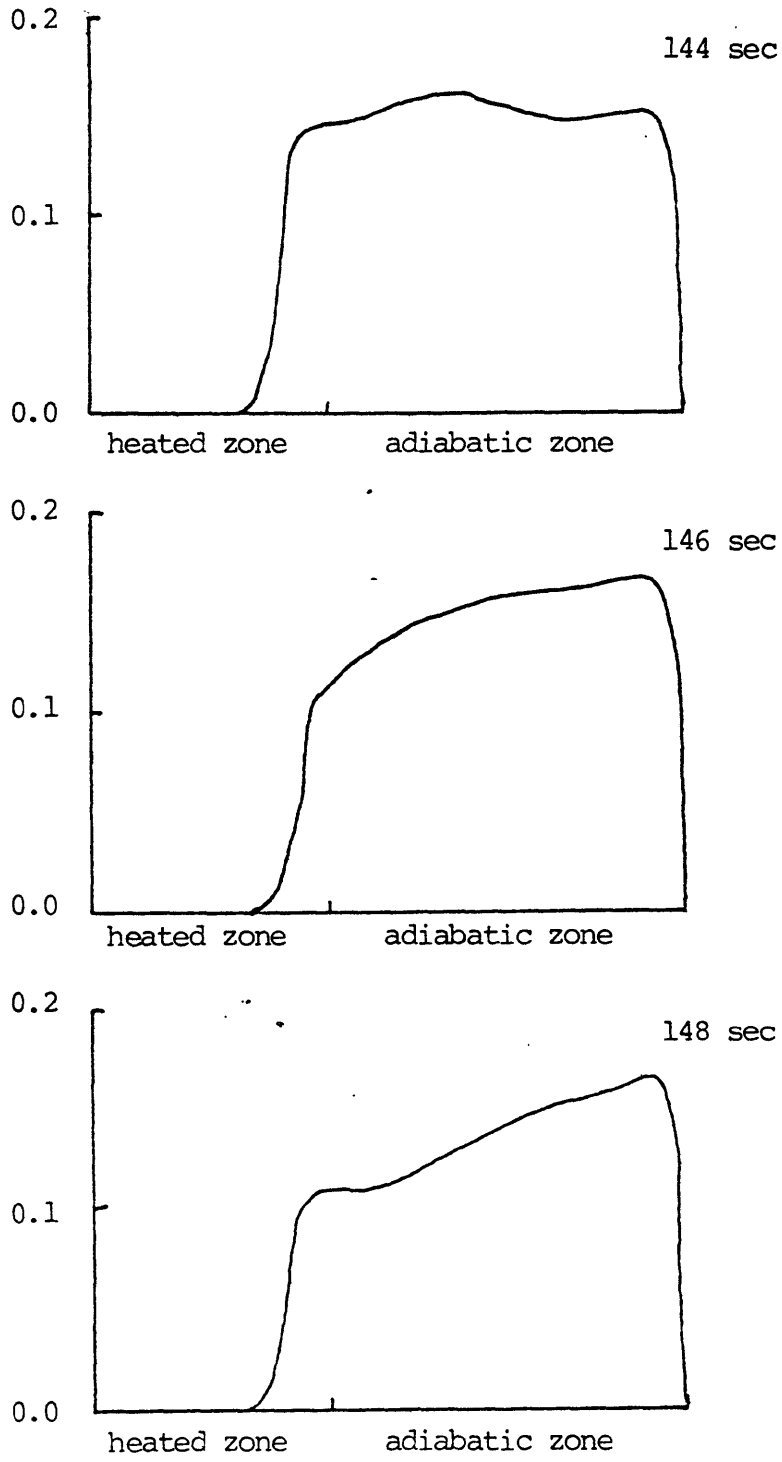

Fig 4.17 Spatial void distribution for simulated 1-D loop with vapor density x200

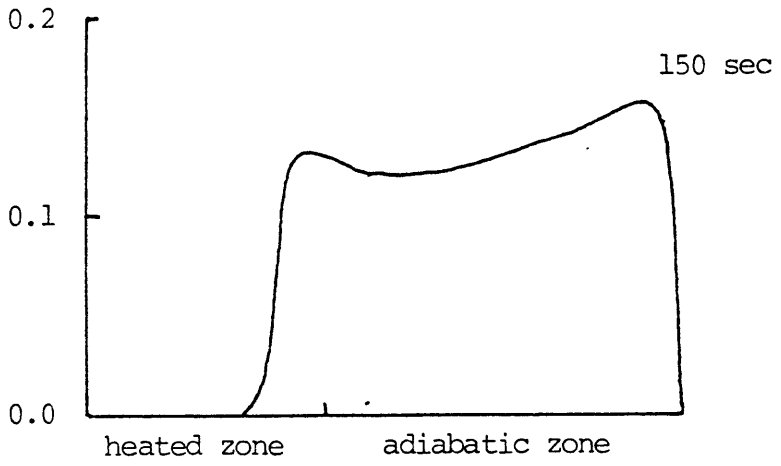

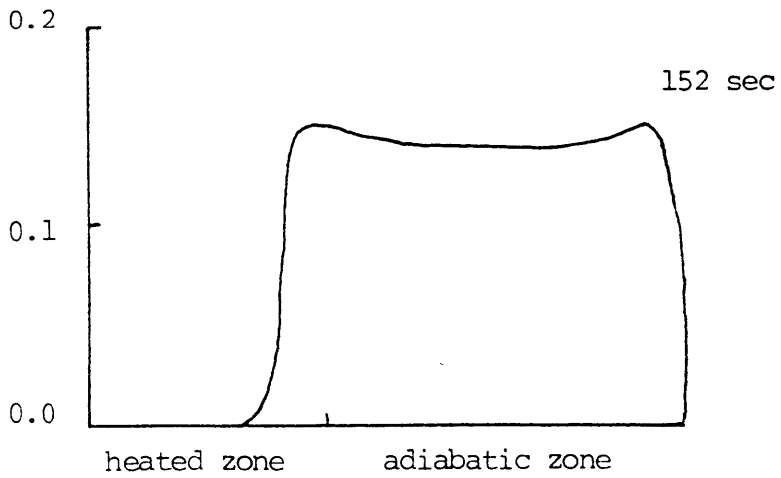

Fig 4.18 Spatial void distribution for simulated 1-D loop with vapor density x200

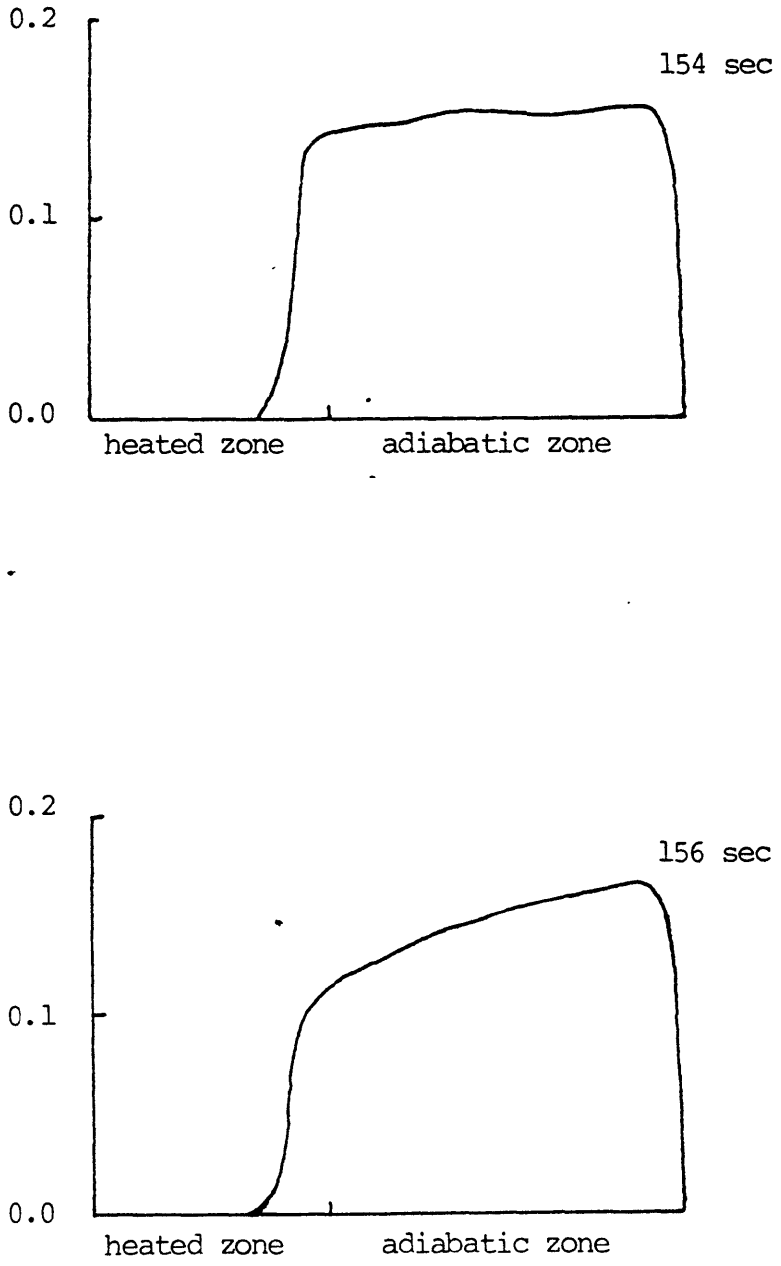

Fig 4.19 Spatial void distribution for simulated 1-D loop with vapor density x200

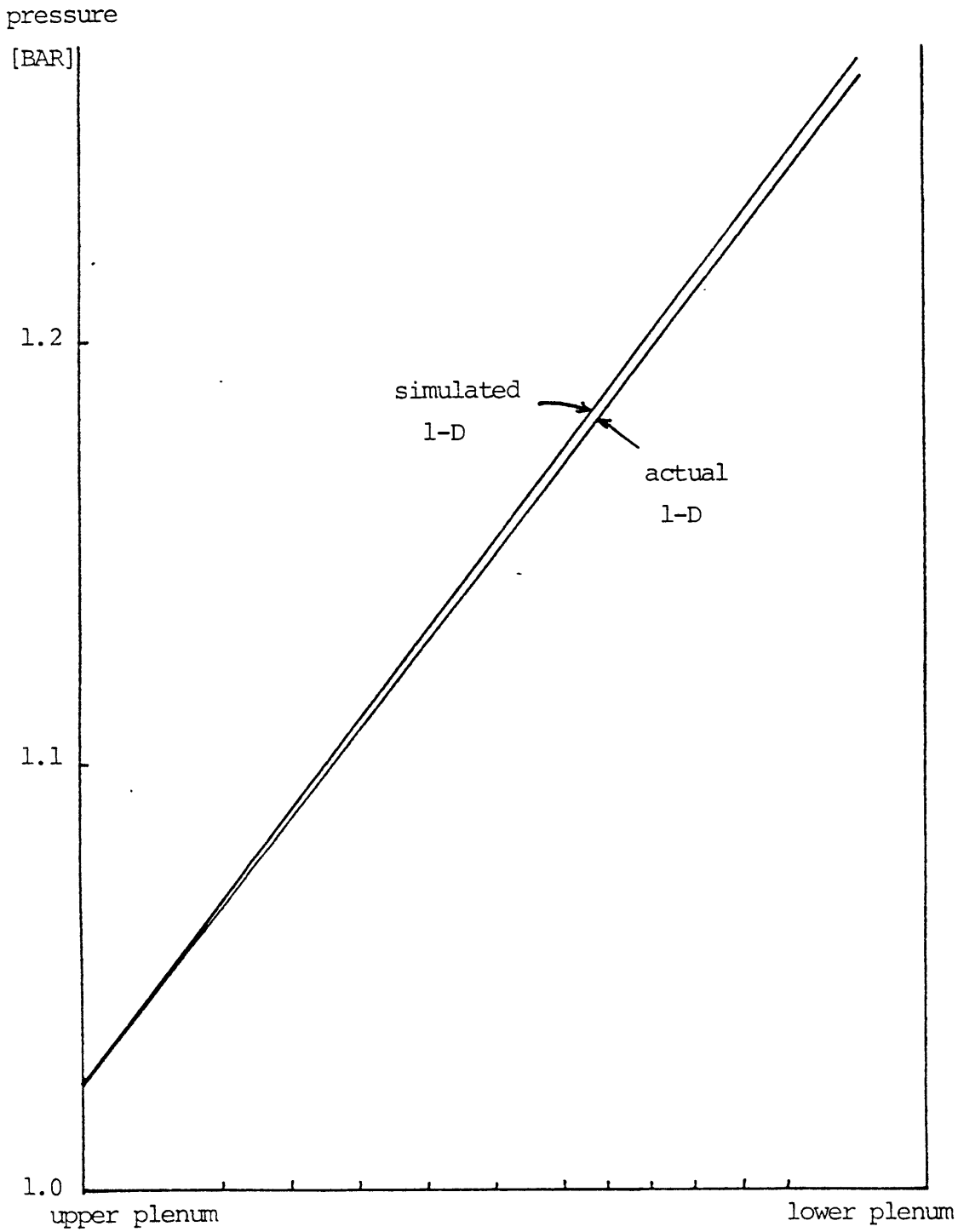

Fig 4.20 Pressure distribution for single phase loop analysis for the test run 107R2

simulated 1-D loop is a little steeper as shown in Fig 4.20. Since the simulated and actual 1-D loop have the same geometry and heat input, they should give exactly the same result. The deviation in the steady-state pressure distri--bution and inlet velocity of the two analyses is due to the different treatment of the transverse wall friction. In the simulated 1-D loop, all the wall friction is treated axially, whereas in the actual 1-D loop a separate correlation is used for the transverse wall friction.

Another source of the deviation in the velocity is the thermal expansion of sodium. In the simulated 1-D loop it adds to the axial velocity, whereas in the actual 1-D loop it adds to the vertical velocity component at the top face of the rectangular pool. However the thermal expansion effect has no relevance for the steady-state results.

4.2 Forced convection

The calculation results for the simulation of the French forced-convection experiment are presented here. Simulation is done for the hypothetical geometry of uniform flow area in axial direction.

Table 4.7 and 4.8 show the calculation results for two different radii tubes, r = 0.002 m and r = 0.003 m. Fig 4.21 is the plot of the results on coordinates of inlet mass flow rate and total pressure drop over the test section.

Table 4.7 Forced-convection calculations for r = 0.002 m

Run	v_{inlet} [m/s]	$\dot{m}$ [kg/s]	ΔP[BAR]	enthalpy rise[kW]	max. slip ratio	max. void fraction	% loss in energy
1-2	10.0	0.106	3.12251	9.962	1.0	0.0	0.38
2-2	5.0	0.053	1.02615	9.994	1.0	0.0	0.06
3-2	4.0	0.042	0.73875	9.996	1.0	0.0	0.04
4-2	3.0	0.032	0.49989	9.998	1.0	0.0	0.02
5-2	2.0	0.021	0.31207	9.999	1.0	0.0	0.01
6-2	1.75	0.019	0.27329	9.999	1.0	0.0	0.01
7-2	1.5	0.016	0.67066	9.996	3.01	0.8192	0.04
8-2	1.4	0.015	1.13522	9.985	3.64	0.8690	0.15
9-2	1.3	0.014	1.72212	9.969	4.18	0.8916	0.31
10-2	1.2		F A I L				

Table 4.8 Forced-convection calculations for r = 0.003 m

Run	v_{inlet} [m/s]	$\dot{m}$ [kg/s]	ΔP[BAR]	enthalpy rise[kW]	max. slip ratio	max. void fraction	% loss in energy
1-3	4.44	0.106	0.57404	9.993	1.0	0.0	0.07
2-3	2.22	0.053	0.26603	9.998	1.0	0.0	0.02
3-3	1.78	0.042	0.22303	9.999	1.0	0.0	0.01
4-3	1.33	0.032	0.18641	9.999	1.0	0.0	0.01
5-3	0.89	0.021	0.15550	10.000	1.0	0.0	0.0
6-3	0.78	0.019	0.14835	10.000	1.0	0.0	0.0
7-3	0.67	0.016	0.39279	9.992	3.83	0.8603	0.08
8-3	0.62	0.015	0.60586	9.978	4.76	0.8971	0.22
9-3	0.58	0.014	0.81121	9.957	5.60	0.9173	0.43
10-3	0.53	0.013	1.00211	9.930	6.42	0.9308	0.70

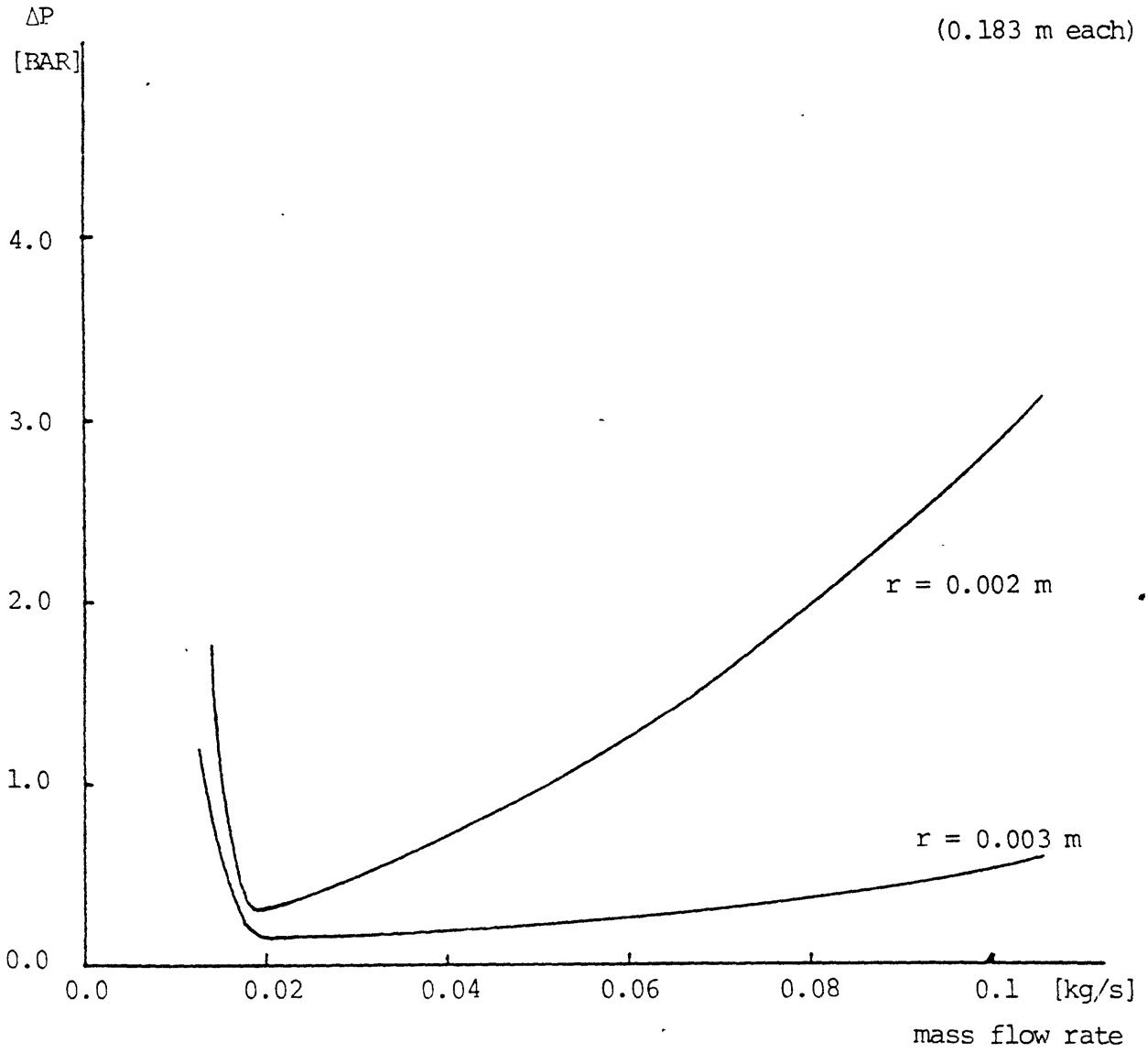

Fig 4.21 S-curve for two different flow areas for the hypothetical French experiment

Note that the minimum point in the so-called S-curve is the boiling inception point.

The code failed at some point in the two-phase region and the inlet mass flow rate could not be reduced any more. As the physical models and the numerical scheme are improved to the state that the S-curve can be completed to the zero mass flow rate, the suggested form of the energy conservation equations in Chapter 3 would have to be used.

A higher velocity will result in a higher frictional pressure drop and more dissipation of the mechanical energy into thermal energy. Hence the fraction of the dissipation thermal energy will increase.

At high inlet velocities the flow is single-phase. As the inlet velocity is decreased and the flow remains single--phase, the energy loss decreases. However upon further flow decrease, boiling begins and the vapor slip increase offsets the flow decrease effect and the net energy loss increases.

The results in Table 4:7 and 4.8 are an indication that the energy loss problem of the present energy conservation equations will become more severe as the calculation goes to a higher void fraction region.

Chapter 5. Discussion of the results

5.1 Natural convection

5.1.1 Test section simulation

5.1.1.1 Steady-state

5.1.1.1.1 Pressure drop

The only parameter that can be checked against experiment in the steady-state is the pressure drop over the test section. Fig 4.1 shows that there is a considerable deviation between the 4-Eq/6-Eq model results and experimental data. The HEM model is even much worse than the 4-Eq/6-Eq model.

The calculated pressure drop is determined by the physical models in the code and the specific way that the experiment is simulated. The physical models directly related with the pressure drop are the wall friction, interfacial mass transfer and interfacial momentum transfer

There may be two sources of error in the pressure drop calculation. One is the error in the physical models related with the pressure drop and the other is the error in simulation of the experiment.

In simulating the test section, some features of the experiment are not taken into account. Since the sodium vapor condenses completely in the upper plenum, there is a pressure rise due to deceleration of sodium. The upper plenum in the

experiment is a single-phase liquid region, whereas the top end in the calculation is a two-phase region. Thus the pressure rise due to deceleration should be considered as an additional term.

Another source of error in simulation is whether the exact positions of manometers coincide with the mesh centers where the pressure is calculated. If the manometer position does not coincide with the center point of a mesh, the pressure difference due to gravity should be taken into consideration.

These two errors are bounded for the test run 129R1.

$$(\text{position deviation}) < 0.5 \text{ m}$$

$$(\text{pressure drop due to position deviation}) < 4000 \text{ Pa}$$

$$(\text{pressure rise due to deceleration}) = \dot{m}[xv_v + (1-x)v_\ell]/A$$
$$= 540 \text{ Pa} < 1000 \text{ Pa}$$

Therefore

$$(\text{Total deviation in pressure drop due to simulation error}) < 5000 \text{ Pa} \quad (0.05 \text{ BAR})$$

The simulation error estimated as 0.05 BAR does not account for the deviation in Fig 4.1. Hence it may be concluded that there is a problem in applying the physical

models in THERMIT to the case of ORNL/TM-7018.

First it is questionable whether the high-speed forced convection correlations in THERMIT give a good result for the low-speed natural convection experiment of ORNL/TM-7018. It is also questionable whether the rod-bundle geometry correlations will be applicable to the circular tube geometry.

One or more of the physical models may be inappropriate due to the different flow condition or geometry, but it is impossible to know which physical model is responsible for the deviation in Fig 4.1. For validation of the physical models, more experimental data are necessary to check with calculation.

The sensitivity of the pressure drop to the wall friction and interfacial momentum transfer will be discussed here. Some intuition for the two-phase wall friction pressure drop can be derived from considering the single-phase case. The single-phase expression for the wall friction pressure drop is,

$$\Delta P = f \frac{L}{De} \frac{\rho v^2}{2} \qquad (5.1)$$

The wall friction factor f is vital for accurate pressure drop prediction, but the calculation in Appendix D shows that f is rather insensitive to the flow condition according to THERMIT wall friction correlations. The error in the wall friction factor is linearly propagated to the pressure drop, i.e. 1% error in f results in 1% error in the pressure drop.

As for the interfacial momentum transfer, it does not affect the pressure drop directly before dryout, but does affect it through the liquid velocity. If there is more inter--facial momentum transfer, a higher liquid velocity will result due to the increased friction force on liquid. A higher liquid velocity will again give rise to a higher pressure drop as Eq 5.1 shows. The interfacial momentum transfer is an import--ant parameter in determining the two-phase condition. It establishes the flow quality and the void fraction, and all the other physical models are strongly dependent on that void fraction.

Moreover the transferred mass carries its own momentum so that the interfacial momentum transfer is composed of two parts, friction forces and momentum carried by the transferred mass.

Sensitivity of the pressure drop to the interfacial momentum transfer is given in Table 4.6. Very large interfa--cial momentum transfer will result in equal velocities of liquid and vapor, therefore the HEM model. The code tends to fail as the interfacial momentum transfer decreases.

5.1.1.1.2 Energy conservation

Table 4.3, 4.7 and 4.8 show that a certain portion of the total energy is lost in THERMIT calculations. The reason for the loss has been given in detail in Chapter 3.

The fraction of the lost energy increases as the total heat input increases. This occurs because at a higher power there is a more interfacial mass transfer and more frictional dissipation due to increased velocities.

The importance of the energy conservation can be illustrated in the following way. A 1% error in the energy corresponds to 1% error in the flow quality. That 1% error in the flow quality may cause a considerable change in the flow condition due to high density ratio between the liquid and vapor phases of sodium at atmospheric pressure. Especially for the dryout point determination, a small amount of error in energy may significantly affect the prediction.

5.1.1.1.3 Comparison of HEM, 4-Eq and 6-Eq models

Table 4.4 and 4.5 show the velocities of the liquid and vapor phases for each model. The HEM model is too far from experimental data, therefore completely erroneous.

As can be seen all through the results, the 4-Eq and 6-Eq models are almost identical. The 6-Eq model can be reduced to the 4-Eq model with the assumption that the liquid and vapor temperatures are equal to the saturation temperature in two-phase region as explained in Chapter 3. Presently THERMIT uses a very large constant for the interfacial heat transfer coefficient so that the liquid and vapor temperatures

are made almost equal to a saturation temperature. Under such a condition, there cannot be much difference between the 4-Eq and 6-Eq model results.

5.1.1.2 Transient

Fig 4.2, 4.3 and 4.4 show that all the parameters oscillate with the same period as the inlet velocity, although with some phase shifts. The phase shift is a characteristic of each parameter and is the final result of all the interac--tions between phases and between the coolant and the wall. Consequently there is no reason that the phase shift of one parameter should be equal to the phase shift of another.

Fig 4.2 shows that the maximum point of the pressure drop corresponds to the minimum point of the inlet velocity, which means a 180° phase shift. Loop analysis results in Chapter 4 show the same behavior between the P and v_{inlet}.

In Fig 4.21, the slope of the S-curve is negative in the two-phase region. If the inlet mass flow rate increases, the pressure drop should decrease and vice versa. Hence the pressure drop should be maximum when the inlet velocity is minimum as Fig 4.2 shows.

5.1.2 Whole loop simulation

5.1.2.1 Oscillation

The simulated 1-D loop analysis has shown that the outputs of the system are oscillatory although all the inputs to the system are constant with respect to time. The experi--mental data also show that the measured parameters oscillate with a certain period, although the inputs are constant.

For the test section simulation in section 5.1.1, the output is constant with constant boundary conditions.

For the simulated 1-D loop analysis, however, a small perturbation from equilibrium state does not damp exponentia--lly, but continues oscillating with constant amplitude. The oscillatory behavior of the two-phase flow in a loop experi--ment is an inherent characteristic of the system.

In early 1960's many people [Ref. 11 - 14] tried to make a general explanation of the two-phase flow oscillations, but were not successful due to lack of knowledge about two-phase flow phenomena and too many parameters that make the analyti--cal analysis impossible.

The calculation of THERMIT with the vapor density 200 times increased has shown that the system keeps on oscilla--ting with a certain period and amplitude after the steady--state boiling has been reached.

5.1.2.2 Mathematical model of oscillation

A mathematical model of the two-phase flow oscillation in a loop is suggested in this section. The idea of the approach is to divide the loop into two regions, the test section and the return loop, and set up mass, momentum and energy conservation equations for both regions. The test section and the return loop conservation equations are coupled through an empirical relation which is obtained from the calculation results and shown in Fig 5.3.

Conservation equations integrated over the test section

Mass

$$\frac{\partial}{\partial t}[V_v\rho_v + V_\ell\rho_\ell + V_{s\ell}\rho_{s\ell}] + \alpha_0\rho_{v0}u_{v0}A + (1-\alpha_0)\rho_{\ell 0}u_{\ell 0}A - \rho_{\ell i}u_{\ell i}A = 0 \qquad (5.3)$$

Energy

$$\frac{\partial}{\partial t}[V_v\rho_v e_v + V_\ell\rho_\ell u + V_{s\ell}\rho_{s\ell}e_{s\ell}] + \alpha_0\rho_{v0}u_{v0}h_{v0}A + (1-\alpha_0)\rho_{\ell 0}u_{\ell 0}h_{\ell 0}A - \rho_{\ell i}u_{\ell i}h_{\ell i}A = Q_w \qquad (5.4)$$

Momentum

$$\frac{\partial}{\partial t}[V_v\rho_v u_v + V_\ell\rho_\ell u_\ell + V_{s\ell}\rho_{s\ell}u_{s\ell}] + \alpha_0\rho_{v0}u_{v0}^2A + (1-\alpha_0)\rho_{\ell 0}u_{\ell 0}^2A - \rho_{\ell i}u_{\ell i}^2A + (P_0'-P_i)A = -F_w - [V_v\rho_v + V_\ell\rho_\ell + V_{s\ell}\rho_{s\ell}]g \qquad (5.5)$$

where Q_w is the total heat input and F_w is the total wall friction force in upward direction.

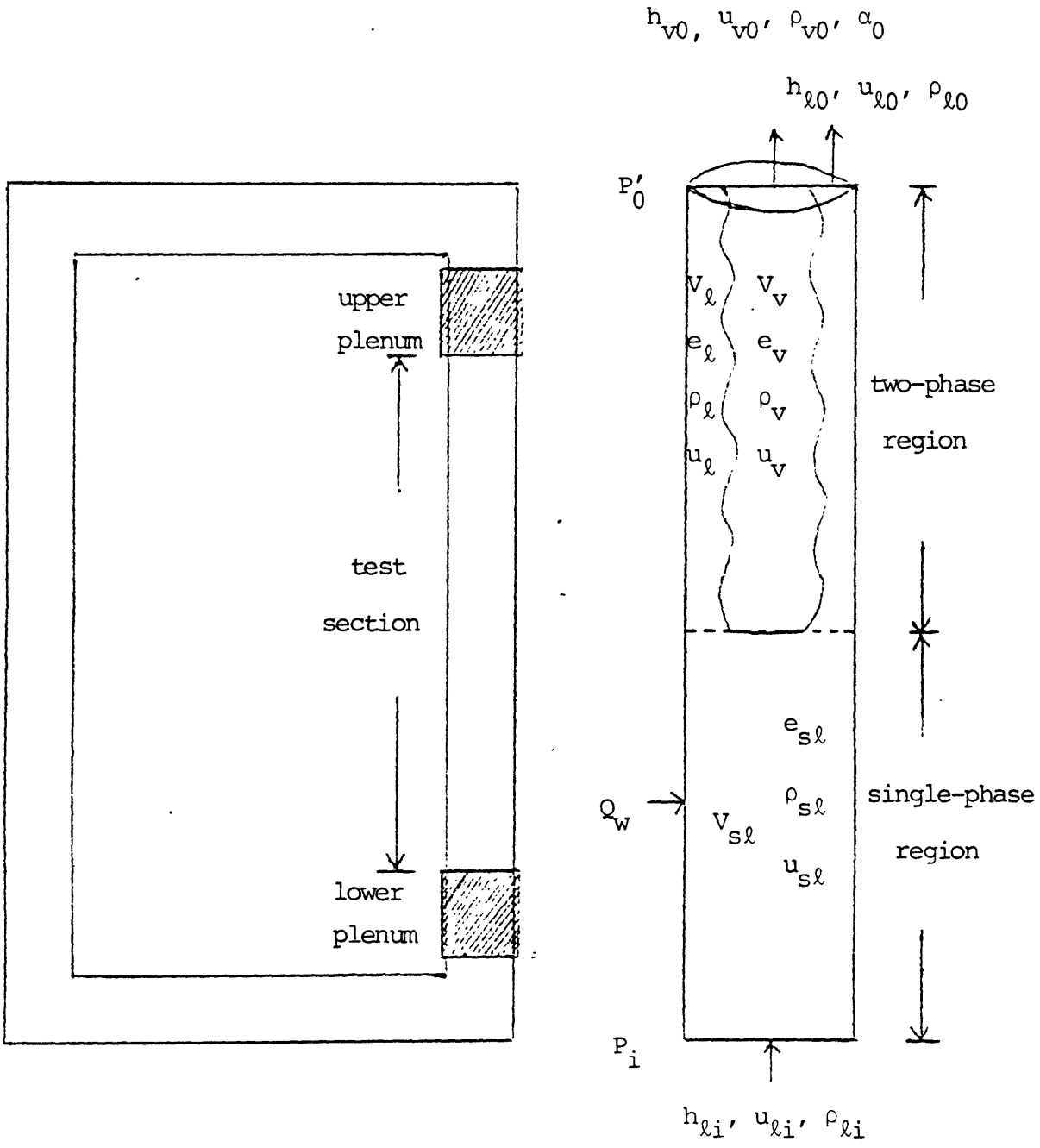

Fig 5.1 Schematic diagram of the loop and the test section

Notations

h_{v0}, $h_{\ell 0}$, ρ_{v0}, $\rho_{\ell 0}$, u_{v0}, $u_{\ell 0}$: enthalpy, density, and velocity of each phase at the outlet

$h_{\ell i}$, $\rho_{\ell i}$, $u_{\ell i}$: enthalpy, density and velocity of liquid at the inlet

α_0 : void fraction at the outlet

A : cross-sectional flow area

V_v, V_ℓ, $V_{s\ell}$: volumes of vapor and liquid in the two-phase region and the liquid in the single-phase region

e_v, e_ℓ, ρ_v, ρ_ℓ, u_v, u_ℓ : spatial averages of internal energy, density and velocity of each phase in the two-phase region

$e_{s\ell}$, $\rho_{s\ell}$, $u_{s\ell}$: spatial averages of internal energy, density and velocity of liquid in the single-phase region

P'_0 : pressure at the bottom face of the upper plenum

P_0 : pressure at the top face of the upper plenum

P'_i : pressure at the bottom face of the lower plenum

P_i : pressure at the top face of the lower plenum

Conservation equations at equilibrium state

$$\frac{\partial}{\partial t} = 0$$

Mass
$$\alpha_0 \rho_{v0} \bar{u}_{v0} A + (1-\alpha_0) \rho_{\ell 0} \bar{u}_{\ell 0} A - \rho_{\ell i} \bar{u}_{\ell i} A = 0 \qquad (5.6)$$

Energy
$$\alpha_0 \rho_{v0} \bar{u}_{v0} h_{v0} A + (1-\alpha_0) \rho_{\ell 0} \bar{u}_{\ell 0} h_{\ell 0} A - \rho_{\ell i} \bar{u}_{\ell i} h_{\ell i} A = Q_w \qquad (5.7)$$

Moemntum
$$\alpha_0 \rho_{v0} \bar{u}^2_{v0} A + (1-\alpha_0) \rho_{\ell 0} \bar{u}^2_{\ell 0} A - \rho_{\ell i} \bar{u}^2_{\ell i} A + (P'_0 - \bar{P}_i) A = -\bar{F}_w - [\bar{V}_v \rho_v + \bar{V}_\ell \rho_\ell + V_{s\ell} \rho_{s\ell}] g \qquad (5.8)$$

In the above equilibrium state equations, it is assumed that u_{v0}, $u_{\ell 0}$, $u_{\ell i}$, V_v, V_ℓ, P_i and F_w are time-dependent variables and all the other parameters are constant. When the equilibrium conservation equations are subtracted from the time-dependent conservation equations, the perturba-tion equations are obtained.

Perturbation equations

Mass
$$\rho_v \frac{\partial}{\partial t}(V_v - \bar{V}_v) + \rho_\ell \frac{\partial}{\partial t}(V_\ell - \bar{V}_\ell) + \alpha_0 \rho_{v0} (u_{v0} - \bar{u}_{v0}) A + (1-\alpha_0) \rho_{\ell 0} (u_{\ell 0} - \bar{u}_{\ell 0}) A - \rho_{\ell i} (u_{\ell i} - \bar{u}_{\ell i}) A = 0 \qquad (5.9)$$

Energy $$\rho_v e_v \frac{\partial}{\partial t}(V_v-\bar{V}_v) + \rho_\ell e_\ell \frac{\partial}{\partial t}(V_\ell-\bar{V}_\ell) + \alpha_0 \rho_{v0}(u_{v0}-\bar{u}_{v0})h_{v0}A$$

$$+ (1-\alpha_0)\rho_{\ell 0}(u_{\ell 0}-\bar{u}_{\ell 0})h_{\ell 0}A - \rho_{\ell i}(u_{\ell i}-\bar{u}_{\ell i})h_{\ell i}A = 0 \qquad (5.10)$$

Momentum $$\rho_v u_v \frac{\partial}{\partial t}(V_v-\bar{V}_v) + \rho_\ell u_\ell \frac{\partial}{\partial t}(V_\ell-\bar{V}_\ell) + \rho_v V_v \frac{\partial}{\partial t}(u_v-\bar{u}_v)$$

$$+ \rho_\ell V_\ell \frac{\partial}{\partial t}(u_\ell-\bar{u}_\ell) + \rho_{s\ell} V_{s\ell} \frac{\partial}{\partial t}(u_{s\ell}-\bar{u}_{s\ell})$$

$$+ \alpha_0 \rho_{v0}(u_{v0}^2-\bar{u}_{v0}^2)A + (1-\alpha_0)\rho_{\ell 0}(u_{\ell 0}^2-\bar{u}_{\ell 0}^2)A$$

$$- \rho_{\ell i}(u_{\ell i}^2-\bar{u}_{\ell i}^2)A - (P_i-\bar{P}_i)A = -(F_w-\bar{F}_w)$$

$$- [(V_v-\bar{V}_v)\rho_v + (V_\ell-\bar{V}_\ell)\rho_\ell]g \qquad (5.11)$$

Since $V_{s\ell}$ is assumed to be constant, $V_v + V_\ell$ = (constant). Thus

$$V_\ell - \bar{V}_\ell = -(V_v - \bar{V}_v) \qquad (5.12)$$

$$\frac{\partial}{\partial t}(V_\ell - \bar{V}_\ell) = -\frac{\partial}{\partial t}(V_v - \bar{V}_v) \qquad (5.13)$$

The perturbation equations may be written as follows.

Mass $$(\rho_v-\rho_\ell)\frac{\partial}{\partial t}(V_v-\bar{V}_v) + \alpha_0 \rho_{v0}(u_{v0}-\bar{u}_{v0})A$$

$$+ (1-\alpha_0)\rho_{\ell 0}(u_{\ell 0}-\bar{u}_{\ell 0})A - \rho_{\ell i}(u_{\ell i}-\bar{u}_{\ell i})A = 0 \qquad (5.14)$$

Energy $$(\rho_v e_v - \rho_\ell e_\ell)\frac{\partial}{\partial t}(V_v - \bar{V}_v) + \alpha_0 \rho_{v0}(u_{v0} - \bar{u}_{v0})h_{v0}A$$

$$+ (1-\alpha_0)\rho_{\ell 0}(u_{\ell 0} - \bar{u}_{\ell 0})h_{\ell 0}A - \rho_{\ell i}(u_{\ell i} - \bar{u}_{\ell i})h_{\ell i}A = 0 \qquad (5.15)$$

Momentum $$(\rho_v u_v - \rho_\ell u_\ell)\frac{\partial}{\partial t}(V_v - \bar{V}_v) + \rho_v V_v \frac{\partial}{\partial t}(u_v - \bar{u}_v) + \rho_\ell V_\ell \frac{\partial}{\partial t}(u_\ell - \bar{u}_\ell)$$

$$+ \rho_{s\ell} V_{s\ell}\frac{\partial}{\partial t}(u_{s\ell} - \bar{u}_{s\ell}) + \alpha_0 \rho_{v0}(u_{v0}^2 - \bar{u}_{v0}^2)A$$

$$+ (1-\alpha_0)\rho_{\ell 0}(u_{\ell 0}^2 - \bar{u}_{\ell 0}^2)A - \rho_{\ell i}(u_{\ell i}^2 - \bar{u}_{\ell i}^2)A - (P_i - \bar{P}_i)A$$

$$= -(F_w - \bar{F}_w) - (V_v - \bar{V}_v)(\rho_v - \rho_\ell)g \qquad (5.16)$$

The momentum conservation equation is simplified to make it a linear differential equation.

$$(\rho_v \bar{u}_v - \rho_\ell \bar{u}_\ell)\frac{\partial}{\partial t}(V_v - \bar{V}_v) + \rho_v \bar{V}_v \frac{\partial}{\partial t}(u_v - \bar{u}_v) + \rho_\ell \bar{V}_\ell \frac{\partial}{\partial t}(u_\ell - \bar{u}_\ell)$$

$$+ \rho_{s\ell} V_{s\ell}\frac{\partial}{\partial t}(u_{s\ell} - \bar{u}_{s\ell}) + 2\alpha_0 \rho_{v0}\bar{u}_{v0}(u_{v0} - \bar{u}_{v0})A$$

$$+ 2(1-\alpha_0)\rho_{\ell 0}\bar{u}_{\ell 0}(u_{\ell 0} - \bar{u}_{\ell 0})A - 2\rho_{\ell i}u_{\ell i}(u_{\ell i} - \bar{u}_{\ell i})A$$

$$- (P_i - \bar{P}_i)A = -(F_w - \bar{F}_w) - (V_v - \bar{V}_v)(\rho_v - \rho_\ell)g \qquad (5.17)$$

Conservation equations integrated over the return loop

For the return loop, the mass and energy conservation equations are not needed because the return loop is adiabatic

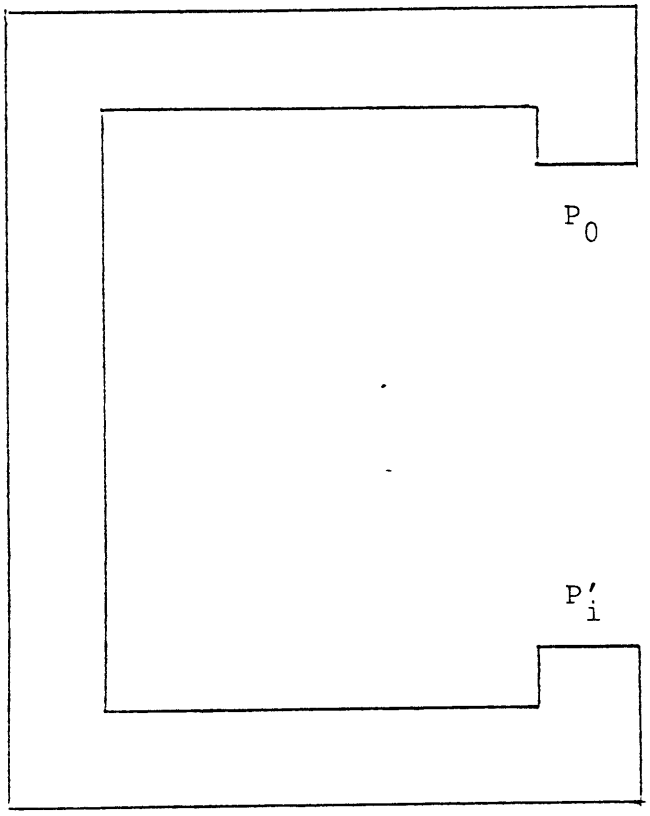

Fig 5.2 Return loop

and has uniform flow area.

Mass u_r is constant all through the return loop.

Energy e_r is constant all through the return loop.

Momentum

$$\frac{\partial}{\partial t}(M_r u_r) + (P_i' - P_0)A = M_{rg} g - F_{rw} \tag{5.18}$$

Momentum at equilibrium

$$(\bar{P}_i' - P_0)A = -M_{rg} g - \bar{F}_{rw} \tag{5.19}$$

Perturbation equation for momentum

$$M_r \frac{\partial}{\partial t}(u_r - \bar{u}_r) + (\bar{P}_i' - \bar{P}_i')A = -(F_{rw} - \bar{F}_{rw}) \tag{5.20}$$

Assume that

$$u_r = C u_{\ell i} \tag{5.21}$$

Since the temperatures of the coolant in the return loop and lower plenum are constant with respect to time, C is constant. Note that C is greater than one because the sodium density increases as the temperature decreases. The following momentum conservation equation for the return loop is obtained.

$$M_r C \frac{\partial}{\partial t}(u_{\ell i} - \bar{u}_{\ell i}) + (P_i - \bar{P}_i)A = -(F_{rw} - \bar{F}_{rw}) \tag{5.22}$$

Now the conservation equations for the test section and the return loop are completely set up and they should be combined together to produce a single ordinary differential equation with respect to time. In the process, the following additional assumptions are made.

$$u_v = u_{v0}$$

$$u_\ell = u_{\ell 0}$$

$$u_{s\ell} = u_{\ell i} \qquad (5.23)$$

$$P_i - \bar{P}_i = P_i' - \bar{P}_i'$$

Up to this point, four Eq's 5.14, 5.15, 5.17 and 5.22 with five unknowns u_{v0}-u_{v0}, $u_{\ell 0}$-$u_{\ell 0}$, $u_{\ell i}$-$u_{\ell i}$, P_i-P_i and V_v-V_v are obtained. Hence we need an additional relation between the unknowns and it is provided by the empirical relation between P_i-$\bar{P}_i$ and V_v-$\bar{V}_v$ in Fig 5.3. Fig 5.3 is a plot of the THERMIT calculational results and is expressed by the following Eq 5.24.

$$P_i - \bar{P}_i = - \frac{K}{A} g(\rho_\ell - \rho_v)(V_v - \bar{V}_v) \qquad (5.24)$$

where K = 0.5

Now the set of Eq's 5.14, 5.15, 5.17, 5.22 and 5.24 can be solved with following wall friction correlations.

$$F_{rw} - \bar{F}_{rw} = f_1(u_{\ell i} - \bar{u}_{\ell i}) \tag{5.25}$$

$$F_w - \bar{F}_w = f_2(u_{\ell i} - \bar{u}_{\ell i}) + f_3(u_\ell - \bar{u}_\ell) \tag{5.26}$$

After some manipulations, the following second-order ordinary differential equation with respect to $V_v - \bar{V}_v$ results.

$$\frac{d^2}{dt^2}(V_v - \bar{V}_v) + C_1\frac{d}{dt}(V_v - \bar{V}_v) + C_2(V_v - \bar{V}_v) = 0 \tag{5.27}$$

where C_1 and C_2 are constants.

Eq 5.27 yields a simple oscillation if the following condition is satisfied.

$$C_1^2 << 4C_2 \tag{5.28}$$

Then the period of the oscillation is,

$$T = \frac{2\pi}{\sqrt{C_2}} \tag{5.29}$$

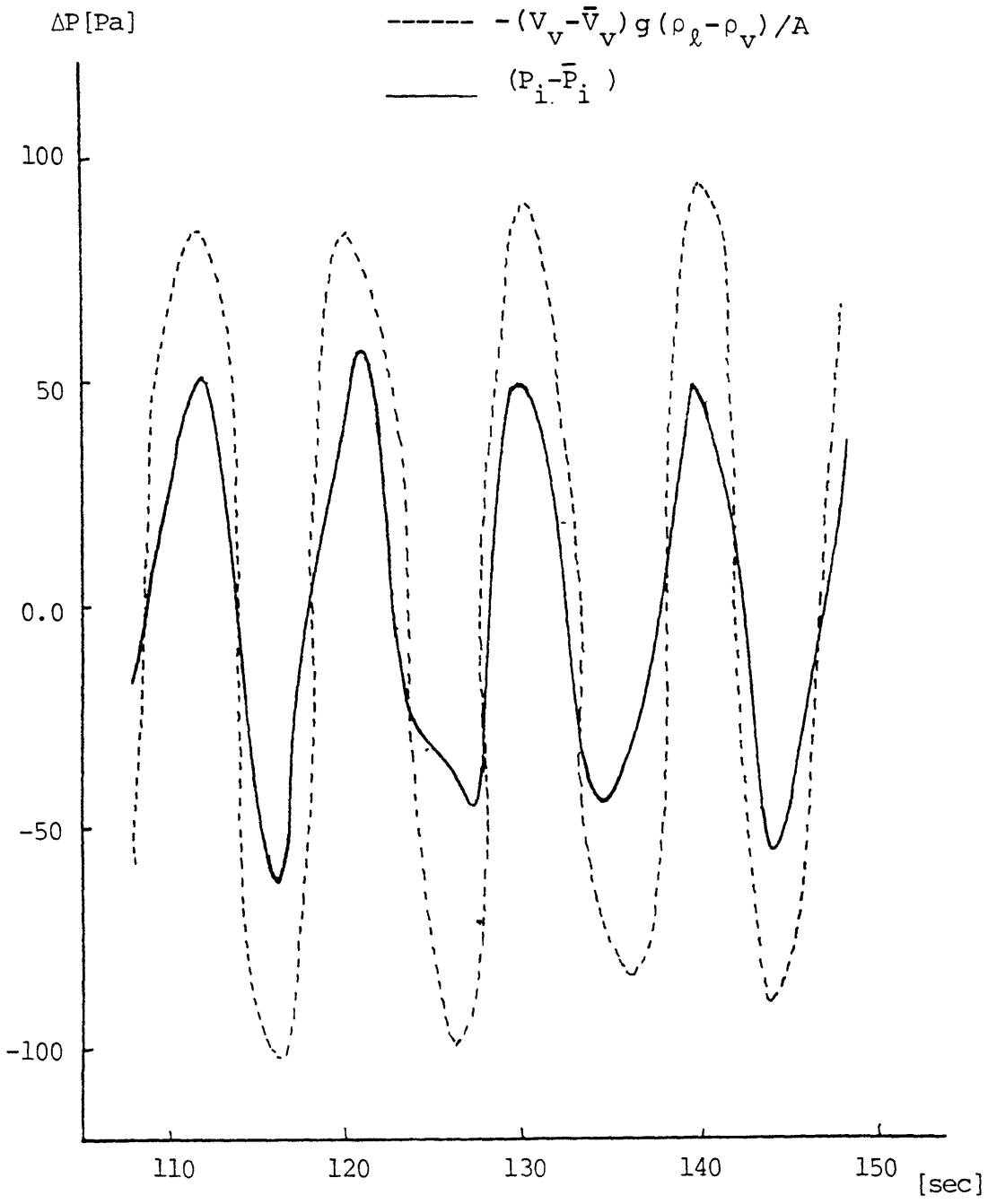

Fig 5.3 Calculation results that show the relationship between $P_i-\bar{P}_i$ and $V_v-\bar{V}_v$

Chapter 6. Conclusions

THERMIT is a good numerical tool for predicting and analyzing sodium two-phase flow phenomena, although there are some problems to be solved.

The two fluid model of THERMIT is a versatile model that can describe a wide range of flow conditions. However, the constitutive relations of the two fluid model are not in a well-established state, especially the interfacial mass and energy transfer terms.

To circumvent the difficulty, the 4-Eq model is deve--loped, in which the interfacial mass and energy transfer occur instantaneously to maintain thermal equilibrium betw--een phases.

The numerical scheme of THERMIT works well for a low density ratio of the liquid and vapor phases. For the high density ratio of sodium at atmospheric pressure, the code fails to converge for conditions of boiling inception and condensation.

For the present the THERMIT calculation results are not in good agreement with the experiment data, but the general tendency and the order of magnitude of the results are right.

THERMIT is a powerful tool in the sense that it can easily accept the developments that will be made in the

future. If more studies on the numerical and physical models would be done, THERMIT might be improved to the state that it can handle a wide range of real LMFBR accident con--ditions.

Chapter 7. Recommendations for future work

1. Improvement of the physical models in THERMIT

   Problems discussed in Chapter 3 will have to be solved.

   a. Forced and natural convection correlations

   b. Flow regime dependence

   c. Condensation modeling

      Interfacial mass transfer

      Interfacial energy transfer

   d. Geometry dependence

2. Validation of the physical models against experiments

   More experiments should be done to test the physical models.

3. Improvement of the overall numerical scheme in THERMIT

   The code failed at a high density ratio of liquid and vapor phases in the present application.

4. Improvement of the loop simulation method

   Implicit numerical scheme may be used to hold the plenum conditions more accurately.

   It is also possible to keep the plenum conditions by a large heat transfer through the structural material.

5. Mathematical model for the oscillation in a two-phase loop experiment

   More general and complete explanation of the two-phase oscillations should be done. THERMIT may be a helpful for this work.

6. Modification of THERMIT momentum conservation equations to accept a variable flow area in axial direction.

References

[1] Reed, W.H., Stewart, H.B., "THERMIT, A Computer pro--gram for Three-dimensional Thermalhydraulic Analysis of LWR Cores," EPRI NP-2032 Project518, Final Report, Sep. 1981.

[2] Garrison, P.W. et al, "Dryout Measurements for Sodium Natural Convection in a Vertical Channel," ORNL/TM--7018 (December 1979)

[3] Costa, J. and Charlety, P., "Forced Convection Boiling of Sodium in a Narrow Channel," in Liquid Metal Heat Transfer and Fluid Dynamics, ASME winter annual meeting, New York, Nov. 1970.

[4] Wilson, G.J., "Development of Models for the Sodium Version of the Two-phase Three-dimensional Thermal--hydraulics Code THERMIT," M.S. Thesis, Department of Nuclear Engineering, MIT, (1980)

[5] Autruffe, M.A., "Theoretical Study of Thermohydraulic Phenomena for LMFBR Accident Analysis," M.S. Thesis, Department of Nuclear Engineering, MIT, (1978)

[6] Collier, J.G., Convective Boiling and Condensation, McGraw-Hill International Book Company, 2nd ed., (1980)

[7] El-Wakil, M.M., Nuclear Heat Transport, International Textbook Company, Scranton, Pa., (1971)

[8] Tang, Y.S., Coffield, R.D., Markley, R.A., Thermal Ana--lysis of Liquid Metal Fast Breeder Reactors, American Nuclear Society, (1978)

[9] Seiler, J.M., "Sodium Boiling Under Single Channel Na--tural Convection Conditions; Calculational Results and Analysis of ORNL/SBT Experimental Results," AIChE, NewOrleans, Nov 8-12, 1981

[10] Lahey, Jr R.T., "Nuclear System Safety Modelling," in Nuclear Reactor Safety Heat Transfer, O.C. Jones, editor Hemisphere McGrawHill, 1981

[11] Quandt, E.R., "Analysis and Measurement of Flow Oscilla--tions," Chem. Eng. Progr., Monograph and Symposium Seri--es No. 32S, p.111.

[12] Wissler, E.H., Isbin, H.S., Amundson, N.R., "Oscillatory Behavior of a Two-phase Natural-circulation Loop," Am. Inst. Chem. Eng. J., 3(1956)2.

[13] Wallis, G.B., Heasley, J.H., "Oscillations in Two-phase Flow Systems," J. Heat Transfer, Trans. ASME Series C, 83(363)369.

[14] Levy, S., Beckjord, E.S., "Hydraulic Instability in a Natural Circulation Loop with Net Steam Generation at 1000 psia," ASME Paper 60-HT-27, 1960.

[15] Personal communications with Dr. Allan Levin in Oak Ridge National Laboratory.

Appendix A. Calibration of heat input

Outer wall temperature data of experiment in adiabatic zone

	107R2	108R2	100R3	100R2	100R4
TE 124	763°C	864°C	907°C	873°C	845°C
TE 125	754	856	898	863	848
TE 126	756	865	906	871	870
TE 127	754	873	900	866	875
TE 128	763	884	893	856	877
TE 129	763	881	881	845	874
TE 130	762	875	886	852	880
AVERAGE	759.3	871.1	895.9	860.9	867.0

The temperature difference between sodium and outer wall is about 11°C. Therefore the sodium temperature is calculated as follows.

107R2	300W	759.3 + 11 = 770.3°C
108R2	500W	871.1 + 11 = 882.1
100R3	700W	895.9 + 11 = 906.9
100R2	700W	860.9 + 11 = 871.9
100R4	800W	867.0 + 11 = 878.0

Test No.	Power given in ORNL/TM-7018	ΔT (measured)	ΔT (calculated with 70% power)
107R2	300 W	350.3°C	279.65°C
108R2	500	462.1	362.35
100R3	700	486.9	455.55
100R4	800	458	472.95

Since the total heat input appears as the enthalpy increase of the single-phase liquid sodium,

$$\dot{Q}_{\substack{\text{actual power} \\ \text{input}}} = \dot{m}\, c_p\, \Delta T_{\text{measured}}$$

$$\dot{m} = (\text{density}) \times (\text{volumetric flow rate}_{\text{measured}})$$

where $c_p = 1447$ J/kg °C

As a result of the calculations,

Test No.	Power given in ORNL/TM-7018	70% Of the power given in ORNL/TM-7018	Actual power input
107R2	300 W	210 W	263.3 W
108R2	500	350	446.6
100R3	700	490	522.9
100R4	800	560	541.1

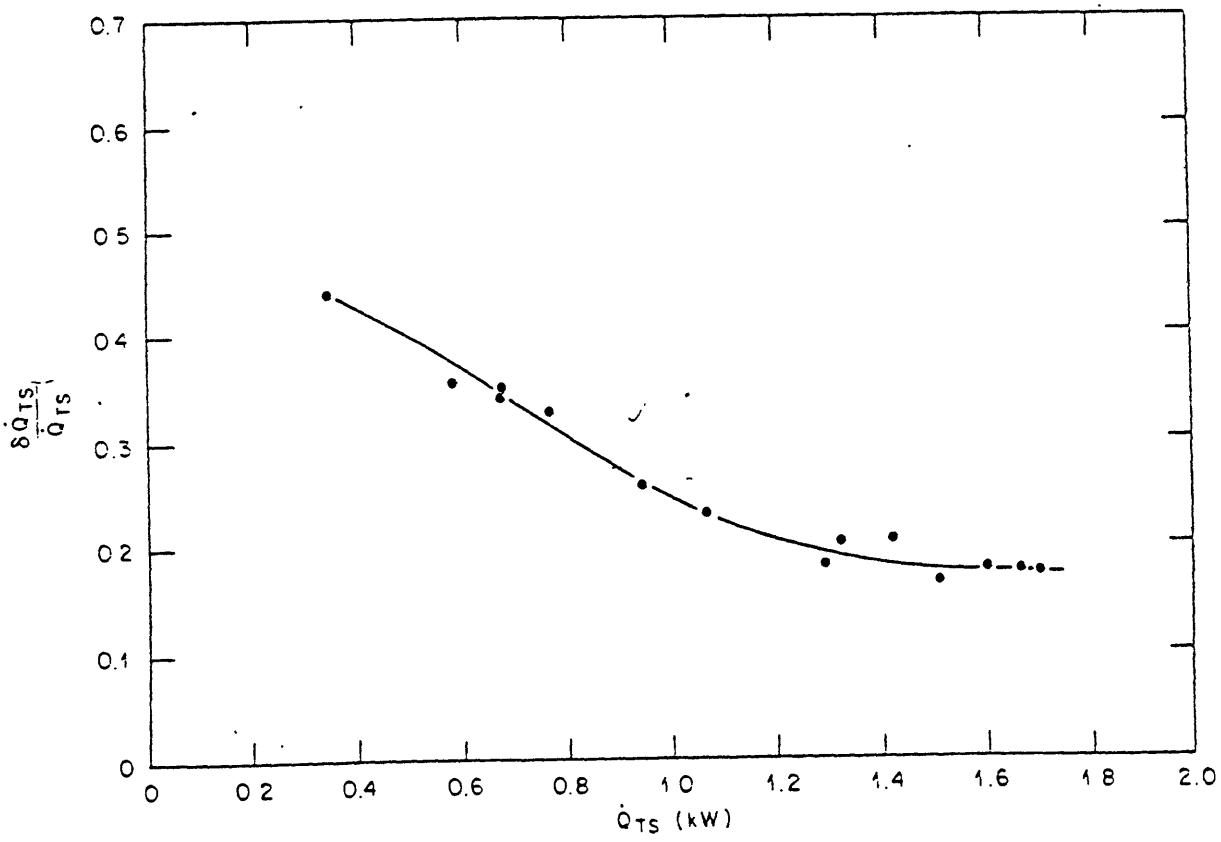

Fig A1. Relative error in test section power determination as a function of test section power

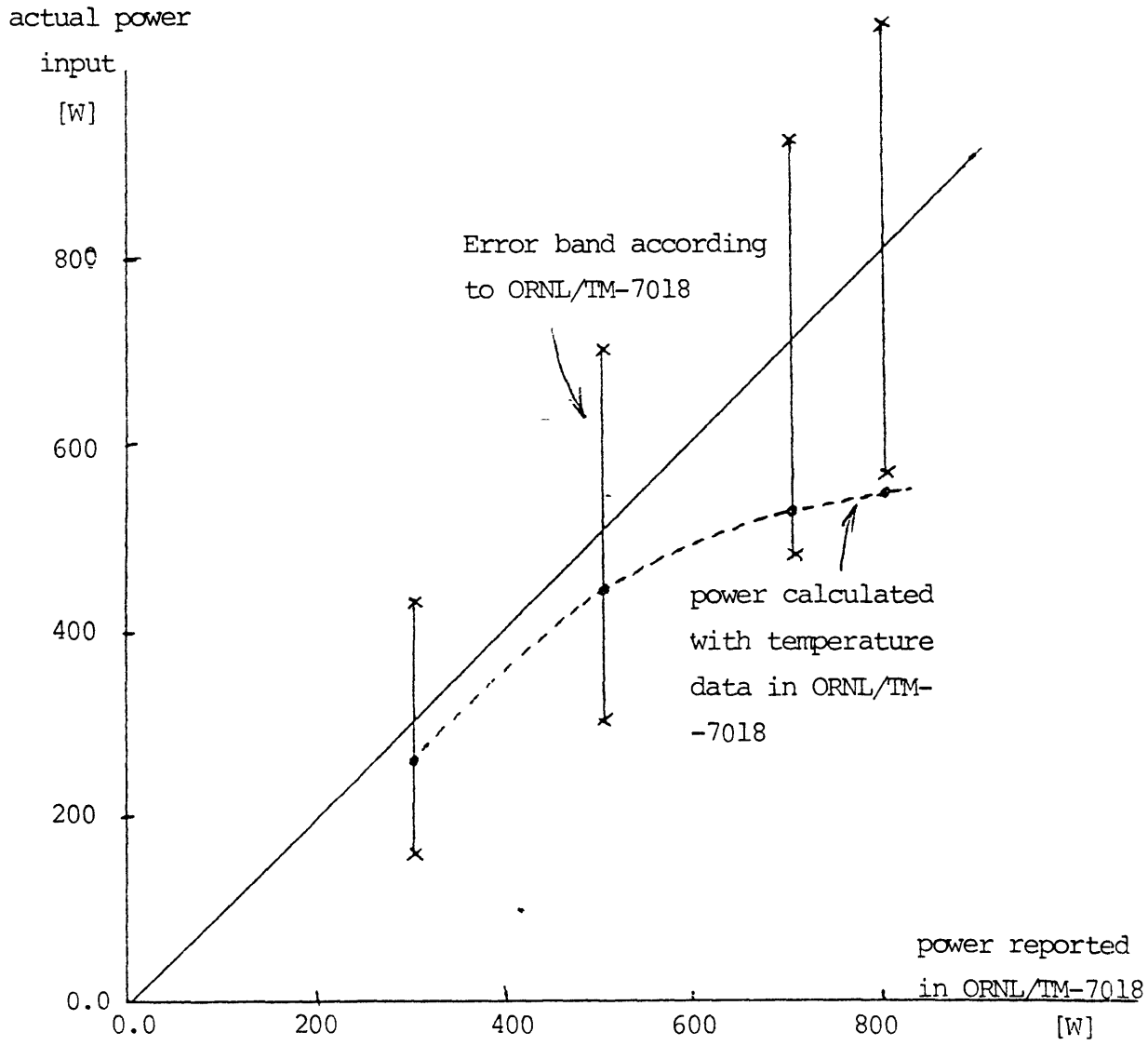

Fig A2. Comparison of the actual power and the reported power in ORNL/TM-7018

Appendix B. Energy conservation of THERMIT

THERMIT conservation equations for 1-D steady-state

Mass

$$\frac{\partial}{\partial z}(\alpha\rho_v v_{vz}) = \Gamma \tag{B1}$$

$$\frac{\partial}{\partial z}[(1-\alpha)\rho_\ell v_{\ell z}] = -\Gamma \tag{B2}$$

Momentum

$$\frac{\partial}{\partial z}(\alpha\rho_v v_{vz}^2) + \alpha\frac{\partial P}{\partial z} = -F_{wv} - F_i - \alpha\rho_v g_z \tag{B3}$$

$$\frac{\partial}{\partial z}[(1-\alpha)\rho_\ell v_{\ell z}^2] + (1-\alpha)\frac{\partial P}{\partial z} = -F_{w\ell} + F_i - (1-\alpha)\rho_\ell g_z \tag{B4}$$

Energy

$$\frac{\partial}{\partial z}(\alpha\rho_v e_v v_{vz}) + P\frac{\partial}{\partial z}(\alpha v_{vz}) = Q_{wv} + Q_i \tag{B5}$$

$$\frac{\partial}{\partial z}[(1-\alpha)\rho_\ell e_\ell v_{\ell z}] + P\frac{\partial}{\partial z}[(1-\alpha)v_{\ell z}] = Q_{w\ell} - Q_i \tag{B6}$$

First law of thermodynamics

$$\frac{\partial}{\partial z}[\alpha\rho_v v_{vz}(h_v + \frac{v_{vz}^2}{2} + g_z z)] = Q_{wv} + Q_i \tag{B7}$$

$$\frac{\partial}{\partial z}[(1-\alpha)\rho_\ell v_{\ell z}(h_\ell + \frac{v_{\ell z}^2}{2} + g_z z)] = Q_{w\ell} - Q_i \tag{B8}$$

Reexpressing Eq B5 and B6 in terms of enthalpy,

$$\frac{\partial}{\partial z}(\alpha\rho_v h_v v_{vz}) - \alpha v_{vz}\frac{\partial P}{\partial z} = Q_{wv} + Q_i \tag{B9}$$

$$\frac{\partial}{\partial z}[(1-\alpha)\rho_\ell h_\ell v_{\ell z}] - (1-\alpha)v_{\ell z}\frac{\partial P}{\partial z} = Q_{w\ell} - Q_i \qquad \text{(B10)}$$

Multiplying Eq B3 and B4 by the respective phasic velocities, the mechanical energy conservations are obtained as follows.

$$-\alpha v_{vz}\frac{\partial P}{\partial z} = v_{vz}\frac{\partial}{\partial z}(\alpha\rho_v v_{vz}^2) + (F_{wv} + F_i + \alpha\rho_v g_z)v_{vz} \qquad \text{(B11)}$$

$$-(1-\alpha)v_{\ell z}\frac{\partial P}{\partial z} = v_{\ell z}\frac{\partial}{\partial z}[(1-\alpha)\rho_\ell v_{\ell z}^2] + [F_{w\ell} - F_i + (1-\alpha)\rho_\ell g_z]v_{\ell z} \qquad \text{(B12)}$$

The THERMIT energy conservation equations are obtained by substituting Eq B11 and B12 into Eq B9 and B10. The terms $v_{vz}\frac{\partial}{\partial z}(\alpha\rho_v v_{vz}^2)$ and $\alpha\rho_v g_z$ and their liquid counterparts are transformed through the following procedure.

$$v_{vz}\frac{\partial}{\partial z}(\alpha\rho_v v_{vz}^2) = \alpha\rho_v v_{vz}^2\frac{\partial v_{vz}}{\partial z} + v_{vz}^2\frac{\partial}{\partial z}(\alpha\rho_v v_{vz}) \qquad \text{(B13)}$$

$$\frac{\partial}{\partial z}(\tfrac{1}{2}\alpha\rho_v v_{vz}^3) = \frac{\alpha\rho_v v_{vz}}{2}\,2v_{vz}\frac{\partial v_{vz}}{\partial z} + \frac{v_{vz}^2}{2}\frac{\partial}{\partial z}(\alpha\rho_v v_{vz})$$

$$= \alpha\rho_v v_{vz}^2\frac{\partial v_{vz}}{\partial z} + \frac{v_{vz}^2}{2}\frac{\partial}{\partial z}(\alpha\rho_v v_{vz}) \qquad \text{(B14)}$$

Therefore

$$v_{vz}\frac{\partial}{\partial z}(\alpha\rho_v v_{vz}^2) = \frac{\partial}{\partial z}(\tfrac{1}{2}\alpha\rho_v v_{vz}^3) + \frac{v_{vz}^2}{2}\frac{\partial}{\partial z}(\alpha\rho_v v_{vz}) \qquad \text{(B15)}$$

Utilizing Eq B1, Eq B15 reduces to

$$v_{vz} \frac{\partial}{\partial z}(\alpha \rho_v v_{vz}^2) = \frac{\partial}{\partial z}(\frac{1}{2}\alpha \rho_v v_{vz}^3) + \frac{\Gamma}{2} v_{vz}^2 \qquad \text{(B16)}$$

Similarly for the liquid, utilizing Eq B2,

$$v_{\ell z} \frac{\partial}{\partial z}[(1-\alpha)\rho_\ell v_{\ell z}^2] = \frac{\partial}{\partial z}[\frac{1}{2}(1-\alpha)\rho_\ell v_{\ell z}^3] + \frac{v_{\ell z}^2}{2} \frac{\partial}{\partial z}[(1-\alpha)\rho_\ell v_{\ell z}]$$

$$= \frac{\partial}{\partial z}[\frac{1}{2}(1-\alpha)\rho_\ell v_{\ell z}^3] - \frac{\Gamma}{2} v_{\ell z}^2 \qquad \text{(B17)}$$

Similar procedure is applied to the potential terms in Eq B7 and B8 so that the following equations result.

$$\alpha \rho_v g_z v_{vz} = \frac{\partial}{\partial z}(\alpha \rho_v g_z v_{vz} z) - z \frac{\partial}{\partial z}(\alpha \rho_v g_z v_{vz})$$

$$= \frac{\partial}{\partial z}(\alpha \rho_v g_z v_{vz} z) - z g_z \Gamma \qquad \text{(B18)}$$

$$(1-\alpha)\rho_\ell g_z v_{\ell z} = \frac{\partial}{\partial z}[(1-\alpha)\rho_\ell g_z v_{\ell z} z] - z \frac{\partial}{\partial z}[(1-\alpha)\rho_\ell g_z v_{\ell z}]$$

$$= \frac{\partial}{\partial z}[(1-\alpha)\rho_\ell g_z v_{\ell z} z] + z g_z \Gamma \qquad \text{(B19)}$$

Utilizing the results of Eq B16, B17, B18 and B19 in in combination with Eq B9, B11 and B10, B12 yields,

$$\frac{\partial}{\partial z}[\alpha\rho_v v_{vz}(h_v + \frac{v_{vz}^2}{2} + g_z z)] + \frac{\Gamma}{2}v_{vz}^2 - zg_z\Gamma + (F_{wv} + F_i)v_{vz}$$

$$= Q_{wv} + Q_i \tag{B20}$$

$$\frac{\partial}{\partial z}[(1-\alpha)\rho_\ell v_{\ell z}(h_\ell + \frac{v_{\ell z}^2}{2} + g_z z)] - \frac{\Gamma}{2}v_{\ell z}^2 + zg_z\Gamma + (F_{w\ell} - F_i)v_{\ell z}$$

$$= Q_{w\ell} - Q_i \tag{B21}$$

Finally upon rearrangement of Eq B20 and B21, the THERMIT energy conservation equations are obtained.

$$\frac{\partial}{\partial z}[\alpha\rho_v v_{vz}(h_v + \frac{v_{vz}^2}{2} + g_z z)] = Q_{wv} + Q_i - \frac{\Gamma}{2}v_{vz}^2 + zg_z\Gamma$$

$$- (F_{wv} + F_i)v_{vz} \tag{B22}$$

$$\frac{\partial}{\partial z}[(1-\alpha)\rho_\ell v_{\ell z}(h_\ell + \frac{v_{\ell z}^2}{2} + g_z z)] = Q_{w\ell} - Q_i + \frac{\Gamma}{2}v_{\ell z}^2 - zg_z\Gamma$$

$$- (F_{w\ell} - F_i)v_{\ell z} \tag{B23}$$

When Eq B22 and B23 are compared with Eq B7 and B8, it can be seen that the present THERMIT energy conservation equations are in contradiction with the first law of thermodynamics.

Appendix C. Plenum temperature

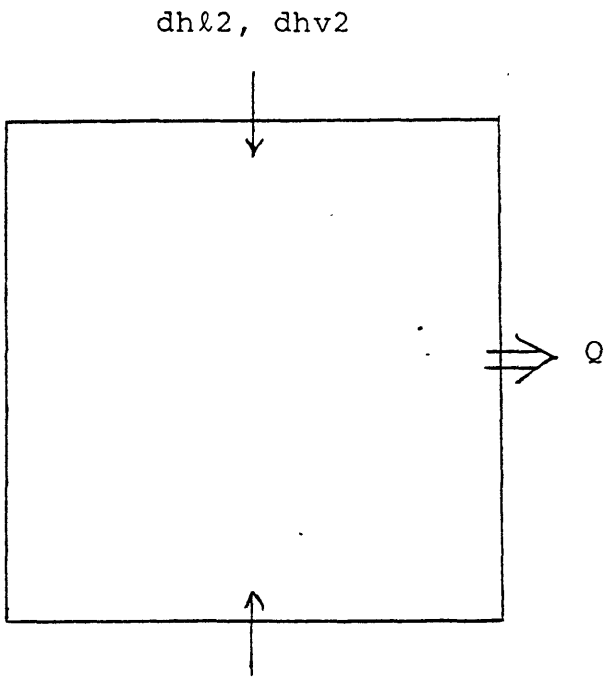

Fig C1. Plenum energy conservation

$$Q = dh\ell 1 + dh\ell 2 + dhv1 + dhv2 + \frac{V\rho_T c_{pT}(T-T_o)}{\Delta t} \qquad (C1)$$

where

Q : the total amount of heat that should be extracted from the plenum at time step n to keep the temperature at T_o.

V : volume of the plenum

c_{pT} : specific heat of sodium at temperature T

ρ_T : sodium density at temperature T

T : the plenum temperature at time step n

T_o : the desired plenum temperature at time step (n+1)

Δt : time step size $(t^{n+1}-t^n)$

$dh\ell 1$: the amount of heat that should be extracted from the plenum to keep the in-flux sodium at bottom face at temperature T.

$dh\ell 2$, dhv1, dhv2 : similarly defined as $dh\ell 1$. $dh\ell 1$ (or $dh\ell 2$, dhv1, dhv2) is equal to zero if the flow is in outward direction.

The scheme of Eq C1 worked very well for single-phase cases, but in two-phase case where there is condensation in the plenum, the error in the plenum temperature was not tolerable. Hence for the two-phase simulated 1-D loop analysis, an iterative method is used to get a constant plenum temperature.

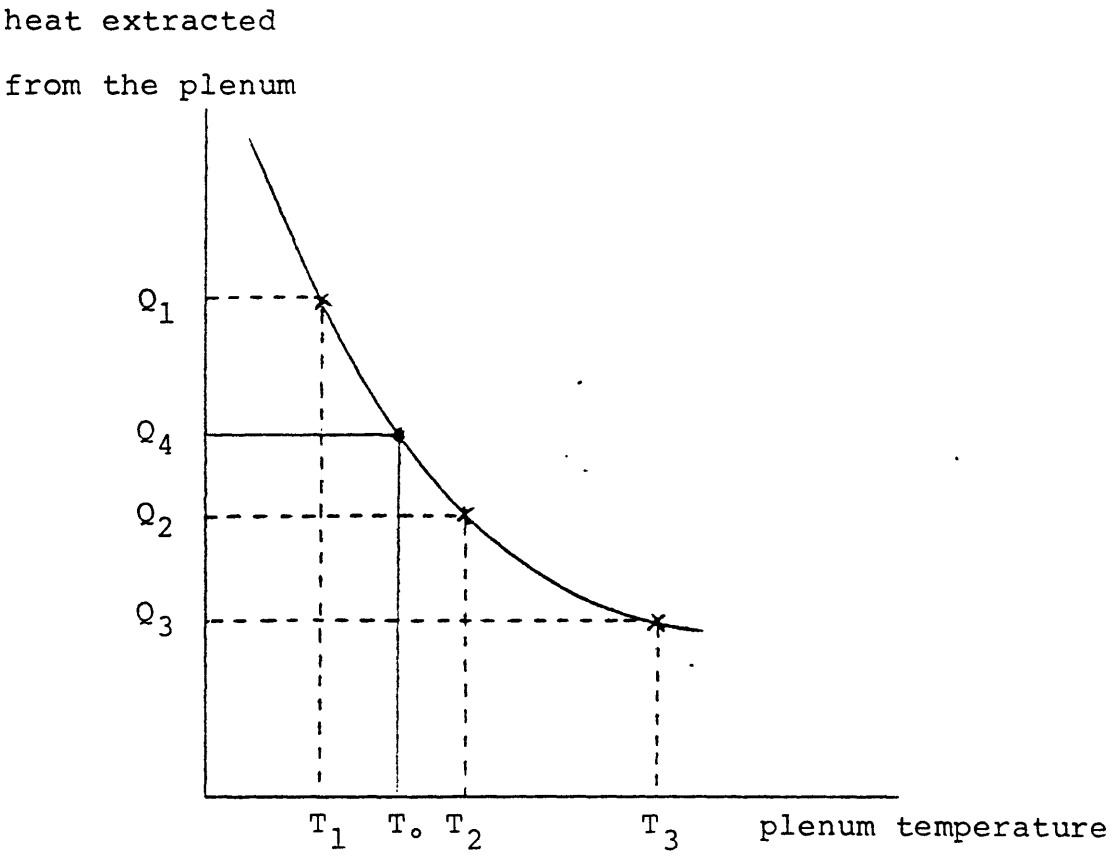

Fig C2. Iterative scheme

In Fig C2, a parabola is drawn with (T_1, Q_1), (T_2, Q_2), (T_3, Q_3) and Q_4 is calculated so that it corresponds to T_o on that parabola. With Q_4, the whole calculation is repeated and a new temperature T_4 is obtained.

Another parabola can be drawn with (T_2, Q_2), (T_3, Q_3) and (T_4, Q_4) and the same procedure is repeated until a satisfactory plenum temperature is obtained.

Appendix D. Dependence of the wall friction on the void fraction

Autruffe's wall friction correlation

For liquid $$F_\ell = \frac{0.18}{2De}[Re_\ell]^{-0.2}\rho_\ell u_\ell |u_\ell| \qquad \alpha < \alpha_{dry} \tag{D1}$$

$$F_\ell = \frac{0.18}{2De}[Re_\ell]^{-0.2}\rho_\ell u_\ell |u_\ell| \frac{\alpha-\alpha_{dry}}{1-\alpha_{dry}} \qquad \alpha>\alpha_{dry} \tag{D2}$$

For vapor $$F_v = \frac{0.18}{2De}[Re_v]^{-0.2}\rho_v u_v |u_v| \frac{\alpha-\alpha_{dry}}{1-\alpha_{dry}} \tag{D3}$$

For $\alpha < \alpha_{dry}$, only the liquid is in contact with the wall.

$$F_T = F_\ell$$

$$f = 0.18[Re_\ell]^{-0.2} \tag{D4}$$

The mass flux G is expressed as follows,

$$G = (1-\alpha)\rho_\ell u_\ell + \alpha\rho_v u_v$$

$$= \rho_\ell u_\ell [(1-\alpha) + \frac{\rho_v}{\rho_\ell} S\alpha] \qquad S = u_v/u_\ell \tag{D5}$$

Since $\rho_v/\rho_\ell \sim 1/2000$,

$$G \simeq \rho_\ell u_\ell (1-\alpha) \tag{D6}$$

$$Re_\ell = \frac{(1-\alpha)\rho_\ell u_\ell De}{\mu_\ell} \simeq \frac{G\ De}{\mu_\ell} \tag{D7}$$

Therefore Re_ℓ is independent of the void fraction if G is constant. It means that the friction factor f is also independent of the void fraction α for constant G.

For $\alpha \geq \alpha_{dry}$, $F_T = F_\ell + F_v$

Table D1 shows that the liquid wall friction is dominant over the vapor wall friction for $\alpha < 0.9999$. Hence it may be said that f is independent of the void fraction for constant G unless the flow is almost single-phase vapor.

Table D1 Wall friction forces by the liquid and vapor phases in contact with the wall

α	$F_\ell/G^{1.8}$	$F_v/G^{1.8}$	$F_T/G^{1.8}$
0.1	0.0254	0.0	0.0254
0.2	0.0321	0.0	0.0321
0.3	0.0419	0.0	0.0419
0.4	0.0570	0.0	0.0570
0.5	0.0821	0.0	0.0821
0.6	0.1282	0.0	0.1282
0.7	0.2277	0.0	0.2277
0.8	0.5111	0.0	0.5111
0.9	2.0312	0.0	2.0312
0.95	8.0199	0.0	8.0199
0.957	10.798	0.0	10.798
0.96	11.58	0.03	11.61
0.97	15.28	0.05	15.33
0.98	22.44	0.10	22.54
0.99	42.17	0.32	42.49
0.995	74.94	1.00	75.94
0.997	107.88	2.16	110.04
0.999	178.77	8.65	187.42
0.9995	189.70	16.01	205.71
0.9999	106.50	32.47	138.97
0.99999	20.76	40.03	60.79
1.0	0.0	41.03	41.03

where $De = 3.25 \times 10^{-3}$ m $\quad S = 2$

$\mu_\ell = 1.6476 \times 10^{-4}$ kg/m s $\quad \rho_\ell = 742.18$ kg/m^3

$\mu_v = 1.9644 \times 10^{-5}$ kg/m s $\quad \rho_v = 0.27$ kg/m^3

Appendix E. Typical experimental data

Some of the typical data from ORNL/TM-7018 are presented here. These are all stable boiling data and Fig E4 and E6 show the void propagation clearly. This void propagation mode can be compared with the simulated 1-D loop results in Fig 4.10 - 4.19 in Chapter 4.

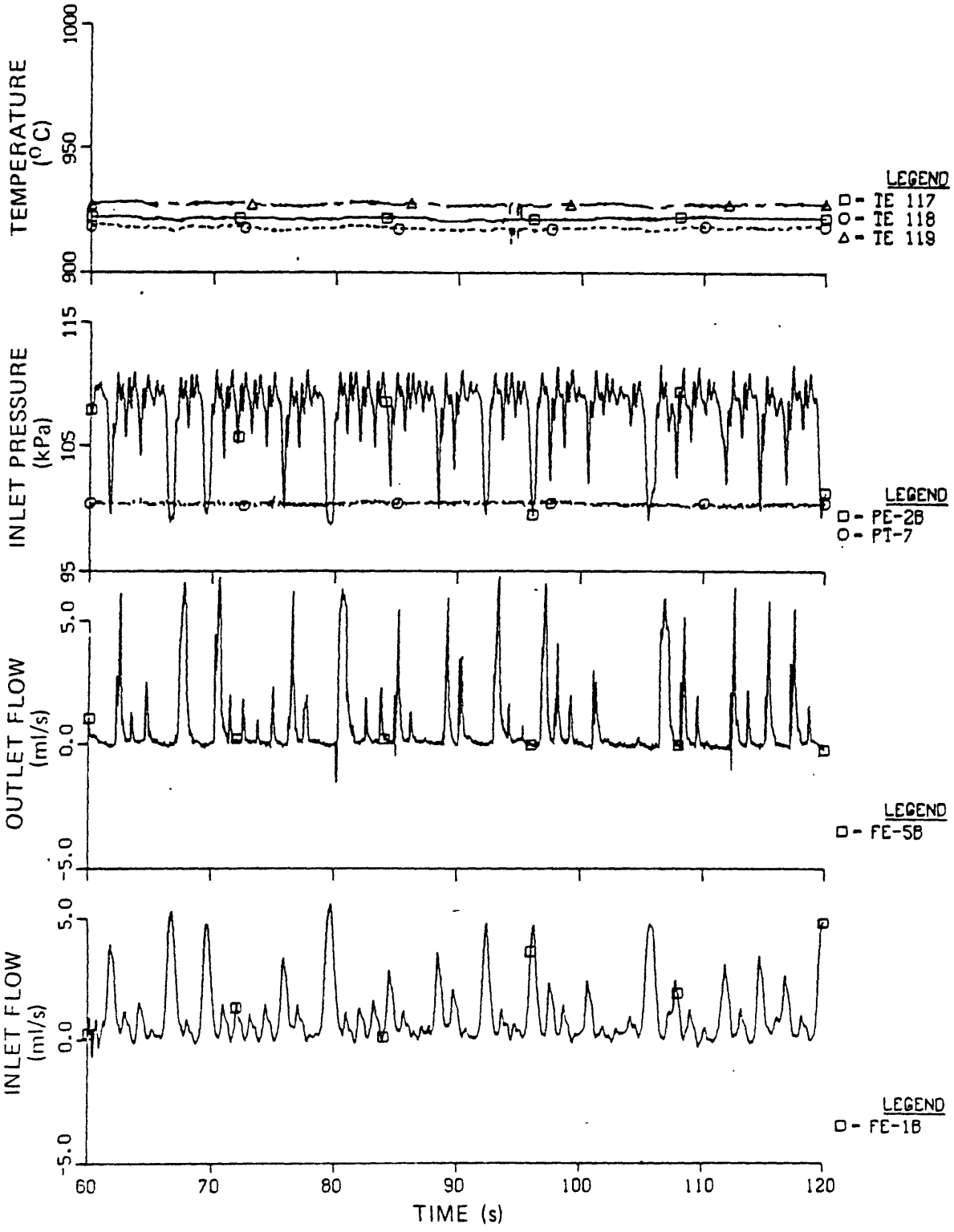

Fig El. Stable boiling of the test run 129R1 at 1.3 kW (taken from ORNL/TM-7018)

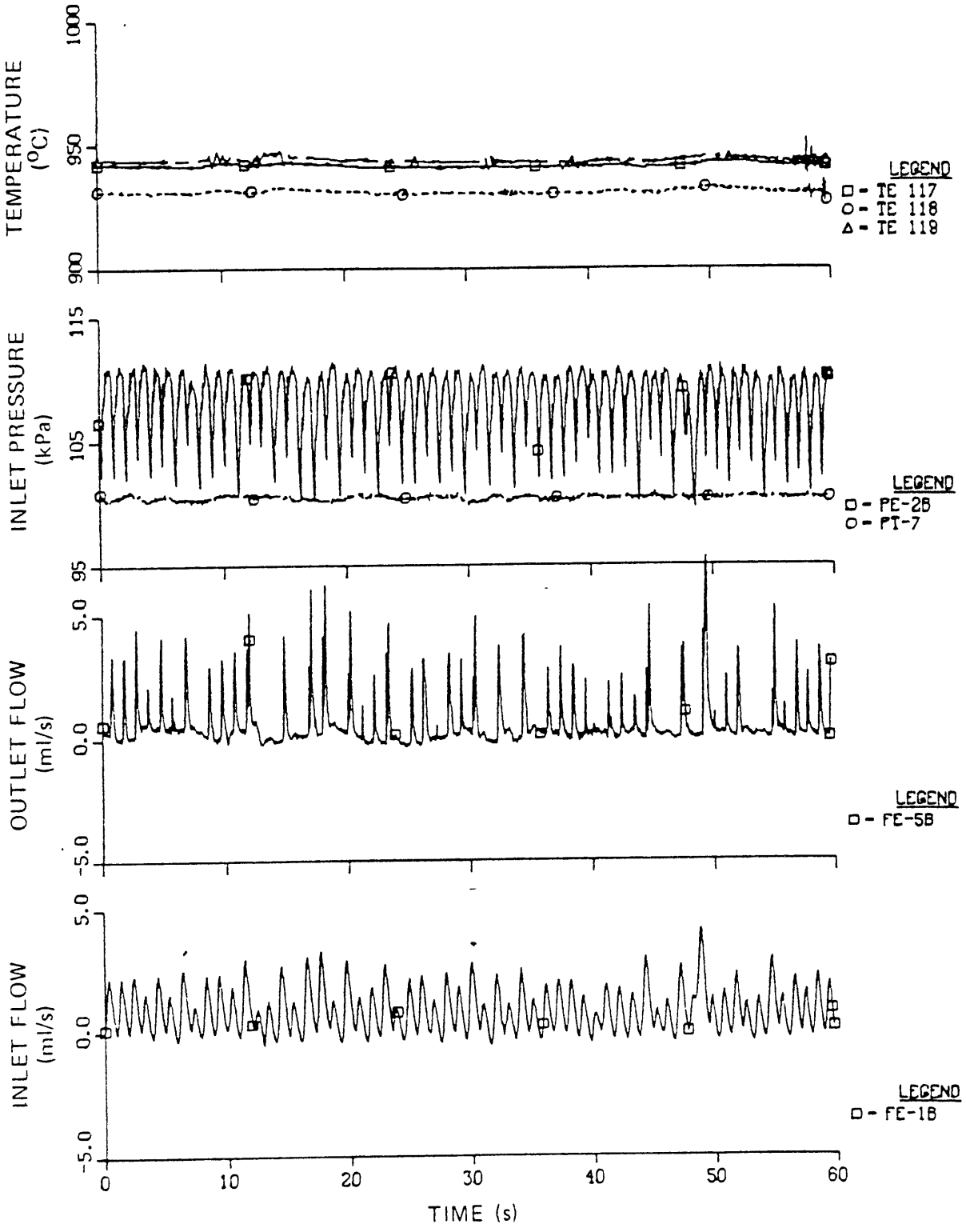

Fig E2. Stable boiling of the test run 127R1 at 1.5kW (taken from ORNL/TM-7018)

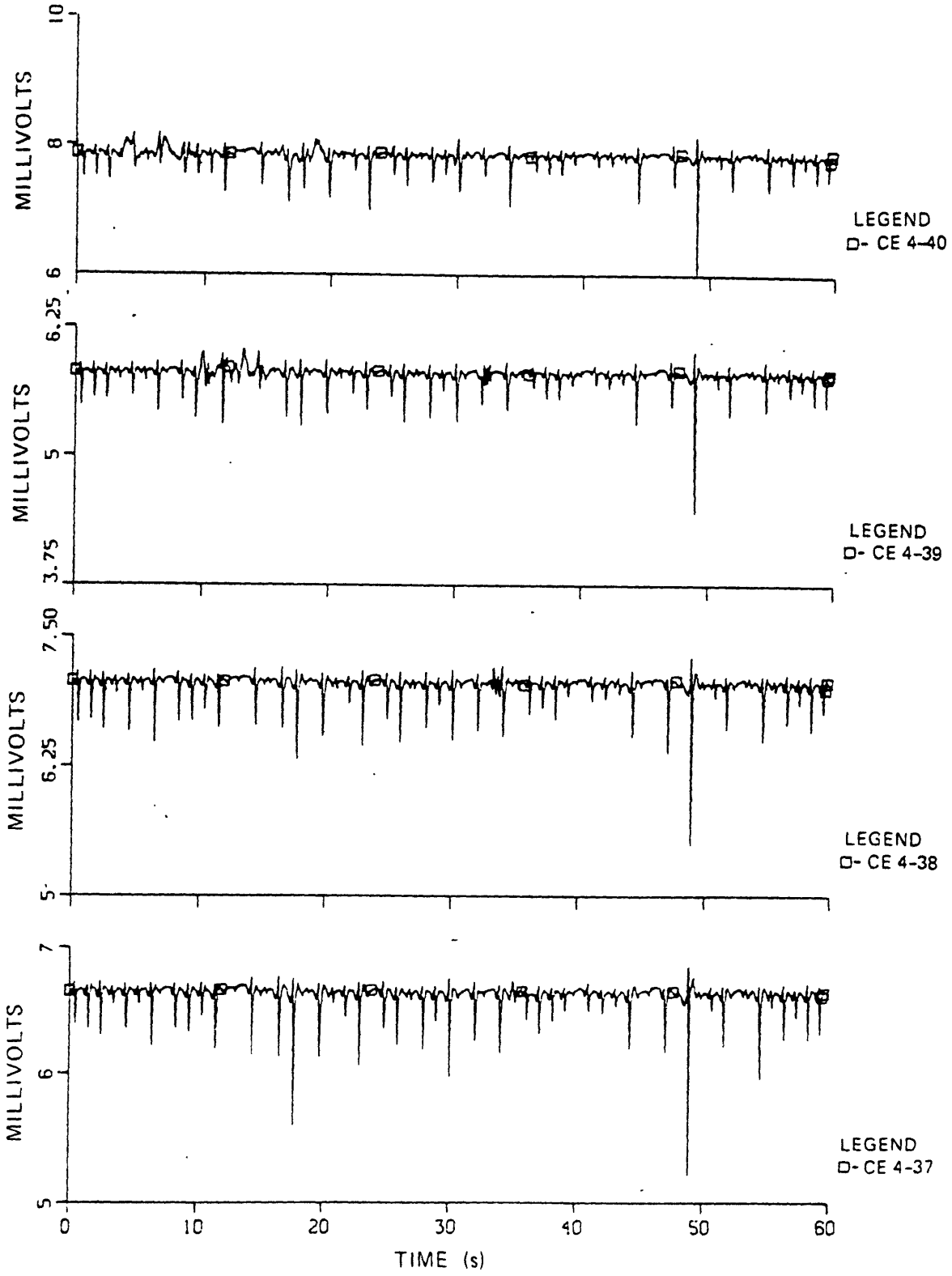

Fig E3. Void detection system data for the test run 127R1 (taken from ORNL/TM-7018)

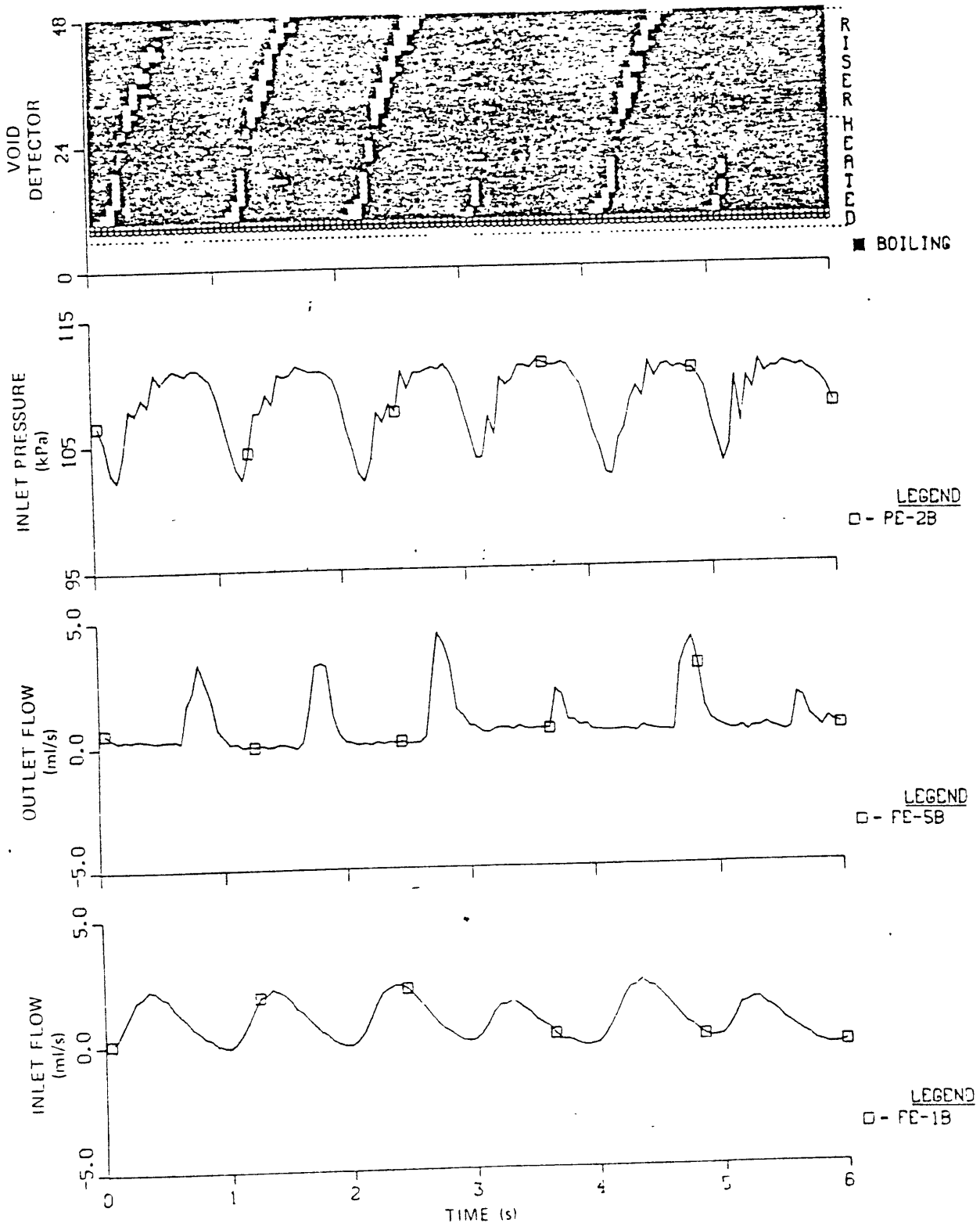

Fig E4. Relationship between voiding pattern, flow and pressure for the test run 127R1 (from ORNL/TM-7018)

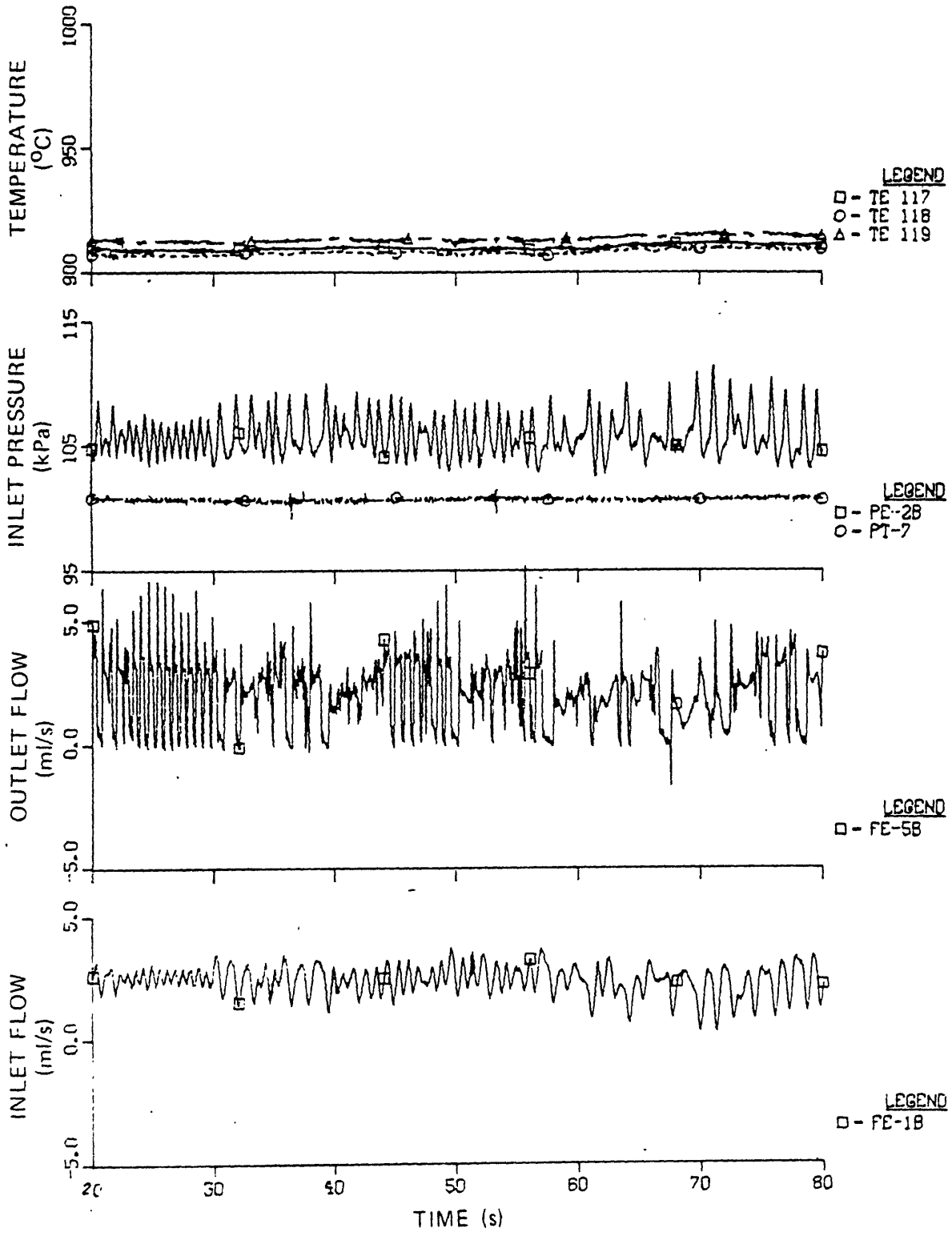

Fig E5. Stable boiling at high flow and low quality for the test run 120R1 at 1.5 kW (taken from ORNL/TM-7018)

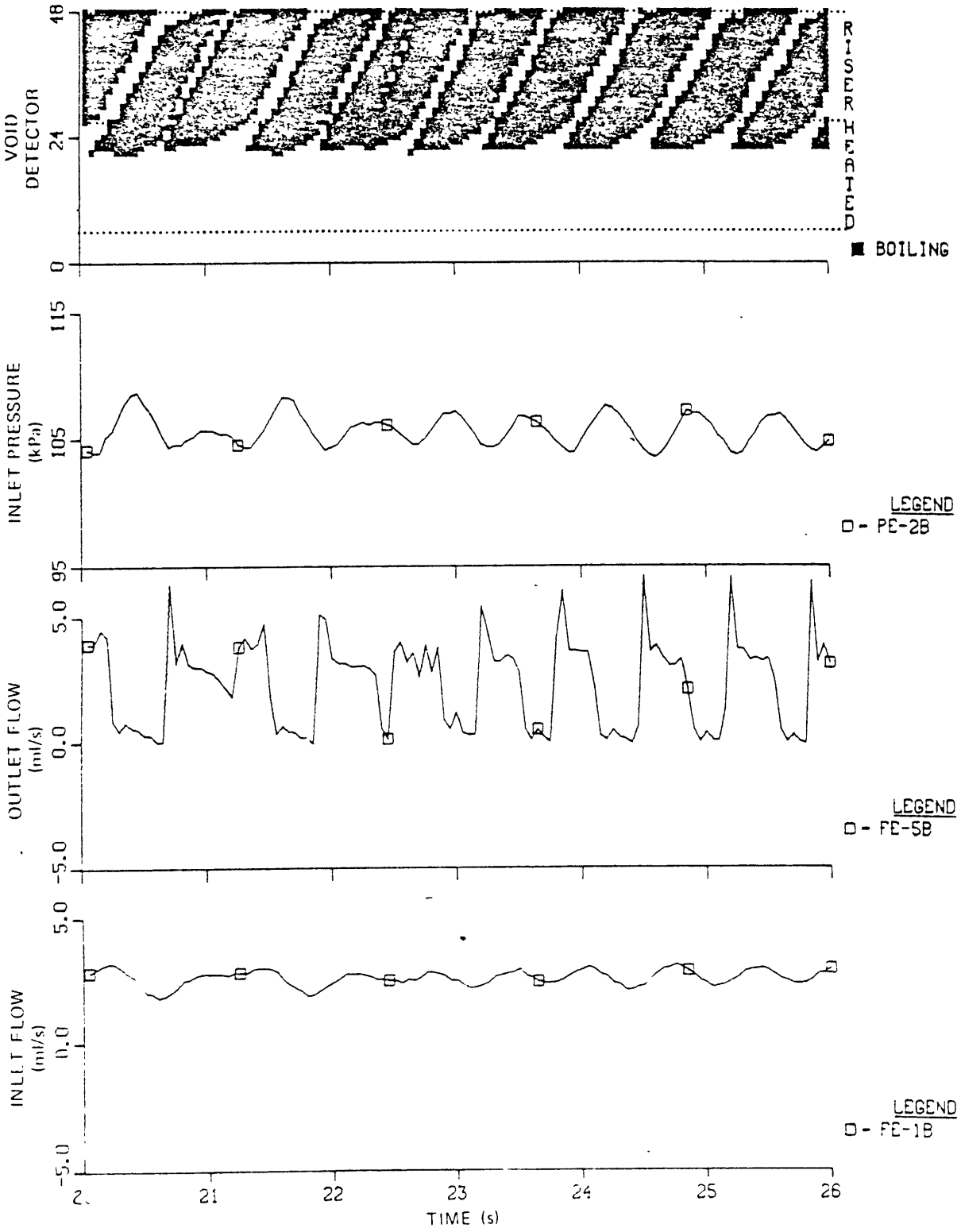

Fig E6. Relationship between voiding pattern, flow and pressure for the test run 120R1 (from ORNL/TM-7018)

Appendix F. Typical computer inputs and outputs

Some of the important computer inputs and outputs are included here. The inputs are for the test run 129R1 and the simulated and actual 1-D loop analysis. The outputs are from the ORNL/TM-7018 test section calculation of the single phase run 107R2 at 210 W with 4-Eq model, the two-phase run 129R1 at 910 W with HEM, 4-Eq and 6-Eq models. The French forced convection results are also listed for the mass flow rate and tube diameter 0.014 kg/s, r = 0.002 m and 0.013 kg/s, r = 0.003 m. The single-phase results of the simulated and actu--al 1-D loop calculations are also shown. Note that the actual 1-D loop calculation has a two-dimensional geometry from the computational point of view, therefore it is composed of four channels. Finally the simulated 1-D loop calculation results with the vapor density 100 and 200 times increased are listed. Note that these are the results at the inception of boiling and a reverse flow is indicated at the inlet of the test sec--tion with the vapor density 100 times increased.

Input for the test section steady-state run 129P1 with 4-Eq model

```
2
ORNL- dryout measurement for sodium natural convection
in a vertical channel  -  SBTF
$intgin nc=1 nz=10 nr=1 narf=1 nx=0 nrzs=0 ihtf=1 ihts=0
        iss=1 ixfl=0 idump=1 ibb=1 iwft=0 ichnge=0 ihtrpr=1
        ishpr=1111 nitmax=3 ipfsol=10 neq=4 ieqvax=1 ieqvtr=1 ntabls=1 ipowt=1 ihtrpr=1   $
$realin epsn=1.e-3 hdt=3.25e-3 pdr=1.2533 hdr=1.0e+10 rnuss=7.0 radf=1.625e-3
        delpr=0.00001 delro=0.00001 delem=0.00001          $
$rodinp q0=910.        $
1                      $  ncr
0                      $  indent
1                      $  ifcar
1                      $  nrzf
1                      $  nrmzf
4                      $  mnrzf
4.07327e-3                $  dx
4.07327e-3                $  dy
6(0.194) 6(0.3)        $  dz
10(0.0)                $  arx
10(0.0)                $  ary
11(8.295768e-6)        $  arz
5(1.609378992e-6) 5(2.4887304e-6)    $  vol
3.25e-3           $  hedz
3.25e-3           $  wedz
6(1.226e+5) 6(1.01e+5)  $  p
12(0.0)                $  alp
12(693.15)                $  tv
11(12.054e-2)           $  vvz
10(693.15)             $  twf
5(1.0) 5(0.0)          $  qz
1.0                    $  qt
1.0                    $  qr
1                      $  rn
1.625e-3                 $  drzf
3
0.0 0.0 50.0 1.0 1000.0 1.0  $table1
$timdat  tend=-1.0 dtmin=1.0e-8 dtmax=5.0
         dtsp=10.0  dtlp=30.0   iredmx=25      $
0
```

Input for the simulated 1-D loop analysis with 4-Eq model

```
1
Input for 1-D loop analysis
$intgin nc=1 nz=26 nr=1 narf=1 nx=0 nrzs=0 ihtf=1 ihts=0 iss=2
        ixfl=0 idump=1 iflash=1 itb=0 ibb=1 iwft=0 ichnge=0 ishpr=1111
        nitmax=3 ipfsol=10 neq=4 ieqvax=0 ieqvtr=1      $
$realin epsn=1.e-4 hdt=3.25e-3 pdr=1.2533 hdr=1.0e+10 rnuss=7.0
        radf=1.625e-3 delpr=1.e-7 delro=1.e-7 delem=1.e-7    $
$rodinp q0=210.              $
1                            $  ncr
0                            $  indent
1                            $  ifcar
1                            $  nrzf
1                            $  nrmzf
4                            $  mnrzf
4.07327e-3                   $  dx
4.07327e-3                   $  dy
2(0.6175) 5(0.193) 5(0.3) 16(0.6175)        $  dz
26(0.0)                      $  arx
26(0.0)                      $  ary
27(8.295768e-6)              $  arz
5.1226368e-6 5(1.6010832e-6) 5(2.4887304e-6) 15(5.1226368e-6)  $  vol
3.25e-3                      $  hedz
3.25e-3                      $  wedz
28(1.29039e+5)               $  p
28(0.0)                       $  alp
28(863.15)                       $  tv
27(8.0e-2)                 $  vvz
26(863.15)                    $  twf
-210. 5(1.0) 5(0.0) 0.0 14(0.0)            $  qz
1.0                          $  qt
1.0                          $  qr
1                            $  rn
1.625e-3                     $  drzf
$timdat tend=-1.0 dtmin=1.e-8 dtmax=5.0 dtsp=5.0 dtlp=10.0 iredmx=25  $
0
```

Input for the actual 1-D loop analysis with 4-Eq model

```
1
Input for loop analysis of 129r1 - 4 channels
$intgin nc=4 nz=14 nr=1 narf=1 nx=0 nrzs=0 ihtf=1 ihts=0 iss=2
        ixfl=1 idump=1 iflash=1 itb=0 ibb=1 iwft=1 ichnge=0
        ivelpr=1 ishpr=1111 nitmax=3 ipfsol=22 neq=4  $
$realin epsn=1.e-4 hdt=3.25e-3 pdr=1.2533 hdr=1.0e+10 rnuss=7.0
        radf=1.625e-3 delpr=1.e-6 delro=1.e-6 delem=1.e-6   $
$rodinp q0=910.                  $
4                                $  ncr
0                                $  indent
1                                $  ifcar
1                                $  nrzf
1                                $  nrmzf
4                                $  mnrzf
8.01106e-2 2(0.915) 4.07327e-3                          $  dx
4(4.07327e-3)                                           $  dy
3(8.01106e-2) 5(0.194) 5(0.3) 3(8.01106e-2)             $  dz
14(0.0) 3(2(4.07327e-3) 10(0.0) 2(4.07327e-3))          $  arx
56(0.0)                                                 $  ary
1.0e-12 14(3.26312e-4) 2(1.0e-12 3.72704e-3 11(1.0e-12) 2(3.72704e-3))
1.0e-12 14(1.659153e-5)                                    $  arz
2(2.614106e-5) 5(6.330455e-5) 5(9.789363e-5) 2(2.614106e-5)
2(2(2.985756e-4) 10(1.0e-12) 2(2.985756e-4)) 2(1.329157e-6)
5(3.218757e-6) 5(4.977459e-6) 2(1.329157e-6)            $  vol
4(3.25e-3)                       $  hedz
4(3.25e-3)                       $  wedz
4(8(1.2e+5) 8(1.0e+5))           $  p
64(0.0)                          $  alp
64(860.)                         $  tv
60(0.0)                          $  vvz
56(860.)                         $  twf
2(-210.) 5(1.0) 5(0.0) 2(-700.)  $  qz
3(0.0) 1.0                       $  qt
1.0                              $  qr
20 2(225) 1                      $  rn
1.625e-3                         $  drzf
$timdat tend=-1.0 dtmin=1.0e-8 dtmax=1.0 dtsp=0.5 dtlp=5.0 iredmx=25  $
0
```

Output of the test section steady-state run 107R2 with 4-Eq model

time step no = 36 time = 34.780457 sec time step size = 0.96364E+00 sec
number of newton iterations = 1
number of inner iterations = 1 0 0

total reactor power = 0.210 kW inlet flow rate = 0.001 kg/s
total heat transfer = 0.210 kW outlet flow rate = 0.001 kg/s
flow enthalpy rise = 0.210 kW

maximum relative changes over the time step
in pressure: 0.0000
in mixture density: 0.0000
in mixture energy: 0.0000

ic	iz	P(bar)	void	% qual	hm	rom	T vap	T liq	T sat	vvz	vlz	rov	rol
1	1	1.2113	0.0000	0.00	913556.	850.63	693.15	693.15	1178.99	0.084	0.084	0.49	850.63
1	2	1.2032	0.0000	0.00	948823.	844.24	720.98	720.98	1178.22	0.085	0.085	0.32	844.24
1	3	1.1952	0.0000	0.00	984091.	837.83	748.82	748.82	1177.45	0.086	0.086	0.32	837.83
1	4	1.1873	0.0000	0.00	1019358.	831.40	776.72	776.72	1176.68	0.086	0.086	0.32	831.40
1	5	1.1794	0.0000	0.00	1054625.	824.93	804.68	804.68	1175.92	0.087	0.087	0.32	824.93
1	6	1.1715	0.0000	0.00	1089892.	818.43	832.68	832.68	1175.16	0.088	0.088	0.31	818.43
1	7	1.1638	0.0000	0.00	1125160.	811.91	860.71	860.71	1174.40	0.088	0.088	0.31	811.91
1	8	1.1561	0.0000	0.00	1160427.	805.37	888.76	888.76	1173.64	0.089	0.089	0.31	805.37
1	9	1.1484	0.0000	0.00	1195694.	798.81	916.80	916.80	1172.88	0.090	0.090	0.31	798.81
1	10	1.1409	0.0000	0.00	1230961.	792.24	944.83	944.83	1172.13	0.091	0.091	0.31	792.24
1	11	1.1333	0.0000	0.00	1266229.	785.66	972.83	972.83	1171.38	0.091	0.091	0.30	785.66
1	12	1.1257	0.0000	0.00	1266228.	785.66	972.83	972.83	1170.61	0.091	0.091	0.30	785.66
1	13	1.1180	0.0000	0.00	1266227.	785.66	972.83	972.83	1169.83	0.091	0.091	0.30	785.66
1	14	1.1103	0.0000	0.00	1266226.	785.66	972.83	972.83	1169.05	0.091	0.091	0.30	785.66
1	15	1.1026	0.0000	0.00	1266225.	785.66	972.83	972.83	1168.26	0.091	0.091	0.30	785.66
1	16	1.0949	0.0000	0.00	1266223.	785.66	972.83	972.83	1167.46	0.091	0.091	0.29	785.66
1	17	1.0872	0.0000	0.00	1266222.	785.66	972.83	972.83	1166.67	0.091	0.091	0.29	785.66
1	18	1.0794	0.0000	0.00	1266221.	785.66	972.83	972.83	1165.86	0.091	0.091	0.29	785.66
1	19	1.0717	0.0000	0.00	1266220.	785.66	972.83	972.83	1165.06	0.091	0.091	0.29	785.66
1	20	1.0640	0.0000	0.00	1266219.	785.66	972.83	972.83	1164.24	0.091	0.091	0.29	785.66
1	21	1.0563	0.0000	0.00	1266218.	785.66	972.83	972.83	1163.43	0.091	0.091	0.28	785.66
1	22	1.0486	0.0000	0.00	1266217.	785.66	972.83	972.83	1162.61	0.091	0.091	0.28	785.66
1	23	1.0409	0.0000	0.00	1266216.	785.66	972.83	972.83	1161.78	0.091	0.091	0.28	785.66
1	24	1.0331	0.0000	0.00	1266213.	785.66	972.83	972.83	1160.95	0.091	0.091	0.28	785.66
1	25	1.0254	0.0000	0.00	1266206.	785.66	972.82	972.82	1160.11	0.091	0.091	0.28	785.66
1	26	1.0177	0.0000	0.00	1266181.	785.66	972.80	972.80	1159.27	0.091	0.091	0.27	785.66
1	27	1.0100	0.0000		1265920.	785.66	972.80	972.80	1158.42			0.31	785.66

Cutput of the test section steady-state run 129R1 with HEM model

time step no = 2764 time = 14.971619 sec. time step size = 0.390630-02 sec
number of newton iterations = 1
number of inner iterations = 1 0 0

total reactor power = 0.910 kW
total heat transfer = 0.910 kW
flow enthalpy rise = 0.598 kW

inlet flow rate = 0.001 kg/s
outlet flow rate = 0.001 kg/s

maximum relative changes over the time step
in pressure: 0.000000
in mixture density: 0.000010
in mixture energy: 0.000000

ic	iz	P(Bar)	void	% qual	hm	rom	T vap	T liq	T sat	vvz	vlz
1	1	5.96754	0.0000	0.000	913556.	350.63	693.15	693.15	1334.10	0.121	0.121
1	2	5.95696	0.0000	0.000	1127519.	811.54	862.32	862.32	1333.48	0.126	0.126
1	3	5.93521	0.0000	0.000	1341460.	771.66	1032.12	1032.12	1332.89	0.133	0.133
1	4	5.92328	0.0000	0.000	1555270.	731.76	1199.32	1199.32	1332.33	0.140	0.140
1	5	5.90654	0.3503	0.767	1769198.	105.22	1331.79	1331.79	1331.79	0.975	0.975
1	6	5.89950	0.9741	4.335	1963022.	19.03	1331.16	1331.16	1331.16	5.392	5.392
1	7	5.63901	0.9769	5.081	1981695.	17.09	1321.41	1321.41	1321.41	6.006	6.006
1	8	5.30358	0.9803	5.427	1979750.	14.71	1307.70	1307.70	1307.70	6.977	6.977
1	9	4.92692	0.9838	5.862	1977148.	12.21	1290.48	1290.48	1290.48	8.402	8.402
1	10	4.47279	0.9875	6.442	1973425.	9.56	1267.55	1267.55	1267.55	10.738	10.738
1	11	3.90696	0.9915	7.296	1967487.	6.67	1233.70	1233.70	1233.70	15.394	15.394
1	12	3.01000	0.9915		1801161.	6.44	1233.70	1233.70	1158.42		

Output of the test section steady-state run 129R1 with 4-Eq model

time step no = 899 time = 13.0140067 sec time step size = 0.8404700-02 sec
number of newton iterations = 1
number of inner iterations = 1 0 0

total reactor power = 0.910 kW inlet flow rate = 0.001 kg/s
total heat transfer = 0.910 kW outlet flow rate = 0.001 kg/s
flow enthalpy rise = 0.900 kW

maximum relative changes over the time step
in pressure: 0.000002
in mixture density: 0.000010
in mixture energy: 0.000002

ic	iz	P(bar)	void	% qual	hm	rom	T vap	T liq	T sat	vvz	vlz
1	1	1.76084	0.0000	0.000	913556.	850.63	693.15	693.15	1223.77	0.121	0.121
1	2	1.74439	0.0000	0.000	1127510.	811.49	862.53	862.53	1222.60	0.126	0.126
1	3	1.72670	0.0000	0.000	1341374.	771.62	1032.28	1032.28	1221.48	0.133	0.133
1	4	1.71378	0.0000	0.000	1554799.	731.61	1199.19	1199.19	1220.41	0.140	0.140
1	5	1.69953	0.8963	3.753	1606647.	75.40	1219.38	1219.38	1219.38	9.723	1.316
1	6	1.67238	0.9413	8.066	1625322.	43.13	1217.39	1217.39	1217.39	20.210	2.207
1	7	1.59059	0.9430	8.214	1616518.	41.91	1211.28	1211.28	1211.28	21.511	2.268
1	8	1.43987	0.9447	8.406	1604648.	40.76	1203.34	1203.34	1203.34	23.345	2.326
1	9	1.38264	0.9467	8.620	1591510.	39.41	1194.45	1194.45	1194.45	25.592	2.400
1	10	1.26833	0.9484	8.863	1576163.	38.27	1184.31	1184.31	1184.31	28.450	2.464
1	11	1.14594	0.9515	9.141	1559615.	36.09	1172.63	1172.63	1172.63	32.125	2.604
1	12	1.01000	0.9515		1554918.	36.06	1172.63	1172.63	1158.42		

Output of the test section steady-state run 129R1 with 6-Eq model

time step no = 1749 time = 18.743907 sec time step size = 0.83948D-02 sec
number of newton iterations = 1
number of inner iterations = 1 0 0

total reactor power = 0.910 kW inlet flow rate = 0.001 kg/s
total heat transfer = 0.910 kW outlet flow rate = 0.001 kg/s
flow enthalpy rise = 0.900 kW

maximum relative changes over the time step
in pressure: 0.000000
in mixture density: 0.000000
in mixture energy: 0.000000

ic	iz	P(bar)	void	% qual	hm	rom	T vap	T liq	T sat	vvz	vlz	rov	rol
1	1	1.76140	0.0000	0.000	913556.	850.63	693.15	693.15	1223.81	0.121	0.121	0.7139	850.63
1	2	1.74495	0.0000	0.000	1127520.	811.48	862.57	862.57	1222.64	0.126	0.126	0.5929	811.48
1	3	1.72926	0.0000	0.000	1341483.	771.51	1032.78	1032.78	1221.52	0.133	0.133	0.5111	771.51
1	4	1.71434	0.0000	0.000	1555441.	731.55	1200.25	1200.25	1220.45	0.140	0.140	0.4508	731.55
1	5	1.70010	0.8970	3.763	1606887.	75.27	1219.50	1219.52	1219.42	9.743	1.318	0.4416	726.92
1	6	1.67289	0.9413	8.076	1625660.	43.11	1217.61	1217.62	1217.43	20.222	2.208	0.4350	727.37
1	7	1.59138	0.9431	8.230	1616634.	41.87	1211.32	1211.32	1211.32	21.535	2.268	0.4155	728.89
1	8	1.49026	0.9448	8.422	1604755.	40.72	1203.38	1203.38	1203.37	23.372	2.327	0.3911	730.80
1	9	1.38313	0.9468	8.637	1591609.	39.37	1194.49	1194.49	1194.48	25.621	2.400	0.3651	732.94
1	10	1.26852	0.9484	8.880	1576251.	38.23	1184.34	1184.34	1184.33	28.483	2.464	0.3371	735.38
1	11	1.14603	0.9516	9.159	1559693.	36.05	1172.66	1172.66	1172.64	32.163	2.605	0.3069	738.18
1	12	1.01000	0.9516		1554988.	36.02	1172.66	1172.66	1158.42			0.2704	738.18

Output of the French experiment with m = 0.014 kg/s and r = 0.002 m

time step no = 1231 time = 2.486363 sec time step size = 0.13904D-02 sec
number of newton iterations = 1
number of inner iterations = 1 0 0

total reactor power = 10.000 kW inlet flow rate = 0.014 kg/s
total heat transfer = 10.000 kW outlet flow rate = 0.014 kg/s
flow enthalpy rise = 9.969 kW

maximum relative changes over the time step
in pressure: 0.000000
in mixture density: 0.000001
in mixture energy: 0.000000

ic	iz	P(bar)	void	% qual	hm	rom	T vap	T liq	T sat	vvz	vlz	rov	rol
1	1	2.92212	0.0000	0.000	955524.	843.05	726.15	726.15	1290.26	1.300	1.300	1.1393	843.05
1	2	2.91222	0.0000	0.000	1137047.	809.75	869.99	869.99	1289.79	1.353	1.353	0.7243	809.75
1	3	2.89237	0.0000	0.000	1318567.	775.92	1014.13	1014.13	1288.84	1.412	1.412	0.7197	775.92
1	4	2.87289	0.0000	0.000	1500088.	742.01	1156.67	1156.67	1287.91	1.477	1.477	0.7153	742.01
1	5	2.85305	0.5822	0.244	1676179.	297.33	1286.95	1286.95	1286.95	6.468	3.682	0.7108	710.63
1	6	2.77086	0.6629	0.347	1673517.	240.35	1282.93	1282.93	1282.93	8.288	4.552	0.6919	711.60
1	7	2.67272	0.7166	0.473	1669365.	202.48	1278.01	1278.01	1278.01	10.800	5.400	0.6694	712.79
1	8	2.54072	0.7639	0.648	1662942.	169.20	1271.17	1271.17	1271.17	14.549	6.454	0.6390	714.45
1	9	2.35472	0.8079	0.908	1652588.	138.21	1261.03	1261.03	1261.03	20.667	7.885	0.5959	716.90
1	10	2.07823	0.8463	1.327	1633902.	111.26	1244.74	1244.74	1244.74	32.342	9.758	0.5312	720.84
1	11	1.64716	0.8961	2.081	1600630.	75.98	1215.53	1215.53	1215.53	59.334	14.194	0.4289	727.88
1	12	1.20000	0.8961		1593772.	75.88	1215.53	1215.53	1177.91			0.3125	727.88

Output of the French experiment with m = 0.013 kg/s and r = 0.003 m

time step no = 1332 time = 3.129023 sec time step size = 0.15117D-02 sec
number of newton iterations = 1
number of inner iterations = 1 0 0

total reactor power = 10.000 kW inlet flow rate = 0.013 kg/s
total heat transfer = 10.000 kW outlet flow rate = 0.013 kg/s
flow enthalpy rise = 9.930 kW

maximum relative changes over the time step
in pressure: 0.000000
in mixture density: 0.000001
in mixture energy: 0.000000

ic	iz	P(bar)	void	% qual	hm	rom	T vap	T liq	T sat	vvz	vlz	rov	rol
1	1	2.20211	0.0000	0.000	955524.	843.05	726.15	726.15	1252.24	0.533	0.533	0.8586	843.05
1	2	2.19544	0.0000	0.000	1152175.	806.93	882.09	882.09	1251.84	0.557	0.557	0.5587	806.93
1	3	2.18253	0.0000	0.000	1348818.	770.24	1038.11	1038.11	1251.07	0.584	0.584	0.5557	770.24
1	4	2.17014	0.0000	0.000	1545428.	733.56	1191.90	1191.90	1250.33	0.613	0.613	0.5528	733.56
1	5	2.15810	0.8852	2.405	1649570.	83.12	1249.61	1249.61	1249.61	22.214	5.311	0.5500	719.66
1	6	2.04965	0.8977	2.574	1643226.	74.24	1242.96	1242.96	1242.96	24.583	5.938	0.5245	721.27
1	7	1.93596	0.9036	2.759	1633963.	70.12	1235.68	1235.68	1235.68	27.588	6.276	0.4977	723.02
1	8	1.81016	0.9094	2.974	1622899.	66.13	1227.21	1227.21	1227.21	31.434	6.640	0.4678	725.06
1	9	1.66862	0.9156	3.230	1609605.	61.78	1217.12	1217.12	1217.12	36.551	7.089	0.4340	727.50
1	10	1.50620	0.9215	3.546	1592626.	57.71	1204.65	1204.65	1204.65	43.816	7.564	0.3949	730.49
1	11	1.31862	0.9308	3.946	1572229.	51.12	1188.85	1188.85	1188.85	54.575	8.503	0.3493	734.29
1	12	1.20000	0.9308		1569407.	51.09	1188.85	1188.85	1177.91			0.3179	734.29

Output of the simulated 1-D loop analysis of 107R2 with 4-Eq model

time step no = 183 time = 183.000000 sec time step size = 0.10000D+01 sec
number of newton iterations = 1
number of inner iterations = 1 0 0

total reactor power = 0.210 kW inlet flow rate = 0.000 kg/s
total heat transfer = -0.000 kW outlet flow rate = 0.000 kg/s
flow enthalpy rise = -0.000 kW

maximum relative changes over the time step
in pressure: 0.000000
in mixture density: 0.000000
in mixture energy: 0.000000

ic	iz	P(bar)	void	% qual	hm	rom	T vap	T liq	T sat	vvz	vlz	rov	rol
1	1	1.00000	0.0000	0.000	1128251.	811.34	863.15	863.15	1157.32	0.070	0.070	0.3396	811.34
1	2	0.97527	0.0000	0.000	1128248.	811.33	863.19	863.19	1154.55	0.070	0.070	0.2643	811.33
1	3	0.97494	0.0000	0.000	1128248.	811.33	863.19	863.19	1154.51	0.070	0.070	0.2643	811.33
1	4	0.97460	0.0000	0.000	1128248.	811.33	863.19	863.19	1154.47	0.070	0.070	0.2642	811.33
1	5	0.97427	0.0000	0.000	1128248.	811.33	863.19	863.19	1154.44	0.070	0.070	0.2641	811.33
1	6	1.02307	0.0000	0.000	1128254.	811.33	863.19	863.19	1159.85	0.070	0.070	0.2763	811.33
1	7	1.07187	0.0000	0.000	1128260.	811.33	863.19	863.19	1165.07	0.070	0.070	0.2885	811.33
1	8	1.12066	0.0000	0.000	1128266.	811.33	863.19	863.19	1170.10	0.070	0.070	0.3006	811.33
1	9	1.16946	0.0000	0.000	1128272.	811.33	863.19	863.19	1174.95	0.070	0.070	0.3127	811.33
1	10	1.21826	0.0000	0.000	1128278.	811.33	863.19	863.19	1179.65	0.070	0.070	0.3247	811.33
1	11	1.26706	0.0000	0.000	1128284.	811.33	863.19	863.19	1184.20	0.070	0.070	0.3367	811.33
1	12	1.31586	0.0000	0.000	1128291.	811.33	863.19	863.19	1188.61	0.070	0.070	0.3487	811.33
1	13	1.31552	0.0000	0.000	1128291.	811.33	863.19	863.19	1188.58	0.070	0.070	0.3486	811.33
1	14	1.31519	0.0000	0.000	1128291.	811.33	863.19	863.19	1188.55	0.070	0.070	0.3485	811.33
1	15	1.31486	0.0000	0.000	1128292.	811.33	863.19	863.19	1188.52	0.070	0.070	0.3484	811.33
1	16	1.26540	0.0000	0.000	913454.	850.63	693.15	693.15	1184.05	0.067	0.067	0.3363	850.63
1	17	1.23131	0.0000	0.000	1002726.	834.44	763.55	763.55	1180.88	0.068	0.068	0.3279	834.44
1	18	1.21532	0.0000	0.000	1092001.	818.04	834.35	834.35	1179.37	0.069	0.069	0.3240	818.04
1	19	1.19965	0.0000	0.000	1181276.	801.50	905.33	905.33	1177.88	0.071	0.071	0.3201	801.50
1	20	1.18430	0.0000	0.000	1270551.	784.85	976.25	976.25	1176.40	0.072	0.072	0.3163	784.85
1	21	1.16926	0.0000	0.000	1359825.	768.16	1046.91	1046.91	1174.93	0.074	0.074	0.3126	768.16
1	22	1.15053	0.0000	0.000	1359823.	768.16	1046.91	1046.91	1173.09	0.074	0.074	0.3080	768.16
1	23	1.12778	0.0000	0.000	1359820.	768.16	1046.91	1046.91	1170.82	0.074	0.074	0.3024	768.16
1	24	1.10503	0.0000	0.000	1359817.	768.16	1046.90	1046.90	1168.51	0.074	0.074	0.2967	768.16
1	25	1.08227	0.0000	0.000	1359813.	768.16	1046.90	1046.90	1166.16	0.074	0.074	0.2911	768.16
1	26	1.05952	0.0000	0.000	1359810.	768.16	1046.90	1046.90	1163.77	0.074	0.074	0.2854	768.16
1	27	1.02473	0.0000	0.000	1128207.	811.34	863.15	863.15	1160.04	0.070	0.070	0.2767	811.34
1	28	1.00000	0.0000		1128251.	811.34	863.15	863.15	1157.32			0.3396	811.34

Output of the actual 1-D loop analysis of 107R2 with 4-Eq model

```
time step no = 2437          time = 143.199102 sec      time step size = 0.58501D-01 sec
number of newton iterations =    1
number of inner iterations =     1   0   0

total reactor power =        0.210 kW          inlet flow rate =        0.000 kg/s
total heat transfer =       -0.000 kW         outlet flow rate =       -0.000 kg/s
flow enthalpy rise =        -0.000 kW

                                        maximum relative changes over the time step
                                                in pressure:          0.000000
                                                in mixture density:   0.000000
                                                in mixture energy:    0.000000
```

ic	iz	P(bar)	void	% qual	hm	rom	T vap	T liq	T sat	vvz	vlz	rov	rol
1	1	1.34223	0.0000	0.000	1128251.	811.34	863.15	863.15	1190.94	0.000	0.000	0.4558	811.34
1	2	1.34191	0.0000	0.000	1128339.	811.33	863.22	863.22	1190.91	-0.063	-0.063	0.3550	811.33
1	3	1.32992	0.0000	0.000	1128338.	811.33	863.22	863.22	1189.86	-0.063	-0.063	0.3521	811.33
1	4	1.29337	0.0000	0.000	1128333.	811.33	863.22	863.22	1186.59	-0.063	-0.063	0.3432	811.33
1	5	1.26128	0.0000	0.000	1128329.	811.33	863.22	863.22	1183.67	-0.063	-0.063	0.3353	811.33
1	6	1.24593	0.0000	0.000	1128328.	811.33	863.22	863.22	1182.25	-0.063	-0.063	0.3315	811.33
1	7	1.23059	0.0000	0.000	1128326.	811.33	863.22	863.22	1180.81	-0.063	-0.063	0.3277	811.33
1	8	1.21524	0.0000	0.000	1128324.	811.33	863.22	863.22	1179.36	-0.063	-0.063	0.3240	811.33
1	9	1.19990	0.0000	0.000	1128322.	811.33	863.22	863.22	1177.90	-0.063	-0.063	0.3202	811.33
1	10	1.18036	0.0000	0.000	1128320.	811.33	863.22	863.22	1176.02	-0.063	-0.063	0.3154	811.33
1	11	1.15663	0.0000	0.000	1128317.	811.33	863.22	863.22	1173.69	-0.063	-0.063	0.3095	811.33
1	12	1.13291	0.0000	0.000	1128314.	811.33	863.22	863.22	1171.33	-0.063	-0.063	0.3036	811.33
1	13	1.10918	0.0000	0.000	1128311.	811.33	863.22	863.22	1168.93	-0.063	-0.063	0.2977	811.33
1	14	1.08545	0.0000	0.000	1128308.	811.33	863.22	863.22	1166.49	-0.063	-0.063	0.2918	811.33
1	15	1.04916	0.0000	0.000	1128303.	811.33	863.22	863.22	1162.67	-0.063	-0.063	0.2828	811.33
1	16	1.01261	0.0000	0.000	1128299.	811.33	863.22	863.22	1158.71	-0.063	-0.063	0.2737	811.33
1	17	1.00032	0.0000	0.000	1128297.	811.33	863.22	863.22	1157.36	-0.063	-0.063	0.2706	811.33
1	18	1.00000	0.0000		1128298.	811.33	863.19	863.19	1157.32			0.3396	811.33

2	1	1.34085	0.0000	0.000	1128251.	811.34	863.15	863.15	1190.82	0.000	0.000	0.4554	811.34
2	2	1.34052	0.0000	0.000	1128338.	811.33	863.22	863.22	1190.79	0.000	0.000	0.3547	811.33
2	3	1.63682	0.0000	0.000	1128305.	811.34	863.17	863.17	1214.75	0.000	0.000	0.4264	811.34
2	4	1.63682	0.0000	0.000	1128305.	811.34	863.17	863.17	1214.75	0.000	0.000	0.4264	811.34
2	5	1.63682	0.0000	0.000	1128305.	811.34	863.17	863.17	1214.75	0.000	0.000	0.4264	811.34
2	6	1.63682	0.0000	0.000	1128305.	811.34	863.17	863.17	1214.75	0.000	0.000	0.4264	811.34
2	7	1.63682	0.0000	0.000	1128305.	811.34	863.17	863.17	1214.75	0.000	0.000	0.4264	811.34
2	8	1.63682	0.0000	0.000	1128305.	811.34	863.17	863.17	1214.75	0.000	0.000	0.4264	811.34
2	9	1.63682	0.0000	0.000	1128305.	811.34	863.17	863.17	1214.75	0.000	0.000	0.4264	811.34
2	10	1.91335	0.0000	0.000	1128364.	811.33	863.19	863.19	1234.19	0.000	0.000	0.4923	811.33
2	11	1.91335	0.0000	0.000	1128364.	811.33	863.19	863.19	1234.19	0.000	0.000	0.4923	811.33
2	12	1.91335	0.0000	0.000	1128364.	811.33	863.19	863.19	1234.19	0.000	0.000	0.4923	811.33
2	13	1.91335	0.0000	0.000	1128364.	811.33	863.19	863.19	1234.19	0.000	0.000	0.4923	811.33
2	14	1.91335	0.0000	0.000,	1128364.	811.33	863.19	863.19	1234.19	0.000	0.000	0.4923	811.33
2	15	1.91335	0.0000	0.000	1128364.	811.33	863.19	863.19	1234.19	0.000	0.000	0.4923	811.33
2	16	1.91335	0.0000	0.000	1128364.	811.33	863.19	863.19	1234.19	0.000	0.000	0.4923	811.33
2	17	1.00032	0.0000	0.000	1128262.	811.33	863.20	863.20	1157.36	-0.000	-0.000	0.2706	811.33
2	18	1.00000	0.0000		1128298.	811.33	863.19	863.19	1157.32			0.3396	811.33
3	1	1.33993	0.0000	0.000	1128251.	811.34	863.15	863.15	1190.74	0.000	0.000	0.4551	811.34
3	2	1.33961	0.0000	0.000	1128335.	811.33	863.22	863.22	1190.71	0.000	0.000	0.3545	811.33
3	3	1.63682	0.0000	0.000	1128305.	811.34	863.17	863.17	1214.75	0.000	0.000	0.4264	811.34
3	4	1.63682	0.0000	0.000	1128305.	811.34	863.17	863.17	1214.75	0.000	0.000	0.4264	811.34
3	5	1.63682	0.0000	0.000	1128305.	811.34	863.17	863.17	1214.75	0.000	0.000	0.4264	811.34
3	6	1.63682	0.0000	0.000	1128305.	811.34	863.17	863.17	1214.75	0.000	0.000	0.4264	811.34
3	7	1.63682	0.0000	0.000	1128305.	811.34	863.17	863.17	1214.75	0.000	0.000	0.4264	811.34
3	8	1.63682	0.0000	0.000	1128305.	811.34	863.17	863.17	1214.75	0.000	0.000	0.4264	811.34
3	9	1.63682	0.0000	0.000	1128305.	811.34	863.17	863.17	1214.75	0.000	0.000	0.4264	811.34
3	10	1.91335	0.0000	0.000	1128364.	811.33	863.19	863.19	1234.19	0.000	0.000	0.4923	811.33
3	11	1.91335	0.0000	0.000	1128364.	811.33	863.19	863.19	1234.19	0.000	0.000	0.4923	811.33
3	12	1.91335	0.0000	0.000	1128364.	811.33	863.19	863.19	1234.19	0.000	0.000	0.4923	811.33
3	13	1.91335	0.0000	0.000	1128364.	811.33	863.19	863.19	1234.19	0.000	0.000	0.4923	811.33
3	14	1.91335	0.0000	0.000	1128364.	811.33	863.19	863.19	1234.19	0.000	0.000	0.4923	811.33
3	15	1.91335	0.0000	0.000	1128364.	811.33	863.19	863.19	1234.19	0.000	0.000	0.4923	811.33
3	16	1.91335	0.0000	0.000	1128364.	811.33	863.19	863.19	1234.19	0.000	0.000	0.4923	811.33
3	17	1.00032	0.0000	0.000	1128240.	811.34	863.18	863.18	1157.36	0.000	0.000	0.2706	811.34
3	18	1.00000	0.0000		1128287.	811.34	863.18	863.18	1157.32			0.3396	811.34

4	1	1.33901	0.0000	0.000	1128251.	811.34	863.15	863.15	1190.66	0.000	0.000	0.4547	811.34
4	2	1.33869	0.0000	0.000	1128335.	811.33	863.22	863.22	1190.63	0.063	0.063	0.3542	811.33
4	3	1.32505	0.0000	0.000	1128332.	811.33	863.22	863.22	1189.42	0.063	0.063	0.3509	811.33
4	4	1.28805	0.0000	0.000	913457.	850.63	693.15	693.15	1186.11	0.060	0.060	0.3418	850.63
4	5	1.25399	0.0000	0.000	1012871.	832.58	771.58	771.58	1182.99	0.061	0.061	0.3335	832.58
4	6	1.23805	0.0000	0.000	1112288.	814.29	850.47	850.47	1181.51	0.063	0.063	0.3296	814.29
4	7	1.22247	0.0000	0.000	1211706.	795.83	929.52	929.52	1180.05	0.064	0.064	0.3257	795.83
4	8	1.20724	0.0000	0.000	1311125.	777.27	1008.41	1008.41	1178.60	0.066	0.066	0.3220	777.27
4	9	1.19237	0.0000	0.000	1410545.	758.68	1086.84	1086.84	1177.18	0.067	0.067	0.3183	758.68
4	10	1.17388	0.0000	0.000	1410552.	758.68	1086.85	1086.85	1175.39	0.067	0.067	0.3138	758.68
4	11	1.15143	0.0000	0.000	1410557.	758.67	1086.85	1086.85	1173.18	0.067	0.067	0.3082	758.67
4	12	1.12898	0.0000	0.000	1410558.	758.67	1086.86	1086.86	1170.94	0.067	0.067	0.3027	758.67
4	13	1.10653	0.0000	0.000	1410551.	758.67	1086.85	1086.85	1168.66	0.067	0.067	0.2971	758.67
4	14	1.08408	0.0000	0.000	1410538.	758.68	1086.85	1086.85	1166.35	0.067	0.067	0.2915	758.68
4	15	1.04975	0.0000	0.000	1128210.	811.34	863.15	863.15	1162.73	0.063	0.063	0.2830	811.34
4	16	1.01276	0.0000	0.000	1128206.	811.34	863.15	863.15	1158.73	0.063	0.063	0.2737	811.34
4	17	1.00033	0.0000	0.000	1128205.	811.34	863.15	863.15	1157.36	0.062	0.062	0.2706	811.34
4	18	1.00000	0.0000		1128252.	811.34	863.15	863.15	1157.32			0.3396	811.34

ic	vvx	vlx	vvy	vly	iz	ic	vvx	vlx	vvy	vly
1	0.000D+00	0.000D+00	0.000D+00	0.000D+00	2	2	3.138D-02	3.138D-02	0.000D+00	0.000D+00
1	0.000D+00	0.000D+00	0.000D+00	0.000D+00	3	2	0.000D+00	0.000D+00	0.000D+00	0.000D+00
1	0.000D+00	0.000D+00	0.000D+00	0.000D+00	4	2	0.000D+00	0.000D+00	0.000D+00	0.000D+00
1	0.000D+00	0.000D+00	0.000D+00	0.000D+00	5	2	0.000D+00	0.000D+00	0.000D+00	0.000D+00
1	0.000D+00	0.000D+00	0.000D+00	0.000D+00	6	2	0.000D+00	0.000D+00	0.000D+00	0.000D+00
1	0.000D+00	0.000D+00	0.000D+00	0.000D+00	7	2	0.000D+00	0.000D+00	0.000D+00	0.000D+00
1	0.000D+00	0.000D+00	0.000D+00	0.000D+00	8	2	0.000D+00	0.000D+00	0.000D+00	0.000D+00
1	0.000D+00	0.000D+00	0.000D+00	0.000D+00	9	2	0.000D+00	0.000D+00	0.000D+00	0.000D+00
1	0.000D+00	0.000D+00	0.000D+00	0.000D+00	10	2	0.000D+00	0.000D+00	0.000D+00	0.000D+00
1	0.000D+00	0.000D+00	0.000D+00	0.000D+00	11	2	0.000D+00	0.000D+00	0.000D+00	0.000D+00
1	0.000D+00	0.000D+00	0.000D+00	0.000D+00	12	2	0.000D+00	0.000D+00	0.000D+00	0.000D+00
1	0.000D+00	0.000D+00	0.000D+00	0.000D+00	13	2	0.000D+00	0.000D+00	0.000D+00	0.000D+00
1	0.000D+00	0.000D+00	0.000D+00	0.000D+00	14	2	0.000D+00	0.000D+00	0.000D+00	0.000D+00
1	0.000D+00	0.000D+00	0.000D+00	0.000D+00	15	2	0.000D+00	0.000D+00	0.000D+00	0.000D+00
1	0.000D+00	0.000D+00	0.000D+00	0.000D+00	16	2	0.000D+00	0.000D+00	0.000D+00	0.000D+00
1	0.000D+00	0.000D+00	0.000D+00	0.000D+00	17	2	-5.080D-05	-5.080D-05	0.000D+00	0.000D+00
3	3.138D-02	3.138D-02	0.000D+00	0.000D+00	2	4	3.138D-02	3.138D-02	0.000D+00	0.000D+00
3	0.000D+00	0.000D+00	0.000D+00	0.000D+00	3	4	0.000D+00	0.000D+00	0.000D+00	0.000D+00
3	0.000D+00	0.000D+00	0.000D+00	0.000D+00	4	4	0.000D+00	0.000D+00	0.000D+00	0.000D+00
3	0.000D+00	0.000D+00	0.000D+00	0.000D+00	5	4	0.000D+00	0.000D+00	0.000D+00	0.000D+00
3	0.000D+00	0.000D+00	0.000D+00	0.000D+00	6	4	0.000D+00	0.000D+00	0.000D+00	0.000D+00
3	0.000D+00	0.000D+00	0.000D+00	0.000D+00	7	4	0.000D+00	0.000D+00	0.000D+00	0.000D+00
3	0.000D+00	0.000D+00	0.000D+00	0.000D+00	8	4	0.000D+00	0.000D+00	0.000D+00	0.000D+00
3	0.000D+00	0.000D+00	0.000D+00	0.000D+00	9	4	0.000D+00	0.000D+00	0.000D+00	0.000D+00
3	0.000D+00	0.000D+00	0.000D+00	0.000D+00	10	4	0.000D+00	0.000D+00	0.000D+00	0.000D+00
3	0.000D+00	0.000D+00	0.000D+00	0.000D+00	11	4	0.000D+00	0.000D+00	0.000D+00	0.000D+00
3	0.000D+00	0.000D+00	0.000D+00	0.000D+00	12	4	0.000D+00	0.000D+00	0.000D+00	0.000D+00
3	0.000D+00	0.000D+00	0.000D+00	0.000D+00	13	4	0.000D+00	0.000D+00	0.000D+00	0.000D+00
3	0.000D+00	0.000D+00	0.000D+00	0.000D+00	14	4	0.000D+00	0.000D+00	0.000D+00	0.000D+00
3	0.000D+00	0.000D+00	0.000D+00	0.000D+00	15	4	0.000D+00	0.000D+00	0.000D+00	0.000D+00
3	0.000D+00	0.000D+00	0.000D+00	0.000D+00	16	4	0.000D+00	0.000D+00	0.000D+00	0.000D+00
3	0.000D+00	0.000D+00	0.000D+00	0.000D+00	17	4	-1.874D-04	-1.874D-04	0.000D+00	0.000D+00

Output of the simulated 1-D loop analysis with vapor density x200 at boiling inception

time step no = 29 time = 3.000000 sec time step size = 0.10000D+00 sec
number of newton iterations = 2
number of inner iterations = 1 1 0

total reactor power = 0.910 kW inlet flow rate = 0.000 kg/s
total heat transfer = 0.903 kW outlet flow rate = 0.002 kg/s
flow enthalpy rise = 1.823 kW

maximum relative changes over the time step
in pressure: 0.001371
in mixture density: 0.039481
in mixture energy: 0.018382

ic	iz	P(bar)	void	% qual	hm	rom	T vap	T liq	T sat	vvz	vlz	rov	rol
1	1	1.00000	0.0000	0.000	1128298.	811.33	863.19	863.19	1157.32	0.006	0.006	67.9204	811.33
1	2	0.97545	0.0000	0.000	1128252.	811.33	863.19	863.19	1154.57	0.006	0.006	52.8764	811.33
1	3	0.97547	0.0000	0.000	1128248.	811.33	863.19	863.19	1154.57	0.006	0.006	52.8777	811.33
1	4	0.97550	0.0000	0.000	1128248.	811.33	863.19	863.19	1154.57	0.006	0.006	52.8790	811.33
1	5	0.97552	0.0000	0.000	1128248.	811.33	863.19	863.19	1154.58	0.006	0.006	52.8802	811.33
1	6	1.02468	0.0000	0.000	1128254.	811.33	863.19	863.19	1160.03	0.006	0.006	55.3411	811.33
1	7	1.07384	0.0000	0.000	1128260.	811.33	863.19	863.19	1165.28	0.006	0.006	57.7922	811.33
1	8	1.12299	0.0000	0.000	1128266.	811.33	863.19	863.19	1170.33	0.006	0.006	60.2340	811.33
1	9	1.17215	0.0000	0.000	1128273.	811.33	863.19	863.19	1175.22	0.006	0.006	62.6668	811.33
1	10	1.22131	0.0000	0.000	1128279.	811.33	863.19	863.19	1179.94	0.006	0.006	65.0910	811.33
1	11	1.27046	0.0000	0.000	1128285.	811.33	863.19	863.19	1184.51	0.006	0.006	67.5070	811.33
1	12	1.31962	0.0000	0.000	1128291.	811.33	863.19	863.19	1188.94	0.006	0.006	69.9150	811.33
1	13	1.31964	0.0000	0.000	1128291.	811.33	863.19	863.19	1188.95	0.006	0.006	69.9163	811.33
1	14	1.31967	0.0000	0.000	1128248.	811.34	863.15	863.15	1188.95	0.006	0.006	69.9175	811.34
1	15	1.31969	0.0000	0.000	1123744.	812.18	859.57	859.57	1188.95	0.006	0.006	69.9188	812.18
1	16	1.27054	0.0000	0.000	913455.	850.63	693.15	693.15	1184.52	0.005	0.005	67.5107	850.63
1	17	1.23671	0.0000	0.000	1432427.	754.59	1104.01	1104.01	1181.39	0.012	0.012	65.8488	754.59
1	18	1.22230	0.0492	2.925	1551804.	703.39	1180.03	1180.03	1180.03	0.425	0.065	65.1401	736.41
1	19	1.20852	0.0848	2.681	1567326.	679.72	1178.73	1178.73	1178.73	0.403	0.119	64.4613	736.72
1	20	1.19516	0.1141	1.106	1580402.	660.21	1177.45	1177.45	1177.45	0.199	0.198	63.8028	737.03
1	21	1.18134	0.1082	1.030	1574938.	664.43	1176.11	1176.11	1176.11	0.263	0.263	63.1207	737.35
1	22	1.16354	0.0000	0.000	1280190.	783.05	983.90	983.90	1174.37	0.246	0.246	62.2413	783.05
1	23	1.13924	0.0000	0.000	1160858.	805.29	889.10	889.10	1171.97	0.246	0.246	61.0391	805.29
1	24	1.11431	0.0000	0.000	1133197.	810.42	867.11	867.11	1169.45	0.246	0.246	59.8031	810.42
1	25	1.08924	0.0000	0.000	1128820.	811.23	863.63	863.63	1166.88	0.246	0.246	58.5585	811.23
1	26	1.06416	0.0000	0.000	1128308.	811.32	863.23	863.23	1164.26	0.246	0.246	57.3107	811.32
1	27	1.02581	0.0000	0.000	1128209.	811.34	863.15	863.15	1160.15	0.246	0.246	55.3977	811.34
1	28	1.00000	0.0000		1128253.	811.34	863.15	863.15	1157.32			67.9226	811.34

Output of the simulated 1-D loop analysis with vapor density x100 at boiling inception

time step no = 27 time = 3.336324 sec time step size = 0.838680-01 sec
number of newton iterations = 2
number of inner iterations = 2 0 0

total reactor power = 0.910 kW inlet flow rate = -0.001 kg/s
total heat transfer = 0.674 kW outlet flow rate = 0.005 kg/s
flow enthalpy rise = 5.728 kW

maximum relative changes over the time step
in pressure: 0.052486
in mixture density: 0.263107
in mixture energy: 0.115685

ic	iz	P(bar)	void	% qual	hm	rom	T vap	T liq	T sat	vvz	vlz	rov	rol
1	1	1.00000	0.0000	0.000	1128302.	811.33	863.19	863.19	1157.32	-0.081	-0.081	33.9601	811.33
1	2	0.97620	0.0000	0.000	1128252.	811.33	863.19	863.19	1154.65	-0.081	-0.081	26.4571	811.33
1	3	0.97774	0.0000	0.000	1128249.	811.33	863.19	863.19	1154.83	-0.081	-0.081	26.4956	811.33
1	4	0.97927	0.0000	0.000	1128249.	811.33	863.19	863.19	1155.00	-0.081	-0.081	26.5341	811.33
1	5	0.98080	0.0000	0.000	1128249.	811.33	863.19	863.19	1155.17	-0.081	-0.081	26.5725	811.33
1	6	1.03147	0.0000	0.000	1128255.	811.33	863.19	863.19	1160.77	-0.081	-0.081	27.8401	811.33
1	7	1.08213	0.0000	0.000	1128261.	811.33	863.19	863.19	1166.14	-0.081	-0.081	29.1025	811.33
1	8	1.13280	0.0000	0.000	1128268.	811.33	863.19	863.19	1171.32	-0.081	-0.081	30.3600	811.33
1	9	1.18346	0.0000	0.000	1128274.	811.33	863.19	863.19	1176.32	-0.081	-0.081	31.6127	811.33
1	10	1.23413	0.0000	0.000	1128280.	811.33	863.19	863.19	1181.15	-0.081	-0.081	32.8610	811.33
1	11	1.28479	0.0000	0.000	1128286.	811.33	863.19	863.19	1185.82	-0.081	-0.081	34.1049	811.33
1	12	1.33546	0.0000	0.000	1128292.	811.33	863.19	863.19	1190.34	-0.081	-0.081	35.3447	811.33
1	13	1.33699	0.0000	0.000	1128254.	811.34	863.16	863.16	1190.48	-0.081	-0.081	35.3821	811.34
1	14	1.33853	0.0000	0.000	1127040.	811.57	862.19	862.19	1190.61	-0.081	-0.081	35.4196	811.57
1	15	1.34007	0.0000	0.000	1103926.	815.84	843.82	843.82	1190.75	-0.081	-0.081	35.4574	815.84
1	16	1.29023	0.0000	0.000	913845.	850.56	693.45	693.45	1186.31	-0.089	-0.089	34.2381	850.56
1	17	1.26036	0.0000	0.000	1336537.	772.52	1028.50	1028.50	1183.58	0.318	-0.410	33.5056	772.52
1	18	1.25770	0.8209	23.083	2387063.	159.19	1183.34	1183.34	1183.34	0.390	0.271	33.4403	735.62
1	19	1.25186	0.4802	5.120	1731457.	398.41	1182.80	1182.80	1182.80	0.659	0.510	33.2967	735.75
1	20	1.23878	0.3837	3.210	1665481.	466.30	1181.58	1181.58	1181.58	0.857	0.720	32.9755	736.04
1	21	1.22303	0.3626	2.802	1650778.	481.17	1180.10	1180.10	1180.10	1.049	0.916	32.5879	736.39
1	22	1.20083	0.0000	0.000	1469082.	747.75	1132.69	1132.69	1177.99	0.675	0.675	32.0410	747.75
1	23	1.17281	0.0000	0.000	1284700.	782.21	987.48	987.48	1175.28	0.674	0.674	31.3497	782.21
1	24	1.14247	0.0000	0.000	1180667.	801.61	904.85	904.85	1172.29	0.674	0.674	30.5995	801.61
1	25	1.11143	0.0000	0.000	1141395.	808.90	873.63	873.63	1169.16	0.674	0.674	29.8303	808.90
1	26	1.08016	0.0000	0.000	1130786.	810.87	865.20	865.20	1165.94	0.674	0.674	29.0534	810.87
1	27	1.03225	0.0000	0.000	1128223.	811.34	863.16	863.16	1160.85	0.674	0.674	27.8597	811.34
1	28	1.00000	0.0000		1128266.	811.34	863.16	863.16	1157.32			33.9610	811.34